

**LOW-TEMPERATURE SELECTIVE CATALYTIC
REDUCTION OF NO_x
CATALYTIC BEHAVIOR AND KINETIC MODELING**

A dissertation submitted to the
SWISS FEDERAL INSTITUTE OF TECHNOLOGY ZURICH
for the degree of
DOCTOR OF TECHNICAL SCIENCES

presented by
RENÉ WILLI
Dipl. Chem. Ing. ETH
born November 11, 1967
citizen of Mels (SG)

accepted on the recommendation of

Prof. Dr. A. Baiker, examiner
Prof. Dr. A. Wokaun, co-examiner

1996

*To my parents who provided the opportunities and to
Sibylle for her love, patience, and understanding.*

Acknowledgments

I am very grateful to Professor Alfons Baiker for the scientific supervision of this work. I appreciated his skill to create an atmosphere for creativity and to find always time for constructive discussions.

I thank Professor Alexander Wokaun for agreeing to be co-examiner and giving expert advice about this work.

My special thanks are due to Dr. René Köppel for being a helpful and untiring teacher. He was always a partner for fruitful discussions and spent a lot of time for proof-reading our publications and this thesis.

The co-operation with Dr. Lukas Padeste, Dr. Marek Maciejewski, Dr. Helmut Schneider and Bertrand Roduit was a great help for my research and I want to thank them for their ideas which are involved in this work.

Thanks are also due to Dr. Ulrich Göbel for carrying out the XPS measurements, to Dr. Michael Schneider for the preparation of the aerogel sample and to Katalysatorwerke Hüls GmbH for providing the commercial catalyst sample.

Financial support of this work by the Nationaler Energie-Forschungs-Fond (Neff-Project 569) is gratefully acknowledged.

Many other people supported me during my thesis. Therefore I express my gratitude to all these unnamed, who contributed in various ways to the success of this work.

In the past few years I won new friends and I am happy for the hours we spent together. I will always remember skiing in Colorado, Triftji, Damüls, mountain biking in the Valais Alps and all the other adventures.

Table of Contents

SUMMARY	1
ZUSAMMENFASSUNG	5
CHAPTER 1: INTRODUCTION	
1.1 Nitrogen cycle	9
1.2 Environmental problems by nitrogen oxide emissions	10
1.2.1 NO _x emission	10
1.2.2 N ₂ O emission	14
1.3 Control technologies for the nitrogen oxides emissions	15
1.3.1 Primary Measures	16
1.3.2 Selective Non-Catalytic Reduction (SNCR)	17
1.3.3 Non-Selective Catalytic Reduction (NSCR)	17
1.3.4 Selective Catalytic Reduction (SCR)	18
1.3.4.1 Process description	18
1.3.4.2 Types of catalysts	23
1.3.4.3 Kinetics and Mechanisms for vanadia containing catalysts	24
1.3.4.4 Kinetics and Mechanisms for chromia containing catalysts	28
1.4 Research Frontiers	29
1.4.1 The direct decomposition of NO to its elements	29
1.4.2 New developments in the selective reduction of NO _x with NH ₃	30
1.4.3 Using hydrocarbons as reducing agent	31
1.5 Scope of the Thesis	32
1.6 References	33
CHAPTER 2: EXPERIMENTAL	
2.1 Apparatus	39
2.2 Analysis	42
2.3 Kinetic Modeling	44

2.4 Notation	47
2.5 References	48
CHAPTER 3: VANADIA-BASED COMMERCIAL CATALYST	
Abstract	49
3.1 Introduction	50
3.2 Experimental	51
3.3 Results	52
3.3.1 Mass and heat transfer	52
3.3.2 Catalyst stability	53
3.3.3 Influence of space velocity	53
3.3.4 Influence of water	54
3.3.5 Influence of oxygen	55
3.3.6 Influence of ammonia	56
3.3.7 Influence of SO ₂	57
3.3.8 Kinetic modeling	58
3.4 Discussion	62
3.5 Conclusions	65
3.6 Notation	66
3.7 References	66
CHAPTER 4: VANADIA-TITANIA AEROGEL CATALYST	
Abstract	69
4.1 Introduction	70
4.2 Experimental	71
4.2.1 Catalyst	71
4.2.2 Catalytic tests	72
4.2.3 Kinetic modeling	72
4.3 Results	73
4.3.1 Mass and heat transfer	73
4.3.2 Catalyst stability	74
4.3.3 Temperature dependence	75
4.3.4 Influence of space velocity	76
4.3.5 Influence of the ammonia concentration	77

4.3.6 Influence of water	78
4.3.7 Influence of oxygen	80
4.3.8 Influence of SO ₂	81
4.3.9 Kinetic modeling	83
4.4 Discussion	85
4.5 Conclusions	89
4.6 Notation	90
4.7 References	90

CHAPTER 5: CHROMIA ON TITANIA CATALYST

Abstract	93
5.1 Introduction	94
5.2 Experimental	97
5.2.1 Catalyst preparation	97
5.2.2 Catalytic tests	98
5.2.3 Kinetic modeling	99
5.2.4 X-ray photoelectron spectroscopy	99
5.2.5 Transmission FTIR spectroscopy	99
5.3 Results	100
5.3.1 Heat and mass transfer	100
5.3.2 Stability of the catalyst	100
5.3.3 Influence of temperature	102
5.3.4 Influence of gas flow rate	103
5.3.5 Influence of the ammonia concentration	105
5.3.6 Effect of water	106
5.3.7 Influence of the oxygen concentration	108
5.3.8 Influence of the feed gas composition	110
5.3.9 Effect of SO ₂	112
5.3.10 XPS analysis	114
5.3.11 Transmission FTIR-spectroscopy	115
5.3.12 Kinetic modeling	116
5.4 Discussion	120
5.5 Conclusions	125
5.6 Notation	126

5.7 References	126
CHAPTER 6: COMPARISON OF THE INVESTIGATED CATALYSTS	
6.1 Catalytic performance in the low temperature range	131
6.2 Influence of the exhaust composition on the kinetics	133
6.3 Conclusions	134
6.4 References	134
FINAL REMARKS	135
LIST OF PUBLICATIONS	137
CURRICULUM VITAE	139

Summary

The aim of this study was to design new catalytic systems for the selective catalytic reduction of NO_x with increased activity and improved dynamic behavior, particularly in the lower temperature range. This included the optimization of the structural and chemical properties of the catalysts and comprehensive investigations of the kinetics. The catalysts, developed in our laboratory, were scrutinized under conditions corresponding to real exhausts and the sensitivity of the activity and selectivity to the different components in the exhaust gas was determined. Additionally, the kinetic behavior of a commercial sample, used as a reference catalyst, was investigated in the low temperature range.

The work can be subdivided in the following main topics:

- Setup of a fully computer controlled pilot plant for exhaust gas catalysts.
- Preparation of chromia on titania catalysts with an improved activity and selectivity.
- Experimental investigations and simulations of the intrinsic kinetics of a commercial catalyst, a vanadia-titania aerogel catalyst and a titania supported chromia catalyst.
- Investigations of the deactivation behavior and of the SO_2 poisoning of titania supported chromia catalysts by kinetic measurements, X-ray photoelectron spectroscopy analysis and transmission FTIR spectroscopy.

Reference experiments were carried out with a commercial vanadia based catalyst provided by Hüls GmbH ($\text{TiO}_2 > 70\%$, V_2O_5 , WO_3 , MoO_3 and additives). The results obtained with this catalyst were used as a base for comparison with data obtained with the own catalysts. The influence of the different exhaust gas components on the kinetics was determined, and a model of the intrinsic kinetics was created. NO reacts stoichiometrically with ammonia to water and nitrogen. Side reactions, as the formation of nitrous oxide or the direct oxidation of ammonia, were not significant in the investigated temperature range.

For temperatures exceeding 473 K, the kinetic data are described well with a model which is based on an Eley-Rideal mechanism. The kinetic rate expression of the model was first order with respect to NO and zeroth order with respect to NH₃. Below 473 K the conversion is higher than predicted with this model, probably due to the contribution of an additional reaction pathway, which occurs only at low temperatures. By the introduction of an additional reaction pathway based on a Langmuir-Hinshelwood mechanism, good fitting of the experimental results with the model predictions could be achieved also below 473 K.

The influence of oxygen was taken into account with a Langmuir adsorption isotherm expression. The impact of the variation in the oxygen concentration on the NO conversion was small for concentrations between 4% and 10%. Lower oxygen concentrations resulted in a marked decrease of the catalytic activity. Water inhibited the reaction. The effect leveled off for water concentrations over 2.5%. Between 2.5% and 7.5% H₂O in the feed gas, no significant dependence of the NO conversion was perceptible. To account for this, the kinetic parameters were separately estimated for water concentrations below and above 2.5%.

Recently, vanadia-titania aerogels developed in our laboratory were found to exhibit high activity for the selective catalytic reduction of NO by NH₃. The highly dispersed vanadia-titania aerogel with a vanadia content of 30 wt.% has been prepared by a two-stage sol-gel process with ensuing high-temperature supercritical drying. This catalyst possesses a specific surface area of 183 m²/g which is several times higher than that usually found for commercial catalysts. The kinetic investigations led to a model which agrees to a large degree with the model proposed for the commercial catalyst. However, no deviations from the model based only on an Eley-Rideal reaction path had been detected in the lower temperature range. The stoichiometry and the reaction orders in ammonia and nitric oxide were the same as found for the commercial catalyst, and the formation of nitrous oxide was not significant.

The addition of up to 3% H₂O to the dry feed significantly reduced the rate of NO conversion. The effect leveled off for higher H₂O concentrations. For high water

concentrations, the reaction rate reduced to about 60% of the value without water and kept constant. In the absence of O_2 in the feed the activity collapsed. Small amounts of oxygen resulted in a sharp increase of the NO conversion, but for oxygen concentrations exceeding 4 % the increase diminished. The influence of oxygen was well described by the assumption of a Langmuir adsorption. The influence of water was modeled with a modified Langmuir adsorption which took into account the constant activity for high water concentration by a constant remainder. The temperature dependence of the estimated adsorption constants was not significant in the investigated temperature range. CO_2 showed no influence, and a high tolerance with respect to sulfur dioxide was observed.

The titania supported chromia catalyst with a nominal chromium content of 6.84 wt.% Cr, corresponding to 10 wt.% Cr_2O_3 , was prepared by wet impregnation of TiO_2 (P25, Degussa) with chromium(III)nitrate nonahydrate. After drying and reduction, the catalyst contained the chromium component mainly in the form of X-ray amorphous Cr_2O_3 . In the past, an important disadvantage of catalysts based on chromium oxide was the undesired formation of nitrous oxide. This side reaction could be strongly suppressed, with an optimized pretreatment of the catalyst, thus maximizing the amount of X-ray amorphous Cr_2O_3 .

Similar to the vanadia based catalysts the kinetic model approach involves the assumption of an Eley-Rideal mechanism. The observed reaction orders were the same for the chromia containing catalyst and for the vanadia based catalysts, for which a reaction rate of first order in NO and zeroth order in NH_3 was determined. It was not possible to explain the influence of oxygen on the conversion of NO by a single Langmuir adsorption model, probably due to an additional reoxidation of the catalyst by gaseous oxygen. Water inhibited the reduction of NO, the undesired formation of N_2O and the reoxidation of the catalyst.

Sulfur dioxide exhibited a severe poisoning effect even at low concentrations. This poisoning of the catalyst by SO_2 was irreversible and occurred at temperatures so high that the formation of ammonium sulfates/bisulfates/sulfites is implausible. The formation of a sulfate species was established by X-ray photoelectron spectroscopy and

transmission FTIR spectroscopy. The precise determination of the nature of this sulfate species needs further investigations.

The final comparison of the investigated catalysts showed that the vanadia titania aerogel and the titania supported chromia catalyst offers a better performance per catalyst weight in the lower temperature range than the commercial catalyst. Due to the high specific surface area, the aerogel exhibited high activity for temperatures even below 473 K. The selectivity of the newly developed chromia on titania catalyst to N_2 and H_2O was distinctly improved compared to the known catalysts. The lack of resistance towards SO_2 poisoning of this catalytic system is the main obstacle for an industrial application. However, present trends in fuel technology show an increasing tendency for the use of fuels with very low sulfur content, which would circumvent the SO_2 poisoning problem.

Zusammenfassung

Das Ziel dieser Studie bestand in der Entwicklung neuartiger Katalysatorsysteme mit höherer Aktivität und verbesserter Dynamik in bezug auf die selektive katalytische Reduktion von NO_x mit NH_3 . Besonders wichtig erschien das Erreichen eines guten Ansprechverhaltens im tieferen Temperaturbereich ($<523 \text{ K}$). Dies bedingte neben der Optimierung der strukturellen und chemischen Eigenschaften der Katalysatoren auch umfassende kinetische Untersuchungen. Die in unserer Gruppe entwickelten Katalysatoren wurden unter möglichst praxisnahen Bedingungen getestet, und die Einflüsse der einzelnen Abgaskomponenten auf die Kinetik wurden bestimmt. Das kinetische Verhalten eines uns zur Verfügung gestellten kommerziellen Katalysators wurde eingehend untersucht und als Referenz für die weitergehenden Studien verwendet.

Die durchgeführten Arbeiten lassen sich in folgende Hauptbereiche unterteilen:

- Aufbau einer computergesteuerten Testanlage für Verbrennungsabgaskatalysatoren.
- Präparation von Chromoxid auf Titanoxid Schichtkatalysatoren, welche eine verbesserte Selektivität und Aktivität aufweisen.
- Experimentelle Untersuchungen und Modellierung der intrinsischen Kinetik eines kommerziellen SCR-Katalysators, eines Vanadiumoxid-Titanoxid-Mischkatalysators und eines Chromoxid auf Titanoxid Schichtkatalysators.
- Untersuchung von Vergiftungs- und Deaktivierungserscheinungen bei Chromoxid auf Titanoxid Schichtkatalysatoren mittels kinetischen Messungen, XPS und Transmissions-FTIR-Spektroskopie.

Die ersten Versuche wurden mit einem kommerziellen, auf Vanadiumoxid basierenden Katalysator der Firma Hüls GmbH durchgeführt ($\text{TiO}_2 >70\%$, V_2O_5 , WO_3 , MoO_3 und Zuschlagstoffe). Dieser Katalysator diente als Vergleichsbasis für die weiteren Versuche mit den eigenen Katalysatoren. Es wurde der Einfluss der einzelnen

Abgaskomponenten auf die Kinetik ermittelt und ein Modell für die Mikrokinetik erstellt. NO reagierte stöchiometrisch mit dem eingesetzten Ammoniak zu Wasser und Stickstoff. Nebenreaktionen, wie die Bildung von Lachgas oder die direkte Ammoniakoxidation, waren im ganzen Temperaturbereich vernachlässigbar.

Für Temperaturen über 473 K konnten die kinetischen Daten gut mit einem auf einem Eley-Rideal Mechanismus beruhenden Modell beschrieben werden. Die ermittelten Reaktionsordnungen waren 1 für Stickstoffmonoxid und Null für Ammoniak.

Unter 473 K wurde ein höherer Umsatz beobachtet als aufgrund der Modellvorhersage erwartet wurde. Dies deutet auf einen zusätzlichen Reaktionsweg hin, welcher nur bei tiefen Temperaturen wirksam ist. Durch die Einführung eines zusätzlichen Reaktionsweges, basierend auf einem Langmuir-Hinshelwood Mechanismus, konnte eine gute Übereinstimmung mit dem beobachteten kinetischen Verhalten erzielt werden.

Der Einfluss von Sauerstoff konnte durch einen Langmuiransatz beschrieben werden. Der Umsatz von NO zeigte für Sauerstoffkonzentrationen oberhalb 4% nur noch eine geringe Abhängigkeit. Sauerstoffkonzentrationen unter 4% führten zu einem deutlichen Einbruch der Aktivität. Wasser inhibierte die Reaktion. Für höhere Wasserkonzentrationen verringerte sich jedoch die Abnahme des Umsatzes, und bei einem Wassergehalt von über 2.5% war kein signifikanter Einfluss der H₂O Konzentration auf die Umsatzrate mehr erkennbar. Aus diesem Grund wurden die kinetischen Parameter jeweils für Abgase mit und ohne Wasser einzeln ermittelt. SO₂ und CO₂ zeigten in den für Dieselabgase typischen Konzentrationsbereichen keinen signifikanten Einfluss.

Bei den Titanoxid-Vanadiumoxid-Mischaerogelen handelt es sich um neuentwickelte Mischoxide, welche in einem zweistufigen Sol-Gel-Prozess hergestellt werden. Diese Katalysatoren weisen eine im Vergleich zu den kommerziellen Katalysatoren mehrfach grössere spezifische Oberfläche auf. Der untersuchte Katalysator wies einen Vanadiumoxidgehalt von 30 Gew.% und eine BET-Oberfläche von 183 m²/g auf. Die kinetischen Untersuchungen ergaben ein Modell, welches die

Erkenntnisse mit dem auf Vanadiumoxid basierenden kommerziellen Katalysator weitgehend bestätigte. Die Abweichung vom Eley-Rideal Mechanismus im unteren Temperaturbereich (<473 K) konnte jedoch nicht mehr festgestellt werden. Es wurde dieselbe Stöchiometrie der Reaktion wie beim kommerziellen Katalysator und ebenfalls keine signifikante Lachgasbildung beobachtet. Die ermittelten Reaktionsordnungen betragen wiederum 1 für NO respektive 0 für Ammoniak.

Wasser zeigte für Konzentrationen unter 4% einen stark inhibierenden Einfluss auf die Reaktion. Bei hohen Wasserkonzentrationen wies der Katalysator eine um etwa 60% verringerte, jedoch konstante Aktivität auf. Dies bedeutet, dass auch bei maximaler Bedeckung des Katalysators durch Wasser, der Katalysator eine auf tieferem Niveau konstante Grundaktivität beibehält. Die Aktivität steigt mit der Sauerstoffkonzentration bis 4% stark an. Diese Zunahme schwächt sich ab 4% O₂ stark ab und die Aktivität nähert sich einem oberen Grenzwert. Ohne Sauerstoff im Feedgas bricht der Umsatz zusammen. Dieses Verhalten konnte wie beim kommerziellen Katalysator sehr gut durch einen Langmuiransatz beschrieben werden. Der Einfluss der Wasserkonzentration auf die Sauerstoffabhängigkeit war nicht signifikant. Die Temperaturabhängigkeit der Adsorptionskonstanten konnte in dem von uns untersuchten Temperaturbereich ebenfalls vernachlässigt werden. CO₂ und SO₂ zeigten zudem in den für Dieselabgase typischen Konzentrationsbereichen keinen Einfluss.

Die Chromoxid auf Titanoxid Katalysatoren mit nominell 6.84 Gew.% Cr, entsprechend 10 Gew.% Cr₂O₃, wurden durch Nassimprägnation von Titanoxid (P25, Degussa) mit Cr(NO₃)₃ · 9 H₂O hergestellt. Nach Trocknung und Reduktion bestand der Chromanteil des Katalysators zu >95% aus röntgenamorphem Cr₂O₃. Ein Hauptproblem bei den DENOx-Katalysatoren auf der Basis von Chromoxiden stellte bis anhin die unerwünschte Bildung von Lachgas dar. Durch eine Optimierung der Vorbehandlung, wobei der Anteil an röntgenamorphen Cr₂O₃ maximiert wurde, konnte diese Nebenreaktion weitgehend unterdrückt werden. Wie bei den auf Vanadiumoxid basierenden Katalysatoren beruht der Modellansatz auf einem Eley-Rideal Mechanismus. Die Reoxidation konnte nicht durch einen reinen Langmuiransatz ausgedrückt werden. Nicht adsorbierter Sauerstoff aus der Gasphase scheint ebenfalls

teilweise für die Reoxidation des Katalysators verantwortlich zu sein. Wasser beeinträchtigte die Oxidation des Katalysators und inhibierte zudem die Reduktion von NO zu N₂, sowie die Bildung von Lachgas. Die Chromoxid auf Titanoxidkatalysatoren zeigen schon bei geringen SO₂ Konzentrationen starke Deaktivierungserscheinungen. Diese Vergiftungserscheinungen traten auch bei Temperaturen über 540 K auf. Es erscheint deshalb unwahrscheinlich, dass es sich um ein Fouling durch Ablagerung von Ammoniumsulfaten/sulfiten handelt, welches in der Praxis bei tiefen Temperaturen auch auf Vanadiumoxid basierenden Katalysatoren auftritt. Durch XPS und Transmissions-FTIR Spektroskopie konnte gezeigt werden, dass sich eine Sulfatspezies auf der Katalysatoroberfläche gebildet hat, deren exakte Natur jedoch noch nicht ermittelt werden konnte.

Der zusammenfassende Vergleich aller untersuchten Katalysatoren bei für Dieselabgasen realistischer Abgaszusammensetzung zeigte deutlich, dass die in unserer Gruppe entwickelten Katalysatoren klare Vorteile im unteren Temperaturbereich aufweisen. Der V₂O₅/TiO₂ Misch-aerogel-Katalysator ist durch seine hohe Oberfläche und den im Vergleich zum kommerziellen Katalysator hohen V₂O₅-Gehalt schon bei sehr tiefen Temperaturen aktiv. Die auf Chromoxid basierenden Katalysatoren zeigten eine ebenfalls höhere Aktivität im tieferen Temperaturbereich, und es konnte eine deutliche Verbesserung der Selektivität bei diesem Katalysatorsystem erreicht werden. Die Empfindlichkeit gegenüber SO₂ bildet noch ein Problem, welches jedoch durch die Entwicklung von neuen Dieselmotorkraftstoffen mit sehr geringem Schwefelgehalt entschärft wird.

Introduction

1.1 Nitrogen cycle

Nitrogen is the main component of the atmosphere as well as a structural component of the ribonucleic acid (RNA), the desoxyribonucleic acid (DNA) and many other organic substances. In the animated world, nitrogen uptake is mainly in the form of nitrate (NO_3^-). There are two ways for the fixation of nitrogen in the ecosystem (1). Firstly via the photochemical reaction of N_2 to NH_3 and NO_x induced by high energy radiation in the upper atmosphere yielding up to $35 \text{ mg m}^{-2} \text{ year}^{-1}$, and secondly via the fixation by bacteria and by bluegreen algae yielding to $140 \text{ mg m}^{-2} \text{ year}^{-1}$. Both processes only amount to 6.7 % of the overall nitrogen cycle. During the industrialization, several new flows in the nitrogen cycle were created by man. By burning the biomass and fossil fuels, nitrogen, contained in the combustion air and nitrogen as components in the biomass and the fuel, oxidize at higher temperatures to NO , NO_2 and N_2O . The chemical transformations of atmospheric nitrogen oxides are depicted in Figure 1-1.

The human impact on the natural nitrogen cycle led to severe problems in the environment. The total NO_x emissions are estimated to an amount of $50 (\pm 25) \text{ Mt(N)/y}$ (2). 66% of them are made by human activities. The human sources are subdivided to 42% from fossil fuel combustion and 24% from biomass burning. Natural sources are lightning (16%), microbiologic activities (16%) and input from the stratosphere (1%).

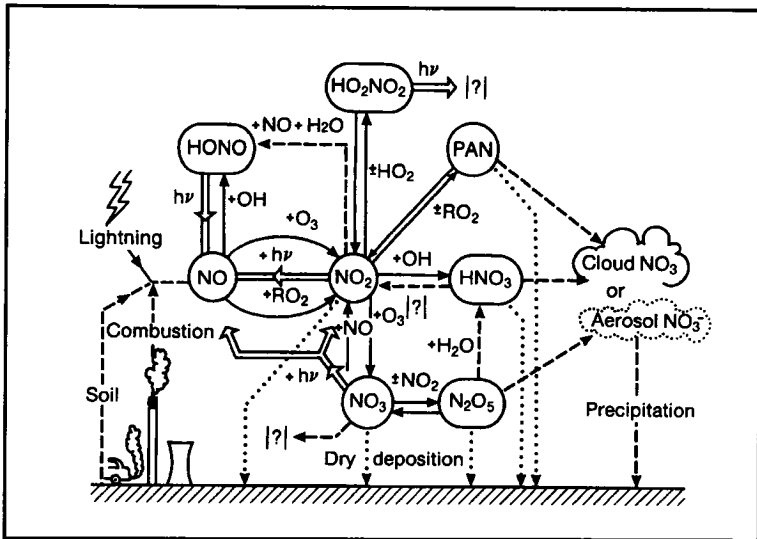


Figure 1-1. Upper atmospheric chemistry of nitric oxide

Reprinted from ref. 3

1.2 Environmental problems by nitrogen oxide emissions

1.2.1 NO_x emission

NO_x formation occurs by three fundamentally different mechanisms (4). The most important mechanism at higher temperatures (thermal NO_x) is based on the thermal dissociation and subsequent reaction of nitrogen and oxygen molecules in the combustion air. Conversion starts at temperatures above approximately 1600 K and increases markedly with rising temperatures. The degree of conversion is proportional to the concentration of atomic oxygen. A mechanism of the thermal NO_x formation was proposed by Zeldovich (5, 6). Under excess of oxygen the kinetic is described by reactions r1 and r2, and under excess of fuel by reaction r3, respectively.

excess O₂:



excess fuel:



The second mechanism (fuel NO_x), involves the reaction of fuel-bound nitrogen components with oxygen. The reactions are not fully known. The nitrogen contents are 0.5 wt.% till 2 wt.% for coal, 0.5 wt.% for heavy oil, trace amounts for light oil and for natural gas virtually none.

The third mechanism (prompt NO_x) has only a minor effect. Nitrogen radicals and hydrocarbons react to HCN (r4-r6) as an intermediate, followed by the oxidation to NO (7, 8). The formation of prompt NO_x is only significant in very fuel-rich flames.



Different sources of anthropogenic NO_x emissions are known. The most important is due to combustion processes (see paragraph 1.1). The transport sector is responsible for 50% of global man-made NO_x emission (9). The remainder originates from stationary sources, like power plants, internal combustion engines, industrial boilers, waste and sludge incinerators, process heaters and gas turbines. In Switzerland the contribution is similar (Fig. 1-2). The lion share of the NO_x emission is produced by traffic. Since 1985 the emission by traffic dropped due to the introduction of catalyst technology for cars. But in the future the part caused by traffic will get bigger due to the increasing volume of traffic (10).

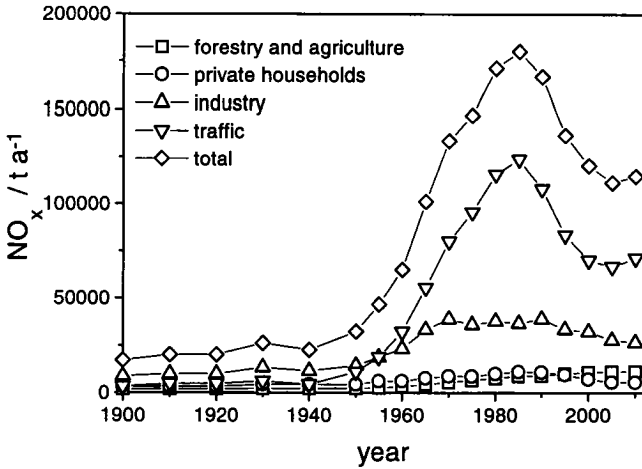


Figure 1-2. Nitric oxide emission in Switzerland 1900-2010

Reprinted from ref. 10.

In the hot waste gas after the burning chamber, the oxidized nitrogen is mainly in the form of nitric oxide (NO), a small amount of the NO is transformed to nitrogen dioxide (NO₂) and nitrous oxide (N₂O). For example in a typical diesel exhaust after the muffler only about 5% of the total NO_x emission is in the form of NO₂, and less than 1% in the form of N₂O. In most of the other combustion types also more than 90 % of nitrogen oxides are in the form of nitric oxide. Dinitrogen trioxide (N₂O₃), dinitrogen tetraoxide (N₂O₄) and dinitrogen pentoxide (N₂O₅) are formed in negligible amounts.

In the troposphere NO is completely oxidized to NO₂, according to reaction r7 (11).



The main problem of the NO_x emission in the troposphere is the formation of photochemical smog. Ozone, NO_x and hydrocarbons are the key substances for the

appearance of photochemical smog. UV radiation ($\lambda < 420$ nm) leads to a photolytical decomposition of NO_2 . The atomic oxygen O reacts with molecular oxygen O_2 to ozone O_3 . Ozone in high concentrations is toxic for men and is supposed to be one cause of the dying of forests. Radicals (CH_2OO^* , HO_2^*) accelerate the formation of ozone. A reaction scheme of the ozone formation in the presence of volatile organic compounds (VOC) is depicted in Figure 1-3. The alternative formation of ozone in the troposphere with carbon monoxide instead of VOC is slow and has only a minor effect.

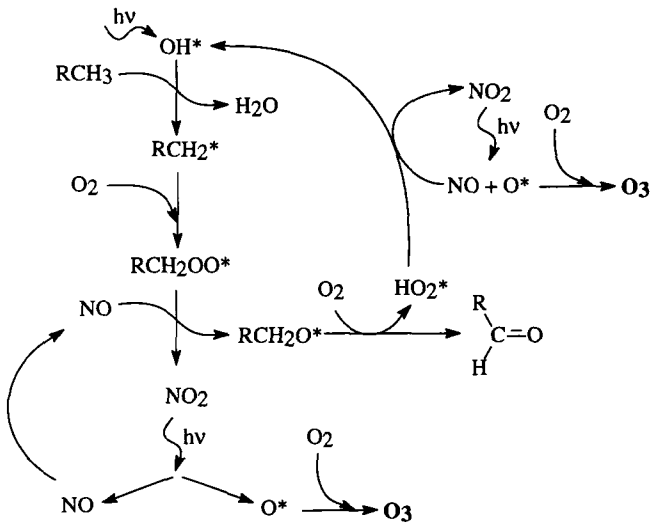
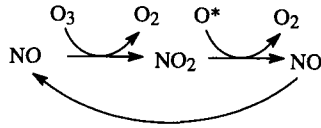


Figure 1-3. Ozone formation in urban air by photochemical reactions.

Reprint from ref. 12.

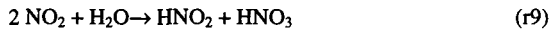
After sunset O_3 reacts with NO (r8). In the stratosphere, the same reaction occurs with NO formed by aircrafts or by the decomposition of N_2O and attacks the vital ozone layer, which protects the earth from the hard UV radiation ($\lambda < 242$ nm).



(r8)

The concentration of PAN (peroxyacyl nitrate), an organic compound which is also formed from NO_2 in presence of aldehydes or ketones, is high in photochemical smog. Daily averages in Los Angeles range from 10 to 30 ppb with maxima up to 210 ppb (13). PAN can cause health problems such as skin cancer and damages the foliage of trees.

An other severe problem caused by NO_x is the acid rain, mainly consisting of sulfuric, nitric and hydrochloric acid. Nitrogen dioxide reacts with water or OH^* radicals to nitric and nitrous acid (reactions r9 and r10). Acid rain is also supposed to be responsible for the dying of forests and led to immense damages at buildings.



1.2.2 N_2O emission

Nitrous oxide leads to stratospheric ozone destruction and greenhouse warming. Because the greenhouse warming potential of N_2O with an atmospheric lifetime of 150 years is 150 times higher than that of CO_2 , strong efforts were made to identify the sources of nitrous oxide and to limit its emission. In the stratosphere 90% of the N_2O is decomposed by photolysis to molecular nitrogen and free oxygen radicals. Another 5% react with free oxygen radicals to N_2 and O_2 and the remaining 5% react with free oxygen radicals to NO. The formed NO leads to a depletion of stratospheric ozone (r8). The total annual emission of N_2O amounts to approximately 20 Mt(N)/y (14). The principal source of nitrous oxide is the microbiological activity within soils. The direct formation of N_2O by burning of fuels is only a minor source. Recent estimates from the

IPPC (15), for the N_2O emissions due to fossil fuel combustion only amounted to approximately 3% of the total N_2O emissions. Most nitrous oxide is not produced during the burning process, but by undesired side reactions in catalytic reduction processes (see paragraph 1.3). In Switzerland about 8% of the nitrous oxide comes from industrial sources, mainly nitric acid plants and waste incinerators (10). The N_2O emission caused by traffic is rising parallel with the number of catalyst equipped vehicles. For Switzerland the share of the traffic at the total emission is estimated to approximately 15% in the year 2010 (10).

1.3 Control technologies for the nitrogen oxides emissions

There is a large number of commercial approaches to NO_x removal from stationary sources. More than 115 control systems are documented in reference 15. A good overview is also given by the comprehensive review from Bosch and Janssen (4). The most important control technologies are listed in Figure 1-4. They can be divided into two mayor groups.

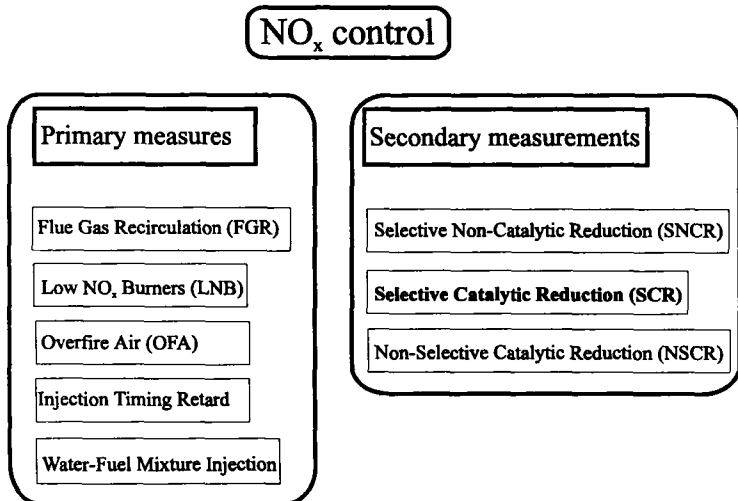


Figure 1-4. Most important techniques for NO_x emission control.

Primary measures prevent the formation of NO_x during the combustion, whereas secondary measures reduce or fix the nitrogen oxides after their formation. Additionally there are many other processes such as adsorption, absorption complexation and radiation induced decomposition which have negligible importance and are not addressed in this paragraph. Table 1-1 presents an overview of the NO_x control technology applications by combustion source type.

Nowadays the strict environmental regulation requires additional post-combustion removal of NO_x (secondary measures) to fulfill the mandatory air quality standards. The best available but also most expensive post-combustion control technology with high removal efficiency is the selective catalytic reduction (SCR).

Table 1-1. Applicability of NO_x control technology (16)

Control Technology	Combustion Turbines	Stationary Combustion Engines	Boilers/ Heaters	Waste Incinerators
Combustion Controls	X	X	X	X
Post-combustion controls				
Selective catalytic reduction	X	X	X	X
Non-selective catalytic reduction		X		
Selective non-catalytic reduction			X	X

1.3.1 Primary Measures

The aim of primary measures is to avoid the formation of NO_x . This can be achieved by modification of the fuel composition or by altering the combustion process.

The substitution of coal or oil by gas or adding of water to the fuel are possibilities of improvements with fuel modifications (17). Examples of in-combustion modifications are Flue Gas Recirculation, Low NO_x Burners, Over Fired Air, etc. (18, 19). The most important advantage of primary measures are the low costs.

1.3.2 Selective Non-Catalytic Reduction (SNCR)

The name indicates that in this process no catalyst is required, which is the main advantage of SNCR. In the SNCR-process, ammonia or another reducing agent like urea or cyanuric acid is injected in the flue gas at temperatures between 1100-1300 K (20). The method gives a lower NO_x reduction degree than SCR (SNCR 25 - 50%; SCR >70%) and has a higher consumption of reducing chemicals (19). A key problem is the narrow temperature window. The temperature of diesel engine exhaust is lower and prevents an economic application of SNCR. Exhaust gases of incinerators operate in this temperature range. In this case SNCR can be the proper and most cost effective technology.

1.3.3 Non-Selective Catalytic Reduction (NSCR)

The best known and one of the earliest techniques to remove nitrogen oxides is the non-selective catalytic reduction. NSCR is used to reduce the NO_x emission of nitric acid plants and gasoline engines.

The abatement of exhaust gases from nitric acid plants is one major application of NSCR (21). The waste gas of a nitric acid plant, based on the high-temperature catalytic oxidation of NH_3 process, contains excess of oxygen. In a first step all the excess of oxygen has to be consumed by combustion of the fuel reductant, due to the nonselectivity of the NSCR-process. Subsequent, the remaining fuel reduces catalytically the NO_x to N_2 .

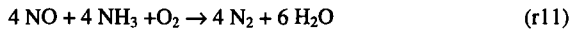
Well known is the automotive three way catalyst for cars, which is based on the same catalytic chemistry. The engine operates near stoichiometric conditions. High conversion of NO_x needs a feedback control loop to ensure the near stoichiometric operation point. The most widely used catalysts are made up of washcoats of platinum, rhodium and palladium on high surface supports.

1.3.4 Selective Catalytic Reduction (SCR)

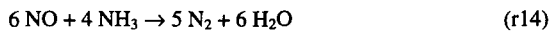
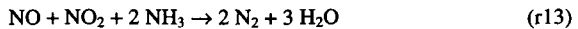
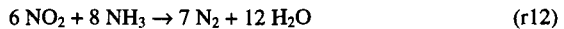
The selective catalytic reduction is the proper technique if a high efficiency of NO_x reduction in excess of oxygen is required. Today, plants with over 90% NO_x reduction are in operation, and a variety of design approaches are in use (16, 22).

1.3.4.1 Process description

In the SCR process, ammonia or an ammonia carrier is used as a reducing agents. Nitrogen oxide and ammonia react over the catalyst with high selectivity to nitrogen and water. The most common overall reaction is:

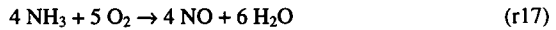
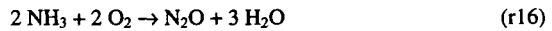
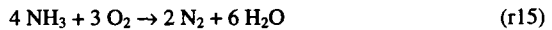


With varying flue gas compositions the overall SCR reactions are frequently written as:



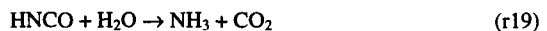
The SCR process is typically applied for flue gases with an excess of oxygen. Therefore, in many cases reaction r14 is not significant. In most flue gases, NO_x contains 90-95% NO and the NH_3 consumption is stoichiometrical to the NO_x reduction,

according to reaction r11 and r13. A change in the stoichiometry was observed by Kato et al. (23), if the NO_2/NO ratio was bigger than 1. For pure NO_2 in the feed gas the mole ratio of NH_3 to NO_2 was found to be about 1.3 (24), which is in accordance with the stoichiometry of reaction r12. Furthermore deviations from the stoichiometry can be caused by side reactions of NH_3 with O_2 . At high temperatures and in the presence of oxygen, ammonia can be oxidized directly to N_2 , N_2O and NO , according to reactions r15-r17.



The selective catalytic reduction of NO with NH_3 is very temperature sensitive, and the operating temperature differs for each class of catalyst material (see paragraph 1.3.4.2). The typical optimum temperature is between 550 K and 700 K.

Reducing agent. Commonly ammonia is used as reducing agent. The storage and transport of the toxic ammonia is problematical. Consequently, often urea is used in place of ammonia as reductant (25, 26). Urea is solid and less toxic than ammonia, which makes the storage and handling more easily. In the process it is dissolved in water and injected into the hot flue gas. The water evaporates and the urea decomposes at 440 K to ammonia and carbon dioxide. The reaction takes place in two steps, forming cyanuric acid as an intermediate, according to reactions r18 and r19.



Most other reducing agents are not suitable, because they react mainly with O_2 rather than with NO_x . Recently great research efforts were made to use hydrocarbons as

reductant (see paragraph 1.4.4), but the efficiency of this route is still too small for commercial application.

Catalyst Location. The catalytic unit can be placed in different positions (see Fig. 1-5 for the example of a coal fired power plant). The flue gas composition and temperature are the decisive criteria for the location. Generally we can distinguish between high dust, low dust and tail end location. All of them have advantages and disadvantages in comparison to each other. For a retrofit in most cases the tail end location is easier to realize, but a great disadvantage is that reheating of the flue gas is necessary. In a low dust case the flue gas is dust free and there are no erosion problems. But a hot gas precipitator is required, which is the main disadvantage for this location. The temperature at the high dust location is in the optimum range for most types of catalysts. Disadvantages are the erosion by the flue gas and poisoning, which cause a shorter catalyst life time.

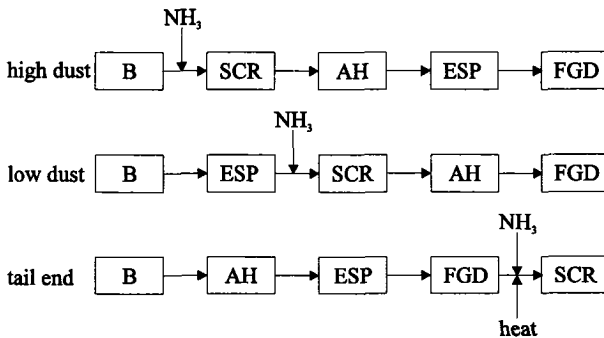


Figure 1-5. Position of catalyst (15)

B = boiler, AH = air preheater, ESP = electrostatic precipitator (or other particulate collector), SCR = selective catalytic reduction, FGD = flue gas desulfurization.

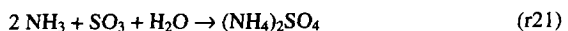
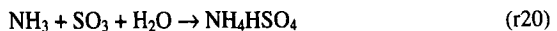
In the year 1990, in Europe 65% of the catalysts were installed at the high dust location and 35% at the tail end location. Only in Japan a significant number of plants equipped with high temperature precipitators are in use, because they need a higher flexibility due to large differences in their coal quality. Therefore they have 66% high dust SCR plants and 34% low dust applications (15).

Catalyst Geometry. The market of SCR plants is dominated by two types of catalyst geometries. Extruded and selfsupported honeycomb catalysts, in the form of squares or honeycombs, and plate type catalysts, which have a metal support covered with the active substance. The plate type catalysts have a higher resistance to erosion and deposition of dust particles than honeycomb catalysts and are often used for high dust installations. Honeycomb catalysts are used in all positions.

Catalyst Degradation. The lifetime of the catalyst dominates the cost of an SCR plant. Usually the replacement costs are higher than the operating costs. Different types of degradations limit the catalyst's lifetime. Important are poisoning, formation and deposition of solids, sintering and erosion.

Alkali ions poison the active sites of most SCR catalysts (27, 28). These elements are contained particularly in lignite and lubricants. Arsenic oxides have also been found to poison catalysts (27, 29, 30, 31) and selenium exhibits the similar poisoning effect as arsenic. If alumina is used as support, SO₂ can react with Al₂O₃ to aluminium sulfate leading to a deactivation of the catalyst (32, 33).

An other problem caused by SO_x is the formation and deposition of ammonium sulfates/sulfites which can plug the downstream process equipment (4). The formation of ammonium sulfates is a function of the flue gas temperature, the sulfur trioxide concentration and the ammonia concentration (see Fig. 1-6). SO₃ is formed by catalytic oxidation of SO₂ (34) and reacts with NH₃ and water (see r20 and r21).



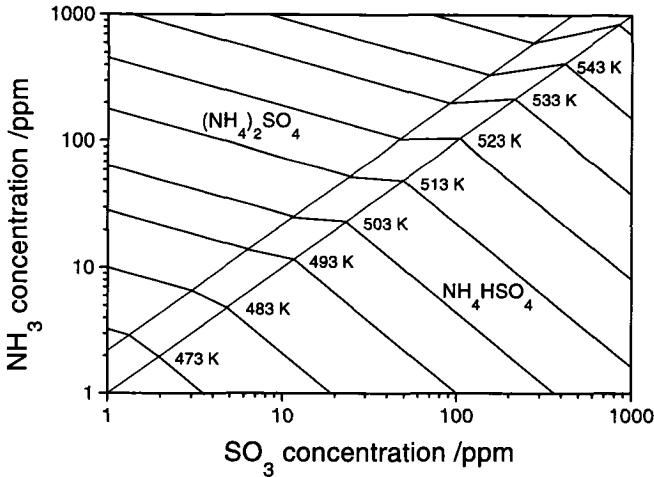
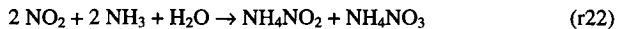


Figure 1-6. Equilibrium partial pressures of NH_3 and SO_3 for ammonium sulfate deposition

Below 480 K ammonium nitrate and nitrite can be formed homogeneously (see r22). Ammonium nitrate has a boiling point of 483 K and ammonium nitrite explodes at about 340 K (35). In some cases these solid salts lead also to problems in the downstream equipment.



Catalyst degradation by sintering occurs only at higher temperatures and reduces the specific surface and the dispersion of the catalytically active material. The pore size distribution is shifting to larger pores, but this will not have a great impact on the NO conversion, due to the diffusion limitation at higher temperatures. In this range, the conversion is proportional to the geometrical (external) surface (36).

Severe problems are caused by solid particles, which leads to physical damage of the catalysts. This reduces the catalyst's lifetime and toxic substances of the catalyst may get in the environment. An advantage of the abrasion is, that fresh catalyst is

always on the top of the surface and the activity remains constant over the whole catalyst's lifetime.

1.3.4.2 Types of catalysts

Titania supported Catalysts. Titanium oxide based catalysts with vanadium oxide and tungsten oxide as active components dominate the market for SCR catalysts. Titania is used in the form of anatase, because of the larger surface area of 50-120 m²/g in comparison to less than 10 m²/g for the rutile phase. The vanadia on titania catalysts with typically 1-5 wt.% V₂O₅ are mainly installed in medium temperature (550 - 700 K) applications. Above 700 K the direct ammonia oxidation is significant and decreases the selectivity to N₂ and H₂O. At 725-775 K the anatase phase of TiO₂ converts irreversibly to rutile and the activity decreases. For lower temperature applications higher vanadia contents are necessary for sufficient activity.

Platinum based Catalysts. In the low temperature range (450 - 525 K), Pt-based catalysts are used. Above 500 K significant amounts of N₂O are produced. Due to the narrow temperature window this type of catalyst is not commonly used today.

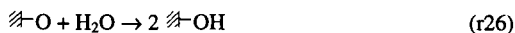
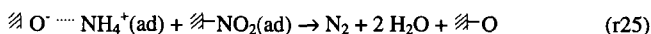
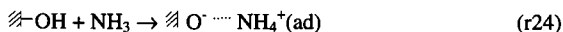
Zeolite Catalysts. In the high temperature range, above 650 K, zeolite catalysts are suitable for SCR. Commercially available zeolite catalysts for SCR can operate at temperatures till 800 K. Zeolite catalysts are manufactured in granular form and also as honeycomb type catalysts. No additional active substances are added in contrast to the catalysts used in SCR with hydrocarbons (see paragraph 1.4 and ref. 16). Zeolite catalysts for SCR is a German development and three SCR plants (3 x 35 MW) at Sandereuth power plant are in operation since 1987 (16).

Several other types of catalysts for example iron based catalysts and activated carbon are frequently used in commercial or test plants. A good overview covering most commercial catalysts and catalyst suppliers is given in reference 16.

1.3.4.3 Kinetics and Mechanisms for vanadia containing catalysts

Many mechanistic studies concerning the selective catalytic reduction of NO with NH₃ were carried out with vanadia based catalysts. Generally, mechanisms are based on a Langmuir-Hinshelwood reaction path involving adsorbed ammonia and nitric oxide or an Eley-Rideal reaction path with weakly bound or gas phase nitric oxide are assumed.

Langmuir-Hinshelwood mechanism. Based on IR-spectroscopy, mass-spectrometry, XPS measurements and kinetic studies under reaction conditions, Takagi et al. (37) postulated, that in the presence of oxygen, nitric oxide adsorbs in the form of NO₂(ad). In the absence of oxygen nitric oxide was not adsorbed on the vanadia surface. Oxygen was found to be essential for the reaction. They proposed that the reaction proceeds via the two adsorbates, NO₂(ad) and NH₄⁺(ad), which react on the catalyst surface through a Langmuir-Hinshelwood mechanism to form N₂ and H₂O according to reactions r23 - r26.



Eley-Rideal mechanism. In contrast to the postulated mechanism of Takagi et al., Inomata et al. (38) established the following mechanism for the selective catalytic reduction under dilute gas condition in the presence of oxygen: NH₃ is strongly adsorbed adjacent to V⁵⁺=O as NH₄⁺(ad), whereas NO is hardly adsorbed on the catalyst. Then, gaseous NO reacts with adsorbed NH₃, i.e., NH₄⁺(ad), to form N₂, H₂O, and V-OH. The V-OH species is reoxidized to V⁵⁺=O by either gaseous O₂ or bulk V⁵⁺=O species.

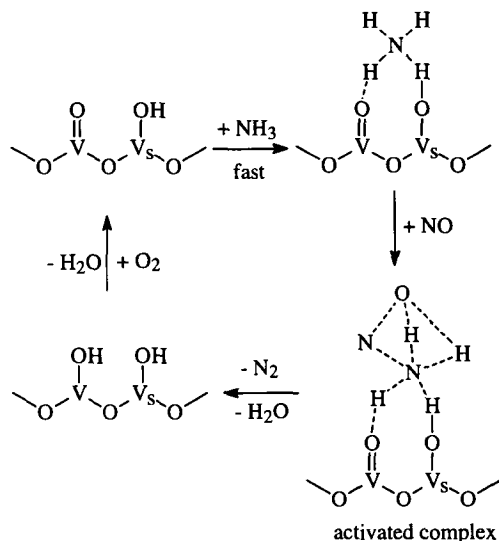


Figure 1-7. Mechanism of the NO-NH₃ reaction on the vanadium oxide catalyst in the presence of oxygen proposed by Inomata et al. (38).

Miyamoto et al. (39) investigated the mechanism by ¹⁵N tracers studies in a pulse reactor over V₂O₅, supported V₂O₅ and V₂O₄ catalysts. Their results supported the previously proposed mechanism in the presence of oxygen. In absence of oxygen the mechanism on the partly reduced vanadium oxide is almost the same. At first NH₃ is strongly adsorbed at the Brønsted acidic site, i.e., V_S-OH, on the surface of the V₂O₄ catalyst. Then, a gaseous NO attacks the adsorbed NH₃ to form N₂, H₂O, and a V-H species. The V-H species reacts readily with NO to form N₂O and H₂O, and vacant vanadium ion sites are produced. Although N₂O is formed by the reaction of NO with the V-H species a high selectivity to N₂ and H₂O can be achieved due to the successive reaction of N₂O with the V-H species leading to the formation of N₂ and H₂O.

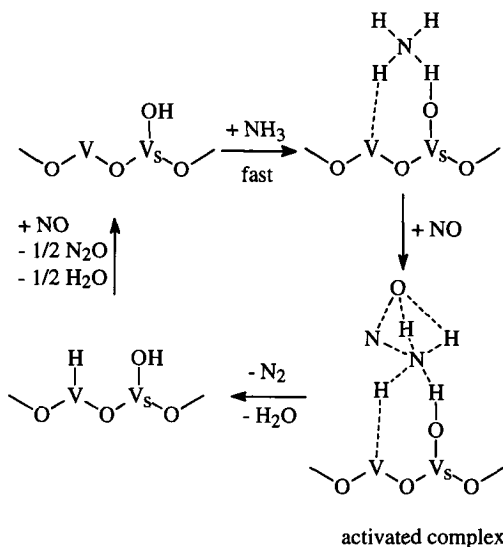


Figure 1-8. Mechanism of the NO-NH₃ reaction on the vanadium oxide catalyst in the absence of oxygen proposed by Myamoto et al. (39).

Janssen et al. (40) investigated the mechanism of the selective reduction of nitric oxide with ammonia in the presence of labeled oxygen over pure and supported vanadia catalysts. The results confirmed that lattice oxygen participates in the reaction. They proposed a participation based on a reduction/oxidation mechanism. Water was formed at two sites; the first part came from the reaction of gaseous nitric oxide and adsorbed ammonia via an Eley-Rideal mechanism and the other came from a surface dehydration process. They assumed that ammonia adsorbs differently on a group of two V=O sites and on a group of a V-OH site next to a V=O site. The adsorption on the group of a V-OH site next to a V=O site leads to the mechanism proposed by Inomata et al. (38), which is illustrated in Figure 1-7. On the other hand, they suggested that ammonia can adsorb dissociatively on two adjacent V=O sites, which involves breaking of the N-H

bond of ammonia. Until now, the proposed NH_2 species was not proved and remains speculative.

Recent investigations of vanadia-titania catalysts by *in situ* FTIR-spectroscopy (41, 42) and by the analysis of the microkinetic (43) supported the mechanism proposed by Inomata (38). The results of Topsøe (43) showed a direct correlation between the concentration of the Brønsted acid sites (associated with V-OH surface groups) and the NO_x conversion. No correlation was found for the Lewis acid sites, which were assumed by Janssen et al. (40) to be responsible for an alternative reaction path. But the V=O groups are also crucial for the catalytic activity. Topsøe found a weakening of the V=O bond, due to the NH_3 adsorption, and she proposed the formation of an activated complex by the partial transfer of H to the vanadyl group, in accordance to the reaction scheme proposed by Inomata (see Fig. 1-7). She proposed two separate catalytic function for the vanadia-titania catalyst. Figure 1-9 illustrates the two cycles of the acid and redox function of the catalyst, which are based on the same mechanism as proposed by Inomata.

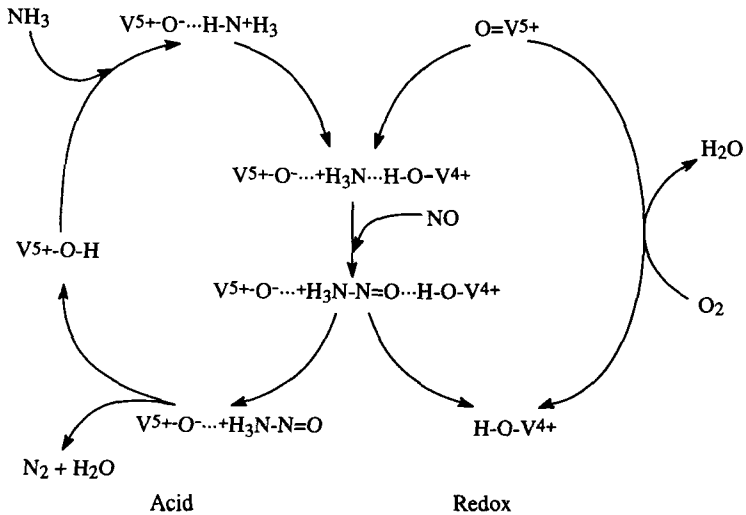
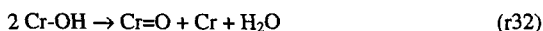
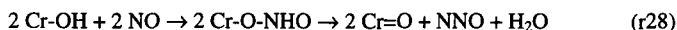


Figure 1-9. Catalytic cycles for the SCR reaction of NO by NH_3 over vanadia-titania catalysts in the presence of oxygen proposed by Topsøe (43).

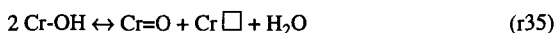
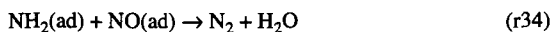
1.3.4.4 Kinetics and Mechanisms for chromia containing catalysts

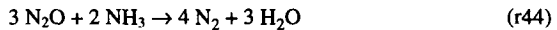
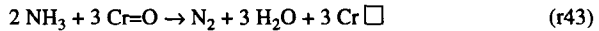
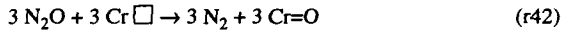
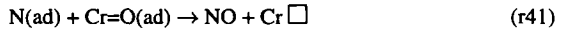
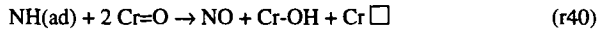
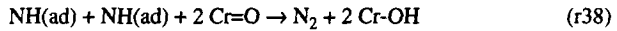
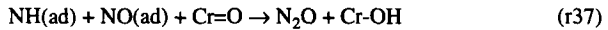
Besides investigations with vanadia containing catalysts, in this work chromia on titania catalysts were in the focus of our attention. In comparison to the numerous studies concerning vanadia based catalysts only few investigations were carried out for chromia containing catalysts.

Based on investigations of the kinetic behavior and isotope labeling studies Niyame et al. (44, 45) proposed a mechanism involving reactions r27 - r32. Due to the significant improvement in the catalytic activity by preoxidation; they suggested surface oxygen as the active site and proposed the formation of nitrous oxide via the reaction of two NO molecules or via the reaction of NO with NH₃



More recently, Duffy et al. (46) carried out activity studies and isotopic labeling experiments in the absence and presence of oxygen using amorphous and crystalline chromia catalysts. They studied the effect of water on the activity and selectivity and tentatively suggested a mechanism, according to reactions r33 -r44, which considers also the direct oxidation of ammonia and the reactions involving N₂O.





1.4 Research Frontiers

1.4.1 The direct decomposition of NO to its elements

The catalytic decomposition of NO_x into its elements in the presence of oxygen would be the ideal method for controlling NO_x emissions.



This reaction is thermodynamically strongly favored at temperatures below 1000 K. Despite the fact that numerous catalytic systems were investigated until now, no catalyst was found, which was able to overcome the kinetic barrier under lean exhaust conditions. Promising results were published by Iwamoto et al. (47, 48). They found that Cu exchanged zeolite catalysts decompose NO_x directly to N_2 and O_2 . With rising temperatures the reaction passes through a maximum at 750 - 850 K. Further studies by Li and Hall (49, 50) showed a strong inhibition by oxygen which decreases with rising temperatures. Water vapor inhibits reversibly the NO decomposition (51) and the presence of SO_2 completely poisons the active sites, requiring regeneration at higher temperatures. Due to the typical water concentration of combustion effluents in

the range of 5 - 15 %, an industrial implementation of this catalytic system is not possible. In spite of the setbacks the search for a suitable catalyst is still on because a NO_x decomposition catalyst which needs no reducing agent would be a breakthrough of tremendous ecological and economical importance.

1.4.2 New developments in the selective reduction of NO_x with NH_3

At present the selective catalytic reduction of nitrogen oxides with ammonia on vanadia/titania catalysts is the most frequently used catalytic technique to remove nitrogen oxides. Recently, main development efforts concern ammonia slip, improvement of the catalyst durability, the decrease of the SO_2 oxidation, pressure drop, the handling and storage of ammonia and the catalytic performance, especially in the lower temperature range (below 525 K).

To minimize the ammonia slip the NH_3 distribution system has to be improved by optimizing the NH_3 injection and the mixing section (52).

Poisoning and abrasion are the key factors which determine the durability of the catalyst. The influence of the catalyst location on the catalyst lifetime and the catalyst degradation by poisoning are described in paragraph 1.3.4.1. Most commercial catalysts contain additives like WO_3 or MoO_3 which increase the poison resistance but have also an impact on the catalyst's activity (53). Other additives are used to harden the surface and to improve the mechanical strength of the catalyst.

The oxidation of SO_2 is an undesired side reaction which is catalyzed by vanadia catalysts (5). The oxidation of SO_2 is slow in comparison to the reduction of NO with NH_3 and is only significant for the temperature range at which the selective catalytic reduction of NO with NH_3 is mass transfer controlled. In that case the NO conversion is proportional to the geometric surface whereas the oxidation of SO_2 to SO_3 uses the whole specific surface and is proportional to the mass of the catalyst (54, 55). A decrease in the SO_2 oxidation can be achieved by the development of thin-walled monoliths, by low vanadia loadings or by the addition of WO_3 .

Pressure drop caused by the down stream equipment after a turbine or a diesel engine can markedly affect the overall efficiency. To minimize the pressure drop the cross-sectional area of the catalyst and the wall thickness have to be optimized.

The problem of handling and storage of ammonia can be solved by the use of urea. But for a non stationary application the control of the NH_3 supply is difficult due to the dynamic behavior of the temperature and exhaust gas flow and the ammonia storage capacity of the catalyst. At the moment, a NH_3 metering system to avoid NH_3 slip which allows also a high conversion would be too complex and expensive for commercial applications in trucks or cars and needs further investigations.

An increase in the intrinsic activity can be achieved by optimizing the morphological and chemical properties of new catalysts. In the lower temperature range the widely used vanadia supported on titania catalyst exhibits a low activity and a slow dynamic behavior (56). Recently, catalytic systems based on pillared interlayered clays (57, 58), chromium oxides (59, 60), aerogels (61 - 63), activated carbon (64, 65) and grafted vanadia on titania (66) were investigated.

1.4.3 Using hydrocarbons as reducing agent

Since the last years, the use of hydrocarbons instead of ammonia or urea as reducing agents is in the focus of the research with regard to mobile applications such as diesel and lean-burn engines. Important drawbacks of ammonia as reductant are difficult handling, costs and ammonia slip.

The main development direction in the SCR with hydrocarbons is related to zeolitic catalysts (67). Among this group of catalysts, Cu-ZSM-5 is the most promising catalytic system. But the addition of water to the stream causes an instantaneous reversible deactivation effect. Furthermore catalysts based on acidic supports, such as alumina, silica-alumina or zirconia, doped with transition metals, have been found as another group of active catalysts for SCR applications. A major problem arising with all

the catalysts mentioned is the insufficient selectivity because the hydrocarbons are mainly burned by the oxygen present in the exhaust.

Although considerably research efforts are currently undertaken for the development of HC-SCR catalysts, a large gap remains to the practical realization due to numerous selectivity, inhibition and durability problems. In addition, recent investigations in our group revealed the formation of HCN and other harmful compounds over Cu-ZSM-5 and alumina catalysts in the selective catalytic reduction of nitrogen oxides by olefins which is a further severe hurdle for an industrial application (68 - 70).

1.5 Scope of the Thesis

The aim of this study was to develop novel catalytic systems for the selective catalytic reduction of NO with NH₃ with an improved activity, particularly in the low temperature range. From preliminary measurement with vanadia-titania aerogels (61, 62) and chromia on titania catalyst (60), we assumed a high potential of these catalytic systems, especially at low temperatures. These types of catalyst were not yet investigated under real SCR conditions. There was a lack of knowledge about the kinetic behavior, the long time stability and the resistance against poisoning.

The kinetic behavior in the low temperature range of a commercial vanadia based catalyst was studied and modeled in order to have a base for comparing the novel catalytic systems with that of catalysts reflecting the state of the art. The ultimate goal was to uncover possibilities to improve the structural and chemical properties of the novel catalysts under real SCR conditions.

1.6 References

1. Heinrich, D. and Hergt, M. "dtv-Atlas zur Ökologie", 2rd Ed., p 65, Deutscher Taschenbuch Verlag GmbH & Co. KG, München, 1991.
2. Singh, H. B. *Environ. Sci. Technol.* **21**, 320 (1897).
3. Cox, R. A. and Penkett, S. A. in: "Acid Deposition" (Beilke, S. and Elshout, A. J.), p 56, D. Reidel Publishing Co., Dordrecht, 1983.
4. Bosch, H. and Janssen, F. *Catalysis Today* **2**, 369 (1988).
5. Zeldovich, J. *Acta Physicochimica U.S.S.R.* **21**, 577 (1946).
6. Zeldovich, J. *Compt. Rend. Acad. Sci. U.S.S.R.* **51**, 217 (1946).
7. Fenimore, C. P. "13th Int. Symp. on Combustion, 1970, Pittsburgh", p 373, The Combustion Institute, Pittsburgh, 1971.
8. Fenimore, C. P. *Combust. Flame* **19**, 289 (1972).
9. CONCAWE 1989 "Trends in motor vehicle emissions and fuel consumption regulation - Special task force on assesment of trends in motor vehicle emission control", p 86, COCAWE, The Hague, Netherlands, 1989.
10. Bundesamt für Umwelt, Wald und Landschaft (BUWAL) in: "Schriftenreihe Umwelt: Vom Menschen verursachte Luftschadstoff-Emissionen in der Schweiz von 1900 bis 2010." Vol. **256**, BUWAL, Bern, Schweiz, 1995.
11. Bodenstein, M. *Z. Phys. Chem.* **100**, 68 (1922).
12. Hoigné, J. "Umweltchemie I", ETH, Zürich, Schweiz, 1990.
13. Roberts, J. M. *Atmospheric Environment* **24A**, 243 (1990).

14. Thurlow, G. in: "Technological Responses to the Greenhouse Effect" (The Watt Committee on Energy), Vol. 23, Elsevier Science Publishers LTD, London and New York, 1990.
15. IPCC Intergovernmental Panel on Climate. in: "Climate Change"(Houghton, J. T.; Jenkins, G. J. and Ephraums, J. J), Cambridge University Press, Cambridge, UK, 1990.
16. NDC in: "Nitrogen Oxides Control Technology Fact Book" (L. L. Sloss et al.), Noyes Data Corporation, Park Ridge, New Jersey U.S.A., 1992
17. Colannino, J. *Chemical Engineering* , 100 (1993).
18. Makansi, J. *Power* **11**, 11 (1993).
19. Wood, S. C. *Chem. Eng. Prog.* , 32 (1994).
20. Kasuya, F.; Glarborg, P.; Johnsson, J. E. and Dam-Johansen, K. *Chem. Eng. Sci.* **50**, 1455 (1995).
21. Engelhard Corporation Research and Development in: "Catalytic Air Pollution Control: Commercial Technology " (Heck, R. M. and Farrauto, R. J.), Van Nostrand Reinhold, New York, U.S.A., 1995.
22. Cho, S. M. *Chem. Eng. Prog.* , 39 (1994).
23. Kato, A.; Matsuda, S.; Kamo, T.; F.Nakajima; Kuroda, H. and Marita, T. *J. Phys. Chem.* **85**, 4099 (1981).
24. Odenbrand, C. U. I.; Andersson, L. A. H.; Brandin, J. G. M. and Lundin, S. T. *Appl. Catal.* **27**, 363 (1986).
25. Köbel, M.; Elsener, M. and Eicher, H. P. *BWK/TU/Umwelt/Special Luftreinhalung* , 3, E24 (1991).
26. Köbel, M. *VDI Berichte* **1019**, (1993).

27. Chen, J. "Preparation, characterization, and deactivation of the catalysts for the selective catalytic reduction of NO with NH₃.", Dissertation, Buffalo, U.S.A., 1993.
28. Chen, J. P. and Yang, R. T. *J. Catal.* **125**, 411 (1990).
29. Hums, E. and Spitznagel, G. W. *ACS Symposium Series* **587**, 42, (1995)
30. Hilbrig, F.; Göbel, H. E.; Knözinger, H.; Schmelz, H. and Lengeler, B. *J. Catal.* **129**, 168 (1991).
31. Gutberlet, H. *VGB Kraftwerkstechnik* **68**, 287 (1988).
32. Nam, I. S.; Eldridge, J. W. and Kittrell, J. R. *Ind. Eng. Chem. Prod. Res. Dev.* **25**, 192 (1986).
33. Vollenweider, J.; Eyres, A. and Holbrook, R. P. *Trans IMarE* **106**, 163 (1994).
34. Svachula, J.; Alemany, L. J.; Ferlazzo, N.; Forzatti, P. and Tronconi, E. *Ind. Eng. Chem. Res.* **32**, 826 (1993).
35. Weast, R. C et al. "Handbook of Chemistry and Physics", 67th Ed., CRC Press INC., Florida, U.S.A., 1987.
36. Prins, W. L. and Nuninga, Z. L. *Catalysis Today* **16**, 187 (1993).
37. Takagi, M.; Kawai, T.; Soma, M.; Onishi, T. and Tamaru, K. *J. Catal.* **50**, 441 (1977).
38. Inomata, M.; Miyamoto, A. and Murakami, Y. *J. Catal.* **62**, 140 (1980).
39. Miyamoto, A.; Kobayashi, K.; Inomata, M. and Murakami, Y. *J. Phys. Chem.* **86**, 2945 (1982).
40. Janssen, F. J. J. G.; v. den Kerkhof, F. M. G.; Bosch, H. and Ross, J. R. H. *J. Phys. Chem.* **91**, 5921 (1987).
41. Topsøe, N. -Y. *J. Catal.* **128**, 499 (1991).

42. Schneider, H.; Tschudin, S.; Schneider, M.; Wokaun, A.; Baiker, A.
J. Catal. **147**, 14 (1994).
43. Topsøe, N. -Y. *Science* **265**, 1217 (1994).
44. Niiyama, H.; Murata, K.; Ebitani, A. and Echigoya, E. *J. Catal.* **48**, 194 (1977).
45. Niiyama, H.; Murata, K. and Echigoya, E. *J. Catal.* **48**, 201 (1977).
46. Duffy, B. L.; Curry-Hyde, H. E.; Cant, N. W. and Nelson, P. F. *J. Catal.* **154**, 107 (1992).
47. Iwamoto, M.; Yokoo, S.; Sakai, S. and Kagawa, S. *J. Chem. Soc. Faraday Trans. 1*, 1629 (1981).
48. Iwamoto, M.; Furukawa, H.; Mine, Y.; Uemura, F.; Mikuriya, S. and Kagawa M., S. *J. Chem. Soc., Chem. Commun.* , 1272 (1986).
49. Li, Y. and Hall, W. K. *J. Phys. Chem.* **94**, 6145 (1990).
50. Li, Y. and Hall, W. K. *J. Catal.* **129**, 202 (1991).
51. Iwamoto, M.; Furakawa, M. and Kagawa, S. in: "New Developments in Zeolite Technology" (Murukami, Y.; Ijima, A.; Ward, J. W.), p 943, Elsevier, Amsterdam, 1988
52. Sulzer Brothers Limited, *The Chemical Engineer* **30**, 17 (1993).
53. Chen, J. P. and Yang, R. T. *Appl. Catal.* **80**, 135 (1992).
54. Binder-Begsteiger, I. *Catalysis Today* **27**, 3 (1996).
55. Beeckman, J. W. and Hegedus, L. L. *Ind. Eng. Chem.* **30**, 969 (1991).
56. Lowe, P. A. *ACS Symposium Series* **552**, 205, (1994).
57. Yang, R. T.; Chen, J. P.; Kikkinides, E. S. and Cheng, L. S. *Ind. Eng. Chem.* **31**, 1440 (1992).
58. Yang, R. T. and Li, W. *J. Catal.* **15**, 414 (1995).

59. Curry-Hyde, E. and Baiker, A. *Ind. Eng. Chem. Res.* **29**, 1985 (1990).
60. Engweiler, J.; Nickl, J.; Baiker, A.; Köhler, K.; Schläpfer, C. W. and von Zelewsky, A. *J. Catal.* **145**, 141 (1994).
61. Engweiler, J. and Baiker, A. *Appl. Catal. A: General* **120**, 187 (1994).
62. Schneider, M.; Maciejewski, M.; Tschudin, S.; Wokaun, A. and Baiker, A. *J. Catal.* **149**, 326 (1994).
63. Amiridis, M. D.; Na, B. K. and Ko, E. I. *ACS Symposium Series* **587**, 32, (1995).
64. Mochida, I.; Kawano, S.; Hironaka, M.; Yatsunami, S.; Korai, Y.; Matsumura, Y. and Yoshikawa, M. *Chem. Lett.* , 385 (1995).
65. Mochida, I.; Kawano, S.; Kisamori, S.; Fujitsu, H. and Maeda, T. *Carbon* **32**, 175 (1994).
66. Baiker, A. and Wokaun, A. *Naturwissenschaften* **76**, 168 (1989).
67. Shelef, M. *Chem. Rev.* **95**, 209 (1995).
68. Radtke, F.; Köppel, R. and Baiker, A. *J. Chem. Soc., Chem. Commun.* , 427 (1995).
69. Radtke, F.; Köppel, R. and Baiker, A. *Env. Sci. & Techn.* **29**, 2703 (1995).
70. Radtke, F.; Köppel, R. and Baiker, A. *Catal. Lett.* **28**, 131 (1994).

Leer - Vide - Empty

Experimental

2.1 Apparatus

Catalytic tests were carried out in a fully computer controlled apparatus equipped with a continuous tubular fixed-bed microreactor. A process flow diagram of the reactor system is shown in Figure 2-1. The flows of the individual reactant gases were controlled by means of mass flow controllers (MFC) and mixed in a hot box (thermostated at 413 K). Water was fed by a step-motor pump and evaporated into the preheated feed stream through a micro capillary. The reaction gas mixture employed in kinetic experiments consisted of 0-1000 ppm NO (99.0%, PanGas), 0-1000 ppm NH₃ (5% NH₃ (99.98%) in N₂ (99.999%), CarbaGas), 0-10% H₂O (bidest.), 0-15% O₂ (99.995%, PanGas), 0-10% CO₂ (99.99%, PanGas) and 0-90 ppm SO₂ (15% SO₂ (99.98%) in N₂ (99.999%), PanGas) in N₂-balance (99.995% PanGas). The conversion of NO to NO₂ in the gas mixing unit was less than 3 % as evidenced by measurements with an empty reactor. Fast responding 3-way solenoid valves allowed rapid changes in the concentrations of O₂, NH₃ and NO. The maximum adjustable gas flow was 25 L (NTP)/min. A bypass controlled by an additional MFC was used for gas flow rates up to 1000 ml(NTP)/min. To avoid condensation in the system, all tubings after the hot box

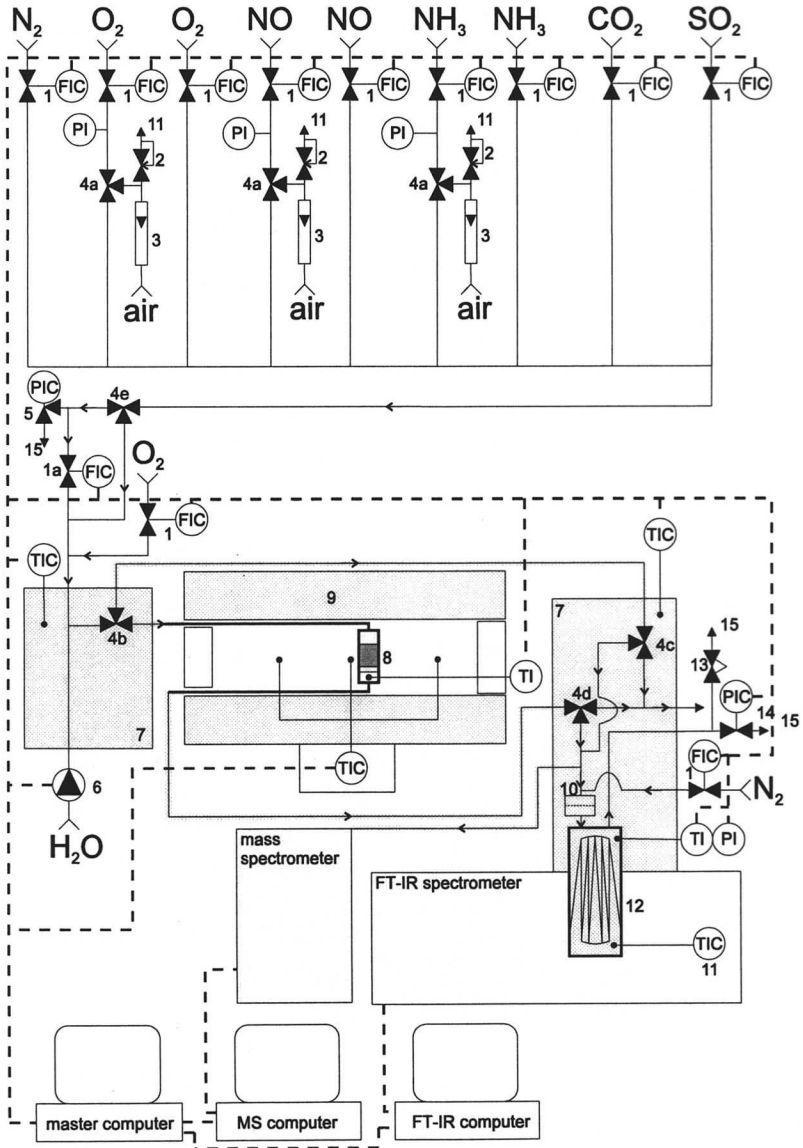


Figure 2-1. Apparatus used for the catalytic tests.

1. mass flow controller, 2. valve to equalize back pressure, 3. rotameter for fine adjusting the back pressure, 4a. solenoid valve for rapid changes in concentration, 4b. pneumatic ball valve to bypass the reactor, 4c-d. pneumatic ball valves to bypass the gas cell, 4e. ball valve to adjust flow rates below 1000 ml(NTP)/min, 5. relief pressure controller, 6. step-motor pump, 7. thermostated box (413 K), 8. fixed bed reactor, 9. tubular furnace, 10. filter (2 μm), 11. digital temperature controller, 12. long path gas cell, 13. safety relief valve, 14. back pressure controller, 15. vent.

were heated at 413 K. The resulting gas stream could either be directed to the reactor or to the analysis system by means of a pneumatic ball valve. Before entering the reactor, the gas mixture was heated to reaction temperature in the first part of the tubular furnace. The quartz glass reactor with an inner diameter of 7.5 mm was placed in the middle of the heated section. The catalyst powder was placed on a porous quartz filter and the free space over the catalyst bed was filled with quartz wool to prevent a radial velocity profile in the bed. The pressure in the reactor was kept constant at $1.1 \cdot 10^5$ Pa for all experiments by an electronic pressure controller.

2.2 Analysis

The temperature of the reactor effluent was adjusted to 413 K in a second hot box and the product stream was then either directed to the analysis system or to the purge. A filter (Nupro 2 μm) prevented solid particles from entering the analysis system, which consisted of a Fourier transform infrared (FT-IR) spectrometer (Perkin Elmer System 2000) and a quadrupole mass spectrometer (GAM 400 Balzers). The FT-IR spectrometer was equipped with a multiple pass gas cell operated at 415 K (Infrared Analysis, 100 ml volume, 2.4 m path length) and a liquid nitrogen cooled MCT detector. The pressure in the gas cell was measured by a pressure transducer (Haenni ED 513). O_2 and N_2 were measured with the mass spectrometer using the QuadStar+ software by Balzers (1), whereas NO , NO_2 , N_2O , NH_3 , SO_2 , CO_2 , CO and H_2O were analyzed by FT-IR spectroscopy. For each spectrum 350 scans with a resolution of 2 cm^{-1} were taken. After each measurement the gas cell was purged with nitrogen and a reference spectrum was taken. For calibration two sets of spectra (one for water concentrations below 2%) of specially prepared gas mixtures were recorded for each component. Based on the characteristic absorption frequencies of the different compounds (see Table 2-1) the spectral ranges specified in Table 2-2 were used for quantification. The software package QUANT+ by Perkin Elmer, which is based on a partial least square method, was used to calculate the concentrations of the feed and effluent gases (2, 3). The accuracy in the concentration measurements was within $\pm 5\%$ for FT-IR spectroscopy and within $\pm 2\%$ for mass spectroscopy, respectively, as evidenced by measurements with calibration gas mixtures.

Table 2-1. Components measured by FT-IR spectroscopy.

Component	Location of bands or lines (cm^{-1})	Comments
H ₂ O	Almost everywhere in the spectrum	Interferes with detection of nearly everything else.
CO ₂	2400 - 2200, 2077, 741	
CO	2250 -2040	Small amounts of CO (<300 ppm) are difficult to detect if N ₂ O or CO ₂ (>5%) are present.
NO	1960 - 1780, 1875 (Q branch)	Interference with water.
NO ₂	2920, 1629, 1595	Strong bands at 1620 cm^{-1} and 1595 cm^{-1} , which are obscured by water and a weaker one at 2920 cm^{-1} with no interference with water.
N ₂ O	2581, 2238, 2214, 1302, 1271	Interference with CO ₂ around 2220 cm^{-1} and with water around 1280 cm^{-1} , weak band at 2581 cm^{-1} .
NH ₃	3500 - 3200, 1800 -1400, 1250-700	Strong bands at 967 cm^{-1} and 931 cm^{-1} , which have little interference with water.
SO ₂	1374, 1361, 1344	Interference with water.

Table 2-2. Spectral Regions used for Quantification.

method 1. 0-2000 ppm H ₂ O [cm ⁻¹]	method 2. 0.2 - 10 % H ₂ O [cm ⁻¹]
2230-2093	2945-2830
1920-1873	2300-2165
1610-1580	2155-2145
1546-1400	2110-2093
1360-1342	1920-1873
978-900	1610-1580
750-730	1360-730

2.3 Kinetic Modeling

The model parameters were estimated from the experimental data by linear and non-linear regression analysis (4, 5, 6). For the non-linear regression analysis the simulation software "Simusolv™" (version 3.0-120, Dow Chemical Company) was used (7). As objective function the maximum likelihood of the partial pressures of the relevant gases was chosen (8). The used simulation software maximized the Log Likelihood Function (LLF, equation 2-1), which is equivalent to maximizing the Likelihood Function itself. The Likelihood Function is based on the assumptions that replicated experimental measurements result in values which are normally distributed and that the errors in the

measured values are independent of each other. In the used Simusolv™ version the number of estimated parameters was not taken into consideration by the estimation of the standard deviation s (equation 2-2).

$$LLF = \Phi = -\frac{n}{2} \left(\ln(2\Pi) + 1 + \ln \left(\frac{\sum_{i=1}^n (z_i - f_i)^2}{n} \right) \right) \quad (2-1)$$

$$s^2 = \frac{\sum_{i=1}^n (z_i - f_i)^2}{n} \quad (2-2)$$

In practice, the experimental error involves an absolute error and an error relative to the magnitude of the measured value. In the used software, the degree of dependence of s is taken into consideration by an adjustable parameter γ , called the heteroscedasticity parameter. The modified standard deviation of the observation i is given by the square root of equation 2-3 and the objective function is expressed by equation 2-4. The parameter γ is optimized in the range of 0 - 2 together with the other adjustable parameters. If γ is zero, maximizing the Φ is equivalent to maximizing the sum of squares of the residuals, and the objective function is controlled by the residuals for the high value of the variables. Even large relative errors in the small values will have very little influence. In contrast, if γ is 2, the relative errors or residuals are important in determining the Φ . Thus the small values of the variables are just as influential in controlling the objective function as the large ones.

$$s^2 = f_i^\gamma \left(\frac{1}{n} \sum_{i=1}^n \frac{(z_i - f_i)^2}{f_i^\gamma} \right) \quad (2-3)$$

$$\Phi = -\frac{n}{2} (\ln(2\pi) + 1) - \frac{n}{2} \ln \left(\frac{1}{n} \sum_{i=1}^n \left(\frac{(z_i - f_i)^2}{f_i^\gamma} \right) \right) - \frac{\gamma}{2} \sum_{i=1}^n \ln(f_i) \quad (2-4)$$

The modified LLF was used if the data, involved in the model, varied over a wide range, else the obtained value for γ was zero or near by zero. In this case the LLF according to equation 2-1 was applied.

The discrimination between different models and the judging of the significance of the model parameters were made using the LLF and variance analysis. The F-test was carried out with a significance level of $\alpha=0.05$ and if several models were not rejected due to the F-test, the model with fewer adjustable parameters was chosen. The standard deviation of the experimental error σ (equation 2-5, 9) was determined separately for both calibration ranges (see paragraph 2.2), because the experimental error of the concentration measurement was strongly influenced by the water concentration. If the parameter estimation included data with water concentration above 2%, always the estimated standard deviation of the experimental error for the calibration range over 2% water was applied.

$$\sigma^2 = \frac{\sum_{j=1}^n (z_j - \bar{z})^2}{n-1} \quad (2-5)$$

The standard deviation of the estimated parameters was given by the square root of the diagonal element of the variance-covariance matrix, which was estimated by the inverse of the Hessian matrix. The Hessian matrix is defined as the matrix of second partial derivatives of the LLF with respect to each pair of parameters. In the applied software the Gauss approximation to the Hessian was used.

The fourth-order Runge-Kutta method (10) was used for the numerical integration and the procedure of Nelder-Mead direct search method (11) for maximizing the objective function.

2.4 Notation

LLF	= Logarithm of the Likelihood function
Φ	= objective function
n	= number of measurements
z	= measured partial pressure, Pa
\bar{z}	= average value of the measured partial pressure, Pa
f	= predicted partial pressure, Pa
s	= estimated standard deviation of the model prediction, Pa
γ	= heteroscedasticity parameter
σ	= estimated standard deviation of the experimental error, Pa
i	= ith data point
j	= jth measurement of a data point

2.5 References

1. Balzers AG, "User's Guide QUADSTAR PLUS V 3.0", Balzers, FL, 1990.
2. Perkin-Elmer Ltd., "Quant+ User' Guide", Beaconsfield, UK, 1992.
3. Griffiths P. R. and de Haseth J. A., "Fourier Transform Infrared Spectrometry", John Wiley & Sons, Inc., New York, U.S.A., 1986.
4. Bard, Y., "Nonlinear Parameter Estimation", Academic Press, Inc., Orlando, U.S.A., 1974.
5. Ratkowsky, D. A., "Nonlinear Regression Modeling", Marcel Dekker, Inc., New York, U.S.A., 1983.
6. Seber, G. A. F. and Wild, C. J., "Nonlinear Regression", John Wiley & Sons, Inc., New York, U.S.A., 1989.
7. The Dow Chemical Company, "Simusolv Reference Guide", Midland, U.S.A., 1989.
8. Edwards, A. W. F., "Likelihood", Cambridge University Press, Cambridge, 1987.
9. Ineichen, R., "Stochastik", 6. Aufl., p. 19, Raeber Verlag, Luzern und Stuttgart, 1984.
10. Collatz, L., "Numerische Behandlung von Differentialgleichungen", 2. Aufl., Springer, Berlin-Heidelberg-New York, 1955.
11. Nelder, J. A. and Mead, R. A., *Comp. J.*, 7, 308 (1965).

Vanadia-based commercial catalyst: Analysis and modeling of the kinetics

Abstract

The kinetics of the selective catalytic reduction of nitric oxide by ammonia have been investigated over a vanadia-based commercial DeNO_x-catalyst. For temperatures exceeding 473 K the kinetic data are described well with a model which is based on an Eley-Rideal mechanism. Below 473 K the conversion is higher than predicted with this model, probably due to the contribution of an additional reaction pathway, which occurs only at low temperatures. Regarding the influence of water and oxygen on SCR, O₂ accelerated and H₂O decreased the reaction rate. The addition of up to 2% H₂O to the dry feed notably reduced the rate of NO conversion. The effect levels off for higher H₂O concentrations, and between 2.5% and 7.5% H₂O no significant dependence was perceptible. Similarly, the conversion of NO is almost independent on O₂ for concentrations between 4% and 10%. Lower oxygen concentrations resulted in a marked decrease of the catalytic activity. The estimated activation energies for the dry and wet feed amounted to 87 kJ/mol ± 3 kJ/mol and 99 kJ/mol ± 9 kJ/mol, respectively (95% confidence limits).

3.1 Introduction

In paragraph 1.3 it was mentioned that the selective catalytic reduction (SCR) by ammonia is the most widely employed technique for the removal of NO_x from stationary combustion sources. Several kinetic and mechanistic studies for vanadia containing catalysts are published in the literature (1). Some of them have been performed on the basis of empirical power-law rate equations (2-4). For a well defined catalyst and with no variation of the experimental parameters an empirical model is sufficient for the reactor design (5), but the determined kinetic parameters have limited physical or chemical background and are not suitable for being used in a wide experimental range. Including mechanistic information in the kinetic approach usually results in more global models. Most of them are based on an Eley-Rideal or a Langmuir-Hinshelwood mechanism (see paragraph 1.3.4.3). On the basis of IR an Eley-Rideal type mechanism involving gaseous or weakly adsorbed nitric oxide and ammonia adsorbed as NH_4^+ was proposed by Inomata et al. (6) and Miyamoto et al. (7). Janssen et al. (8) further supported this mechanism by transient isotopic studies with labeled oxygen and Gasior et al. (9) found from IR and XPS measurements that the reaction proceeds via participation of ammonia adsorbed on Brønsted acid sites. In contrast, a Langmuir-Hinshelwood type mechanism involving NO adsorbed as NO_2 and ammonia adsorbed as NH_4^+ was favored by Takagi et al. (10). Smak et al. (11) concluded from TPR/TPD studies that depending on the reaction conditions both reaction mechanisms are effective for the SCR of NO_x and proposed an activation energy, amounting to about 84 kJ/mol, independent of the reaction mechanism. Under typical SCR reaction conditions the Eley-

Rideal mechanism was expected to be dominant. The adsorption of NO under reducing conditions was also proposed by other groups (12, 13). Recently, Tufano and Turco (14) reported an underestimation of the NO_x conversion at lower temperatures. The authors postulated a reaction mechanism involving the formation of a relatively stable nitrosamidic intermediate. The resulting rate equation is similar to the equations based on the assumption of a Langmuir type adsorption of NO.

The most studies of the intrinsic kinetics in the selective catalytic reduction of NO with NH₃ were carried out for temperatures above 573 K (15-17). In practice, using honeycomb or plate type catalysts, the kinetics in this temperature range are usually determined by mass transfer limitation. Only in low temperature applications is the overall reaction rate dominated by the intrinsic kinetic. In order to explore the kinetic behavior in the relevant temperature range, we have first studied systematically the influence of all important exhaust components on the kinetics and developed a model for temperatures below 573 K. Additionally the results of the commercial catalyst were used as a reference for subsequent experiments with catalysts designed in our laboratory.

3.2 Experimental

A commercial catalyst (ZERONOX[®], Katalysatorwerke Hüls GmbH) containing: TiO₂ (>70%), V₂O₅, WO₃ and MoO₃ was used. In industrial applications the catalyst is used in the form of honeycombs. The BET surface area determined by N₂-physisorption at 77 K using a Micrometrics ASAP 2000 instrument amounted to 55 m²/g_{catalyst}. Before the tests the catalyst was crushed and calcined for 2h at 623 K in a flow of 20% oxygen (99.995%, PanGas) in nitrogen (99.995% PanGas). This pretreatment was repeated at the

start of each test series. With this conditioning it was possible to obtain reproducible activity measurements and no activation or deactivation phenomenon was perceptible. The catalytic studies were carried out in the continuous tubular fixed-bed microreactor described in paragraph 2.1. The steady-state was established for all measurements. The reaction gas mixture consisted of 1000 ppm NO (99.0%, PanGas), 300-1000 ppm NH₃ (99.98%, PanGas), 0-7.5% H₂O (bidest.), 0-11.5% O₂ (99.995%, PanGas), 0-10% CO₂ (99.99%, PanGas) and 0-90 ppm SO₂ (15% SO₂ (99.98%) in N₂ (99.999%), PanGas) in N₂-balance (99.995% PanGas). Standard experiments were carried out using 0.4 g of catalyst (180-300 μm sieve fraction) and a reactant flow rate of 200-1000 ml (NTP) min⁻¹ (60'000-300'000 h⁻¹ (NTP) GHSV) at a constant pressure of 1.1 bar in the temperature range 393-563 K. The model parameters were estimated from the experimental data by linear and non-linear regression analysis as described in paragraph 2.3. As objective function the maximum likelihood of the NO partial pressure was chosen.

3.3 Results

3.3.1 Mass and heat transfer

The small particle size (180 - 300 μm) in comparison to the reactor diameter (7.5 mm) prevented significant bypassing along the walls. The quartz wool plug on top of the catalyst bed ensured that no radial gas velocity profil was established. This experimental set up let us assume that plug flow was established over the whole catalyst bed, which was additionally confirmed by measurements with varying the catalyst bed height. Theoretical calculations using the criterion of Weisz and Prater (18) indicated that no internal mass transfer limitation occurred in the investigated temperature range.

Experiments with larger catalyst particle sizes (300 - 500 μm) showed no influence on the catalytic behavior and confirmed the results of the theoretical calculations. The calculated maximum adiabatic temperature rise for a feed containing 1000 ppm NO was about 13 K. The measured experimental temperature raise over the catalyst bed for full conversion at the highest space velocity amounted to 1.5 K. Because of the small particle size and the small temperature increase, no significant temperature gradients in the catalyst bed and in the catalyst particles had to be taken into account.

3.3.2 Catalyst stability

No significant deactivation was perceptible during 24 hours time on stream. If the catalyst was not calcinated before the tests (see paragraph 3.2), the catalyst exhibited a lower activity at the beginning of the measurements. Within several hours the activity of the uncalcinated catalyst approach the activity of the calcinated sample by exposing it to the SCR feed stream. The velocity of this process depends on the oxygen concentration, the catalyst temperature and the water concentration. In the practice the observed lifetime of the catalyst, during which no significant deactivation is observed, amounts to 2-4 years.

3.3.3 Influence of space velocity

Figure 3-1 shows the conversion of NO versus increasing catalyst weight per gas flow (W/F) for temperatures in the range 473-513 K. With raising temperature the influence of space velocity on NO conversion increases. The measured conversions are in good accordance with the simulated conversions based on the model described in

paragraph 3.3.8. Integral analysis of the data also showed that a first order kinetic in NO describes the experimental behavior properly.

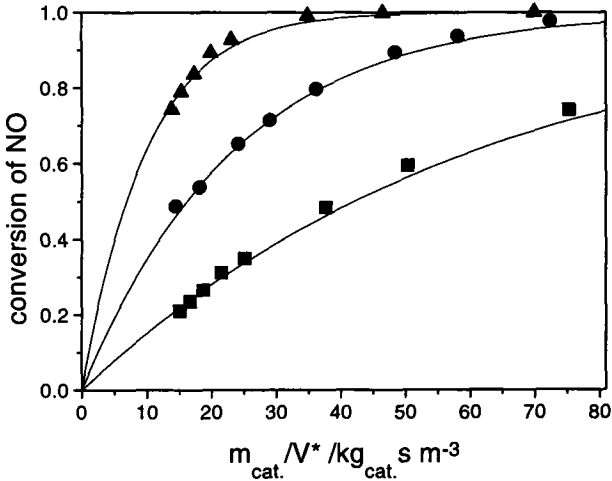


Figure 3-1. The influence of the gas flow per catalyst weight on the conversion.

■ 473 K, ● 493 K, ▲ 513 K, — simulated. Feed: 10% O₂, 1000ppm NO, 1000ppm NH₃, balance N₂, flow rate = 200-1000 ml(NTP)/min, catalysts weight = 0.4 g.

3.3.4 Influence of water

Without water in the feed the catalyst showed high activity for the reduction of NO even at low temperatures as emerges from Figure 3-2. Addition of 2.5% water significantly reduced the activity. Similar behavior of vanadia/titania catalysts is described by other authors (19-22). The authors observed an inhibition by water below 653 K and a decrease of the conversion of NO above this temperature. Figure 3-2 also shows that a further increase of the amount of H₂O up to 7.5% resulted in no measurable loss of activity, indicating that NO conversion is almost independent of the H₂O concentration

under practical SCR conditions (5-15% H₂O). Measured activation energies for the dry and wet feed amounted to 87 kJ/mol \pm 3 kJ/mol and 99 kJ/mol \pm 9 kJ/mol, respectively (95% confidence limits).

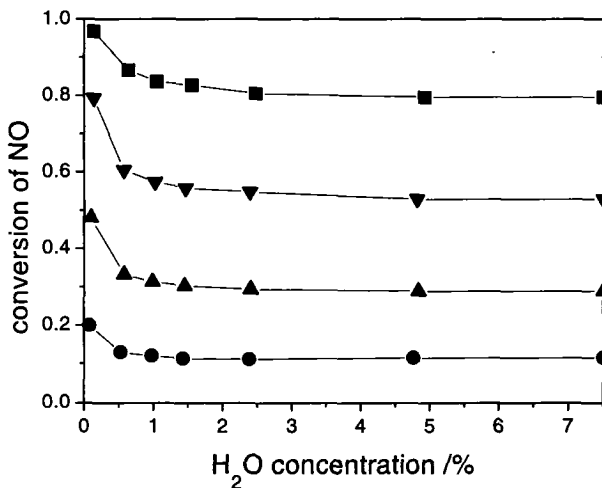


Figure 3-2 Conversion of NO versus H₂O concentration in the feed.

● 463 K, ▲ 483 K, ▼ 500 K, ■ 520 K. Feed: 10% O₂, 1000 ppm NO, 1000 ppm NH₃, 0%-7.5% H₂O, balance N₂, flow rate = 500 ml(NTP)/min.

3.3.5 Influence of oxygen

The oxygen concentration was varied in the range 0%-11.5%. Without oxygen in the feed the reaction rate was almost completely suppressed in the investigated temperature range of 473-533 K. Low oxygen concentrations were sufficient to maintain the activity of the catalyst. A further increase in oxygen concentration over 4% enhanced the reaction rate only slightly (see Fig. 3-3).

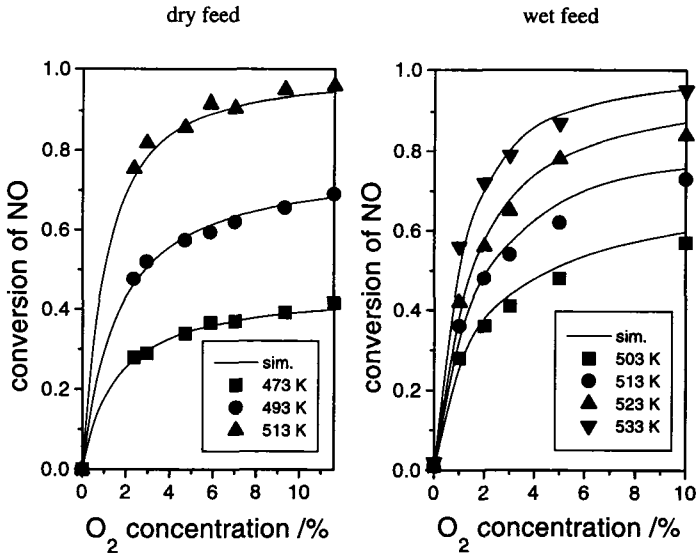


Figure 3-3. Conversion of NO versus oxygen concentration for dry and wet feed.
 Feed: 0-11.5% O₂, 1000 ppm NO, 1000 ppm NH₃, 0% , resp. 5% H₂O,
 balance N₂, flow rate: 430 ml/min(NTP) dry feed, 500 ml(NTP)/min wet
 feed.

3.3.6 Influence of ammonia

The influence of ammonia on the kinetic behavior was investigated for feed concentration between 300 and 1000 ppm NH₃. No change in the conversion rate of NO was observed by varying the ammonia concentration. The conversion of NO and NH₃ versus the reaction temperature with 300 or 1000 ppm NH₃ in the feed is depicted in Figure 3-4. The deviations of the NO conversion to the model (will be described in paragraph 3.3.8) were always in the experimental error. Good fitting of the model

prediction with the experimental NH_3 conversion was achieved for a NH_3 feed concentrations of 300 ppm as well as 1000 ppm.

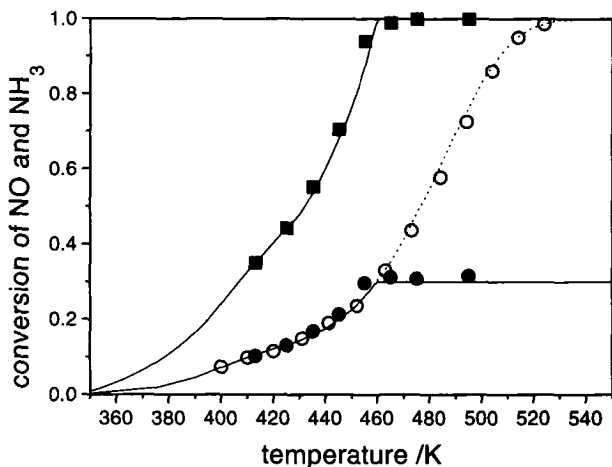


Figure 3-4. Conversion of NO and NH_3 versus temperatures for different ammonia feed concentrations.

○ measured and simulated NO conversion for a feed with 1000 ppm NH_3 , ■ NH_3 conversion, ● NO conversion and — simulated conversions for a feed with 300 ppm NH_3 . Feed composition: 10% O_2 , 1000 ppm NO, 1000 or 300 ppm NH_3 , balance N_2 , flow rate = 430 ml(NTP)/min.

3.3.7 Influence of SO_2 .

Exposing the catalyst alternately to a SO_2 free feed and to a feed containing increasing concentrations of SO_2 , respectively, at 523 K (Fig. 3-5) indicated no

poisoning or deactivation. Additionally no significant amounts of SO_3 were detected. The variation of the NO conversion in the experiment was always in the experimental error.

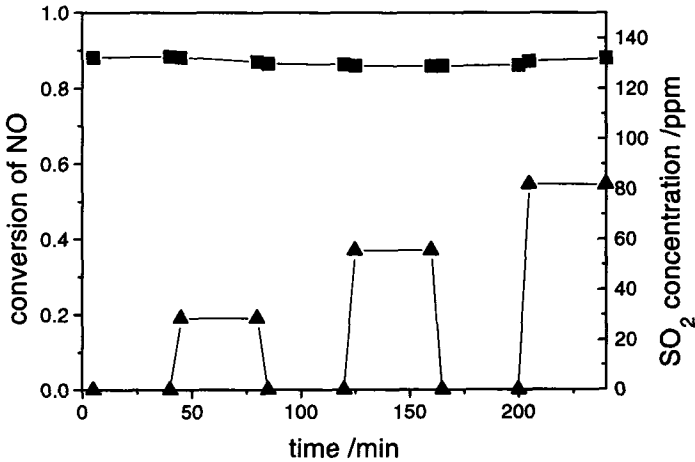
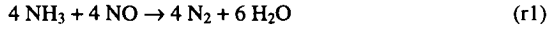


Figure 3-5. Influence of SO_2 on the NO conversion.

■ NO conversion, ▲ SO_2 concentration. Feed: 10% O_2 , 1000 ppm NO, 1000 ppm NH_3 , 5% H_2O , 0-80 ppm SO_2 and balance N_2 , reactor temperature = 523 K, flow rate = 430 ml(NTP)/min.

3.3.8 Kinetic modeling

The kinetic model was based on the reaction stoichiometry shown in equation r1. The selectivity to N_2 and H_2O was higher than 99 % in all experiments. There was no significant impact of carbon dioxide and sulfur dioxide on the reaction rate observable. Consequently, no side reaction had to be taken into account.



Different kinetic equations were investigated. The best description of the experimental data was obtained with the following approach. For temperatures exceeding 473 K the catalytic behavior could be described well with a kinetic rate expression first order with respect to nitric oxide and zeroth order with respect to ammonia. The influence of oxygen was taken into account with a Langmuir adsorption isotherm expression, at which the isotherm is normalized to 10% oxygen in the exhaust gas to allow an independent estimation of k_1 (see equation 3-1). For temperatures below 473 K a significant deviation was perceptible in the case of dry feed. In this temperature range the kinetics could only be properly described by accounting for an additional reaction pathway following a Langmuir-type mechanism (see equation 3-2). For wet feed, the conversion was low in that temperature range and no significant deviation was observable.

$$r_1 = k_1 p_{\text{NO}} \frac{\frac{K_{\text{O}_2} p_{\text{O}_2}}{1 + K_{\text{O}_2} p_{\text{O}_2}}}{\frac{K_{\text{O}_2} p_{\text{O}_2|10\%}}{1 + K_{\text{O}_2} p_{\text{O}_2|10\%}}} \quad (3-1)$$

$$r_2 = k_2 \frac{K_{\text{NO}} p_{\text{NO}}}{1 + K_{\text{NO}} p_{\text{NO}}} \frac{\frac{K_{\text{O}_2} p_{\text{O}_2}}{1 + K_{\text{O}_2} p_{\text{O}_2}}}{\frac{K_{\text{O}_2} p_{\text{O}_2|10\%}}{1 + K_{\text{O}_2} p_{\text{O}_2|10\%}}} \quad (3-2)$$

In order to reduce the correlation between pre-exponential factor (k_i^0 , K_A^0), the activation energy (E_{Ai}), and the enthalpy of adsorption (ΔH_A), respectively, the reaction rate constant (k_i , equation 3-3) and the equilibrium constant of adsorption (K_A , equation 3-4) were expressed as proposed by Himmelblau (23).

$$k_i(T) = k_i^0(T_{Ref.}) \exp\left(\frac{-E_{Ai}}{R} \left(\frac{1}{T} - \frac{1}{T_{Ref.}}\right)\right) \quad (3-3)$$

$$K_A(T) = K_A^0(T_{Ref.}) \exp\left(\frac{-\Delta H_A}{R} \left(\frac{1}{T} - \frac{1}{T_{Ref.}}\right)\right); T_{Ref.} = 500K \quad (3-4)$$

Under dry conditions the simulations were carried out with the same activation energy of 87.4 kJ/mol for both reaction paths. With this approach it was possible to estimate the reaction rate constants k_i independent of the other kinetic parameters and to prevent a correlation between the estimated values of k_i and the adsorption equilibrium constants of oxygen and nitric oxide, respectively. Under wet conditions (more than 2.5% H_2O in the feed), the Eley-Rideal reaction path was dominant for the temperature range investigated (363-463 K) and the simulations were performed with an activation energy of 98.5 kJ/mol.

The temperature dependence of k_i and K_{O_2} are shown in the linearized form in Figure 3-6. For the kinetics under wet conditions only the data over 473 K were used for the linear regression. The Arrhenius-type plot shown in Figure 3-6 demonstrates well the deviation below 473 K. All the model parameters estimates are listed in Table 3-1.

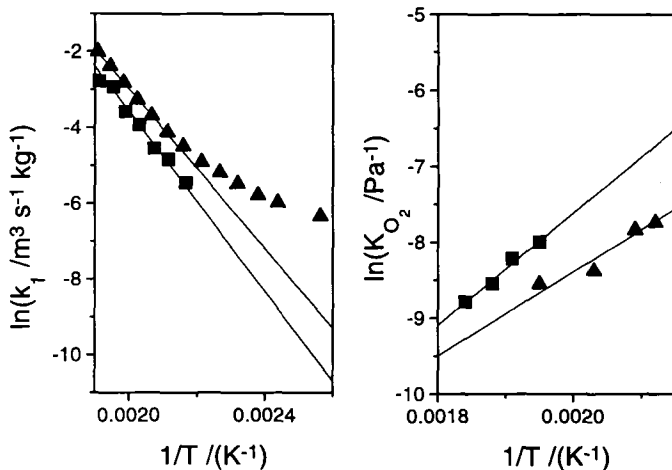


Figure 3-6. Temperature dependency of k_1 and K_{O_2} for dry and wet feed.

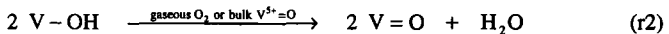
▲ 0% H₂O, ■ 5% H₂O, — simulated. Feed: 10% O₂, resp. 0-11.5%,
1000 ppm NO, 1000 ppm NH₃, balance N₂.

Table 3-1. Model parameters

	units	feed without H ₂ O	standard deviation	H ₂ O conc. >2.5%	standard deviation
$k_1^0(T_{Ref.})$	m ³ /kg s	5.05E-2	6.9E-4	2.79E-2	8.1E-4
E_{A1}	J/mol	87400	1490	98700	4450
$k_2^0(T_{Ref.})$	Pa m ³ /kg	47	32	—	—
E_{A2}	J/mol	87400	—	—	—
$K_{O_2}^0(T_{Ref.})$	Pa ⁻¹	2.27E-4	1.7E-6	4.93E-4	2.21E-6
ΔH_{O_2}	J/mol	-46100	6670	-61500	3300
$K_{NO}^0(T_{Ref.})$	Pa ⁻¹	2.25E-5	1.14E-5	—	—
ΔH_{NO}	J/mol	-112000	19000	—	—

3.4 Discussion

Figure 3-2 shows that water has only an influence up to a concentration of 2.5%. In the temperature range over 473 K the presence of water resulted in an increase of the activation energy from 87.4 kJ/mol (dry condition) to 98.7 kJ/mol (Table 3-1). In comparison to dry conditions the pre-exponential factor decreases about 50% and remains constant for higher water concentrations. This indicates that water only blocks part of the active sites. Because of the higher proton affinity of ammonia compared to water, it is not expected that water blocks the sites for ammonia adsorption (11). However Odriozola et al. (13) reported that ammonia does hardly adsorb on fully hydroxylated vanadia surfaces. The hydroxylation of the vanadia surface could be a possible explanation of the inhibition by water. The influence of water on the oxygen adsorption equilibrium constant is different. In the presence of water the adsorption enthalpy becomes more negative and the pre-exponential factor increases (Table 3-1). Water favors the adsorption of oxygen, because oxygen adsorbs hardly at the V=O sites, whose number is decreasing in the presence of water. This is in accordance with the mechanism proposed by Inomata et al. (6) where V-OH species are reoxidized to V=O species (see equation r2).



In the mechanism proposed by Inomata et al. (6) oxygen is not involved in the rate limiting step. However, the authors also showed that the number of active surface V=O sites is proportional to the reaction rate. The concentration of oxygen has an important

influence on the number of these sites, especially in the low concentration range. Therefore it is necessary to take oxygen into account in the kinetic modeling.

The estimation of the adsorption equilibrium constant of NO contains a high level of uncertainty, due to the low conversion in the temperature range below 473 K, where a significant deviation for k_1 is observable (see Fig. 3-6). But only with the additional Langmuir-Hinshelwood path a good fitting of the kinetic behavior can be reached also in the low temperature range .

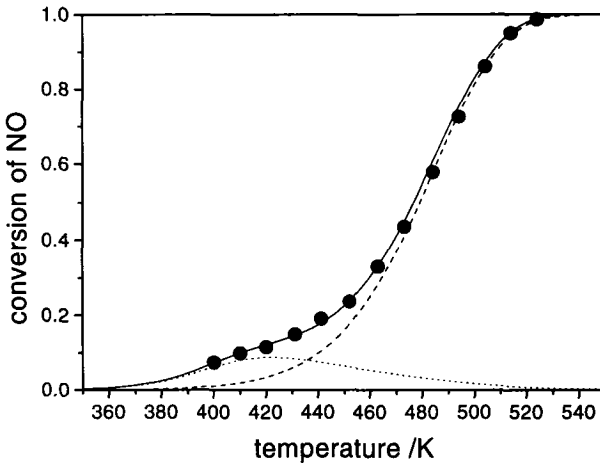


Figure 3-7. Contributions of the different reaction paths to the overall conversion as a function of the temperature.

● experimental data, — simulated overall conversion, conversion via Langmuir-Hinshelwood path, ---- conversion via Eley-Rideal path.

Feed: 10% O₂, 1000 ppm NO, 1000 ppm NH₃, balance N₂, flow rate = 430 ml(NTP)

Figure 3-7 illustrates the conversion of NO versus the temperature and the contributions of each reaction path to the overall conversion. Below 433 K the reaction occurs mainly via the path based on the Langmuir-Hinshelwood mechanism. In the higher temperature range no NO adsorption occurs and the Langmuir-Hinshelwood reaction path can be neglected.

With water in the feed no significant influence was measurable (see Fig. 3-8), due to the very low conversion below 473 K.

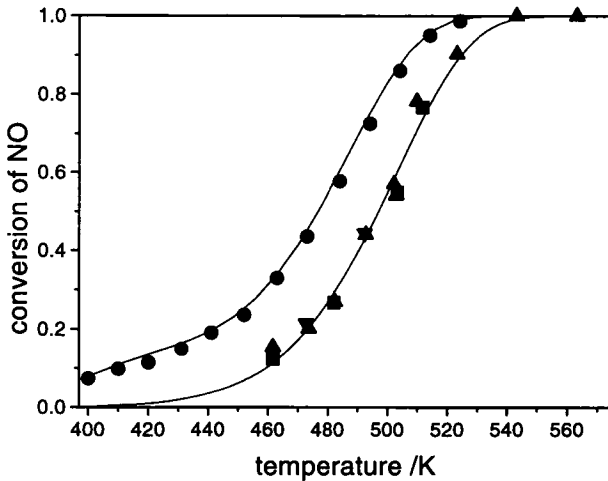


Figure 3-8. Conversion of NO versus temperature for dry and wet feed.

● 0% H₂O, ▼ 2.5 % H₂O, ■ 5% H₂O, ▲ 7.5% H₂O, — simulated.

Feed: 10% O₂, 1000 ppm NO, 1000 ppm NH₃, 0% - 7.5% H₂O, balance

N₂, flow rate = 430 ml/min(NTP).

For the occurrence of a Langmuir-Hinshelwood mechanism the adsorption of NO is necessary. NO adsorption is only reported on TiO₂ and on reduced vanadia but not on oxidized V₂O₅ surfaces (11, 13, 24). In the presence of ammonia a part of the V₂O₅ surface is reduced and the adsorption of NO at this sites becomes possible if the reoxidation by O₂ is not too fast.

An other explanation for the occurrence of a Langmuir-Hinshelwood mechanism is that NO adsorption occurs on the TiO₂ support. In that case NO may be spilled over onto the active vanadia sites and react according to a Langmuir-Hinshelwood mechanism. However this mechanism has so far not been proven and needs direct experimental confirmation. In any case, the suggestion made by Srnak et al. (11) that both an Eley-Rideal and a Langmuir-Hinshelwood mechanism may be relevant to describe SCR kinetics is further supported by this work.

3.5 Conclusions

Below 473 K the kinetic of the selective reduction of NO can not be properly described with the model including a Eley-Rideal mechanism alone. Best fitting is obtained at an additional Langmuir-Hinshelwood pathway. Under typical SCR conditions (5-15% O₂, 5-15% H₂O, 523-723 K) the model with the Eley-Rideal mechanism is sufficient. The influence of oxygen has to be taken into account for the whole temperature range. The importance of oxygen decreases with rising concentrations of oxygen, but can not be completely neglected in the concentration range typical for SCR. Water has no significant influence on the kinetics under typical SCR conditions.

3.6 Notation

m_{cat} = catalyst weight, kg

V^* = flow rate, m^3/s

r_i = reaction rate, $\text{Pa m}^3/\text{kg s}$

k_i = reaction rate constant

K_A = adsorption equilibrium constant, Pa^{-1}

p_i = partial pressure of the component i , Pa

k_i^0 , K_A^0 = pre-exponential factors

E_{Ai} = activation energy, (J/mol)

ΔH_A = adsorption enthalpy, (J/mol)

3.7 References

1. Marangozis, J. *Ind. Eng. Chem. Res.* **31**, 987 (1992).
2. Bauerle, G. L.; Wu, S. C. and Nobe, K. *Ind. Eng. Chem. Prod. Res. Dev.* **17**, 117 (1978).
3. Odenbrand, C. U. I.; Lundin, S. T. and Andersson, L. A. H. *Appl. Catal.* **18**, 335 (1985).
4. Tuenter, G.; van Leeuwen, W. F. and Snepvangers, L. J. M. *Ind. Eng. Chem. Prod. Res. Dev.* **25**, 633 (1986).

5. Robinson, W. R. A. M.; van Ommen, J. G.; Woldhuis, A. and Ross, J. R. H. *Proceedings of the 10th International congress on Catalysis, 19-24 July, Budapest, Hungary*, 2673 (1992).
6. Inomata, M.; Miyamoto, A. and Murakami, Y. *J. Catal.* **62**, 140 (1980).
7. Miyamoto, A.; Kobayashi, K.; Inomata, M. and Murakami, Y. *J. Phys. Chem.* **86**, 2945 (1982).
8. Janssen, F. J. J. G.; v. den Kerkhof, F. M. G.; Bosch, H. and Ross, J. R. H. *J. Phys. Chem.* **91**, 5921 (1987).
9. Gasiot, M.; Haber, J.; Machej, T. and Czeppe, T. *J. Mol. Catal.* **43**, 359 (1988).
10. Takagi, M.; Kawai, T.; Soma, M.; Onishi, T. and Tamaru, K. *J. Catal.* **50**, 441 (1977).
11. Srnak, T. Z.; Dumesic, J. A.; Clausen, B. S.; Törnqvist, E. and Topsøe, N.-Y. *J. Catal.* **135**, 246 (1992).
12. Wu, S. C. and Nobe, K. *Ind. Eng. Chem. Prod. Res. Dev.* **16**, 136 (1977).
13. Odriozola, J. A.; Heinemann, H.; Somorjai, G. A.; de la Banda, J. F. G. and Pereira, P. *J. Catal.* **119**, 71 (1989).
14. Tufano, V. and Turco, M. *Appl. Catal. B: Environmental* **2**, 133 (1993).
15. Svachula, J.; Ferlazzo, N.; Forzatti, P.; Tronconi, E. and Bregani, F. *Ind. Eng. Chem. Res.* **32**, 1053 (1993).
16. Jung, J. and Panagiotidis, T. *Chemie im Kraftwerk 1990*, 1 (1990).
17. Beeckman, J. W. and Hegedus, L. L. *Ind. Eng. Chem.* **30**, 969 (1991).
18. Weisz, P. B. and Prater, C. D. *Advances in catalysis and related subjects* **6**, 144 (1954).
19. Turco, M.; Lisi, L. and Pirone, R. *Appl. Catal. B: Environmental* **3**, 133 (1994).
20. Odenbrand, C. U. I.; Gabrielsson, P. L. T.; Brandin, J. G. M. and Andersson, L. A. H. *Appl. Catal.* **78**, 109 (1991).
21. Topsøe, N. -Y.; Slabiak, T.; Clausen, B. S.; Srnak, T. Z. and Dumesic, J. A. *J. Catal.* **134**, 742 (1992).

22. Duffy, B. L.; Curry-Hyde, H. E.; Cant, N. W. and Nelson, P. F. *J. Phys. Chem.* **98**, 7153 (1994).
23. Himmelblau, D. M. "Process Analysis by Statistical methods", Wiley, New York, 1970.
24. Baltensberger, U.; Ammann, M.; Bochert, U. K.; Eichler, B.; Gäggler, H. W.; Jost, D. T.; Kovacs, J. A.; Türler, A.; Scherer, U. W. and Baiker, A. *J. Phys. Chem.* **97**, 12325 (1993).

Vanadia-Titania Aerogel Catalyst: Catalytic behavior and kinetic modeling

Abstract

The kinetics and the parametric sensitivity of the selective catalytic reduction of NO by NH₃ were investigated for a high surface area vanadia-titania aerogel. The catalyst showed high activity at low temperatures and the selectivity was higher than 99% for all experiments. The addition of up to 3% H₂O to the dry feed significantly reduced the rate of NO conversion. The effect leveled off for higher H₂O concentrations. In the absence of O₂ in the feed the activity collapsed. Small amounts of oxygen resulted in a sharp increase of the reaction rate, but for oxygen concentrations exceeding 4% the increase diminished. A high tolerance with respect to sulfur dioxide was observed. The estimated activation energy amounted to 60 kJ/mol ± 1 kJ/mol. The microkinetic analysis resulted in a model based on an Eley-Rideal mechanism which describes the kinetic behavior over a wide experimental range.

4.1 Introduction

Three different positions are often used as locations for the SCR reactor in the flue gas stream (see paragraph 1.3.4.1). The catalyst location is one of the most important factors which determine the catalyst lifetime. At the tail end position the catalyst lifetime is increased, due to the relatively clean flue gas. However, the flue gas has to be reheated to the SCR operating temperature. The consequence is a 1-4% decrease in the overall thermal efficiency of the power plant (1). In the most cases, these additional costs make the tail end location less economic than the other ones. An economic study of the SCR process for power plant applications indicates, that overall costs could be reduced if a suitable catalyst would allow to carry out the SCR reaction at lower temperatures (2). Today platinum catalysts are utilized for low temperature applications (175 - 250°C). Major disadvantages of the platinum based catalysts are the narrow temperature window, the formation of N₂O as a byproduct and the oxidation of the ammonia reductant to NO_x at higher temperatures, resulting in a decrease in selectivity and conversion. The precise control of the temperature complicates the process design and leads to an increase of the overall costs. Consequently, a demand for new technologies being capable of reducing NO_x at lower temperatures exists today. A new approach to lower the active temperature window of SCR catalysts was recently made by Shell (3). They developed a system based on a granular SCR catalyst in a fixed bed type reactor consisting of numerous shallow slabs of catalysts. The good contact between gas and catalyst allowed an operation temperature between 120 and 350°C. The system has a high catalyst holdup and needs clean gases with low dust concentration. Below 200°C ammonium sulfate deposition can cause a reversible catalyst deactivation.

Recently it has been shown that vanadia-titania aerogels offer a high specific surface area combined with high dispersion and good accessibility of the active vanadia constituent. Due to their unique morphological and textural properties, the aerogel catalysts show excellent catalytic performance in the SCR of NO at low temperatures (4-6).

The aim of the work presented in this chapter is to gain information on the performance and stability of vanadia-titania aerogel SCR catalysts under conditions similar to real lean exhaust conditions, e.g. in the presence of water in the feed. The influence of oxygen, water and sulfur dioxide on catalyst stability, activity and selectivity is investigated. A model of the intrinsic kinetics is developed, which includes the influences of all major exhaust components. It is shown that satisfactory predictions of the kinetic behavior with a single Eley-Rideal based model is possible. The effects of O₂ and H₂O are included by Langmuir-type-adsorption terms.

4.2 Experimental

4.2.1 Catalyst

A highly dispersed vanadia-titania aerogel with high surface area has been used for catalytic tests. The catalyst with a nominal loading of 30 wt.% V₂O₅ was synthesized by a two-stage sol-gel process with ensuing high temperature supercritical drying. Details of the preparation procedure and of the physical and chemical characterizations are described in ref. (5, 6). After calcination at 573 K in 20% O₂/N₂ for 2 hours, the catalyst powder was agglomerated under a pressure of 2.5 MPa for 2 min and then crushed to sieve fractions of 100-250 μm and 250-350 μm, respectively.

N₂-physisorption at 77 K of the fresh catalyst showed a type-IV isotherm with a type-H1 hysteresis according to IUPAC classification (Sing et al., 1985). The average pore diameter of the pronounced meso-to macroporous catalyst was 18 nm and the specific nitrogen pore volume was 1.1 cm³/g_{catalyst}. The BET surface area amounted to 183 m²/g_{catalyst}, with a surface area in micropores < 10 m²/g_{catalyst}. XRD analysis of the agglomerated catalyst showed only reflections due to crystalline anatase. No evidence for crystalline V₂O₅ was found, corroborating a high dispersion of the vanadia component.

4.2.2 Catalytic tests

The catalytic studies were carried out in the continuous tubular fixed-bed microreactor described in paragraph 2.1. The reaction gas mixture employed in kinetic experiments consisted of 100-1000 ppm NO (99.0%, PanGas), 100-1000 ppm NH₃ (5% NH₃ (99.98%) in N₂ (99.999%), CarbaGas), 0-6% H₂O (bidest.), 0-15% O₂ (99.995%, PanGas), 0-10% CO₂ (99.99%, PanGas) and 0-90 ppm SO₂ (15% SO₂ (99.98%) in N₂ (99.999%), PanGas) in N₂-balance (99.995% PanGas). Kinetic experiments at steady-state conditions were carried out in the temperature range 390-510 K at a pressure of 1.1 · 10⁵ Pa using 0.1-0.15 g of catalyst (100 - 250 μm) and a reactant flow rate of 200-1000 ml (NTP) min⁻¹ (60'000-300'000 h⁻¹ (NTP) GHSV). Before catalytic experiments, the catalyst was pretreated in the reactor for 2 h at 573 K in 20 % O₂/N₂.

4.2.3 Kinetic modeling

The model parameters were estimated from the experimental data by linear and non-linear regression analysis as described in paragraph 2.3. The logarithmic maximum

likelihood function of the NO partial pressure was chosen as objective function to estimate the model parameters.

4.3 Results

4.3.1 Mass and heat transfer

The quartz wool plug on top of the catalyst bed and the small particle size (100 - 250 μm) in comparison to the reactor diameter (7.5 mm) ensured that no radial gas velocity profile and no channeling occurred and let us assume that plug flow was established over the whole catalyst bed. Theoretical calculations using the criterion of Weisz and Prater (7) and experiments with larger catalyst particle sizes (250 - 350 μm) indicated that no internal mass transfer limitation occurred in the investigated temperature range. Figure 4-1 shows no deviation of reaction rate due to the particle size for high conversions and thus confirm that intraparticle mass transfer limitations were negligible. A maximum adiabatic temperature increase for a feed containing 1000 ppm NO of 13 K was calculated. The measured experimental raise of the gas temperature for complete conversion at the maximum space velocity was 1.5 K, equal to the increase observed with the commercial catalysts. Due to the small particle size and the negligible increase of the temperature, the kinetic behavior was not significantly affected by temperature gradients in the catalyst bed and in the catalyst.

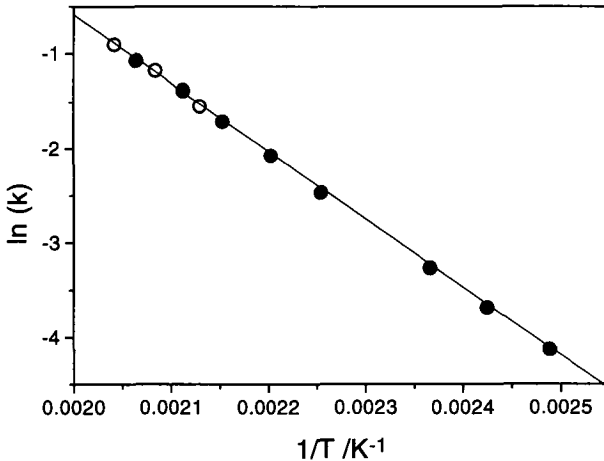


Figure 4-1. Arrhenius plot for kinetic tests with different catalyst particle size

● 100-250 μm , ○ 250-350 μm , — model. Feed: 1000 ppm NO, 1000 ppm NH_3 , 10 % O_2 , balance N_2 .

4.3.2 Catalyst stability

Up to 500 K no significant deactivation was perceptible during 7 hours time on stream (see Figure 4-2). For temperatures exceeding 500 K, a small decrease in activity was observed. This behavior can be explained by a loss of specific surface area due to hydrothermal aging of the aerogel catalyst, as observed previously for vanadia supported on titania-aerogel catalysts (8). After 200 h under SCR conditions the BET surface area decreased by 14% from initially $183 \text{ m}^2/\text{g}_{\text{catalyst}}$ to $158 \text{ m}^2/\text{g}_{\text{catalyst}}$, whereas no change in porosity occurred during the SCR reaction.

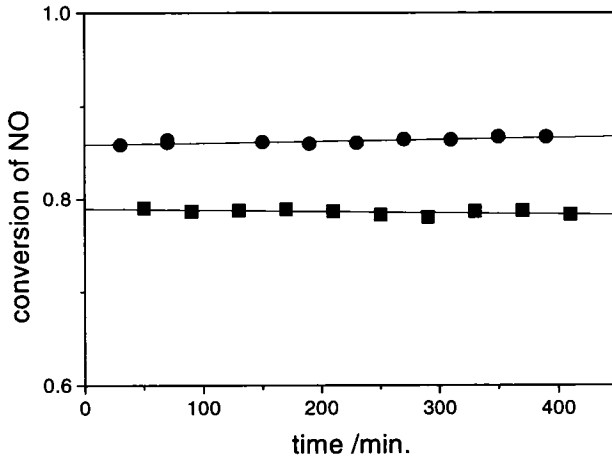


Figure 4-2. Catalyst stability for wet and dry feed.

● 0% H₂O, temperature 473K, ■ 5% H₂O, temperature 493K. Feed: 1000 ppm NO, 1000 ppm NH₃, 10 % O₂, 0 or 5% H₂O, balance N₂, gas flow = 500 ml(NTP)/min, catalyst weight = 0.1 g.

4.3.3 Temperature dependence

In Figure 4-3 the conversion of NO with raising temperature is compared for a dry feed and for a feed containing 5 % water. The temperature necessary to obtain 50% NO conversion ($T_{X_{NO}=0.5}$) is shifted by 25 K to higher temperatures in the presence of water. A selectivity to N₂ higher than 99.5% was observed for the whole temperature range investigated. The reproducibility of the catalytic behavior under steady state SCR conditions is illustrated in Figure 4-3 by comparison of a fresh catalyst with a catalyst which has been on stream for 24 hours at 453 K. The deviations are in the range of the experimental error. A first order kinetics and an Arrhenius type temperature dependence of

the reaction rate constant with an apparent activation energy of $60 \text{ kJ/mol} \pm 1 \text{ kJ/mol}$ (95 % confidence limits) was determined from the data presented in Figure 4-1.

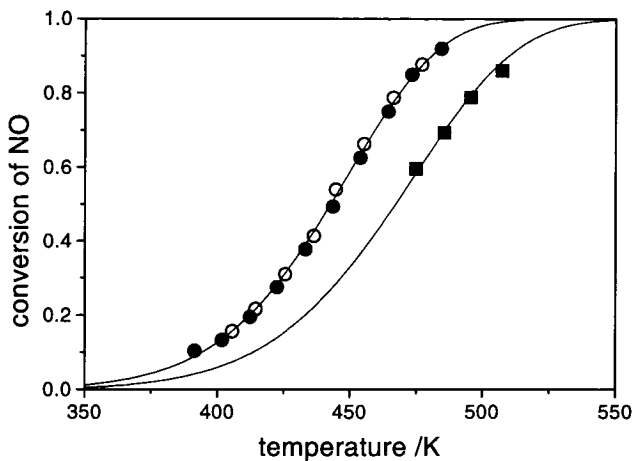


Figure 4-3. NO conversion as a function of temperature

● 0 % H₂O (new catalysts), ○ 0 % H₂O (used catalysts), ■ 5 % H₂O,
 — simulated progress, Feed: 1000 ppm NO, 1000 ppm NH₃, 10 % O₂,
 0 % or 5 % H₂O, balance N₂, gas flow = 500 ml(NTP)/min, catalyst
 weight = 0.1 g.

4.3.4 Influence of space velocity

Figure 4-4 depicts the conversion of NO versus the gas flow per catalyst weight (W/F) for temperatures in the range 405 - 477 K. With increasing temperature a stronger influence of space velocity on NO conversion is perceptible which is most pronounced up to $10 \text{ kg}_{\text{cat}}\text{m}^{-3}\text{s}$. The experimental data are in good accordance with the simulated

progress assuming a first order reaction. Integral analysis of the data also revealed that only a first order kinetic in NO can describe the experimental behavior properly.

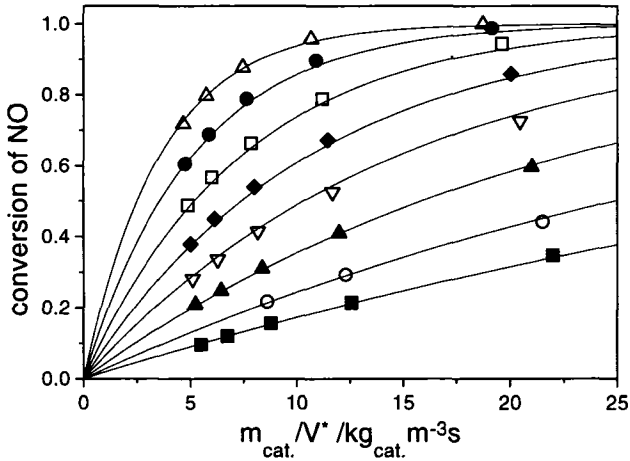


Figure 4-4. NO conversion as a function of the gas flow

■ 405 K, ○ 414 K, ▲ 425 K, ▽ 436 K, ◆ 445 K, □ 455 K, ● 466 K,
 △ 477 K, — simulated progress. Feed: 1000 ppm NO, 1000 ppm NH₃,
 10 % O₂, balance N₂, gas flow = 300 - 800 ml(NTP)/min, catalyst weight
 = 0.1 g.

4.3.5 Influence of the ammonia concentration

The ammonia inlet concentration was varied between 100 and 1000 ppm to investigate the influence of ammonia on the kinetic behavior. The conversion of NO was only sensitive to the ammonia concentration if the reactor outlet concentration of

ammonia was less than 15 ppm. In the measurements depicted in figure 4-5, this occurred only if the conversion was limited by ammonia.

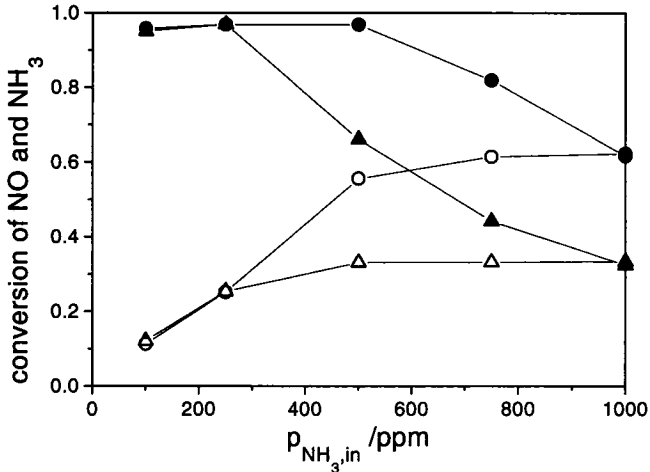


Figure 4-5. NO conversion as a function of the NH₃ reactor inlet concentration.

○ NO conversion and ● NH₃ conversion at 453 K, △ NO conversion and ▲ NH₃ conversion at 428 K. Feed: 1000 ppm NO, 100-1000 ppm NH₃, 10 % O₂, balance N₂, gas flow = 500 ml(NTP)/min, catalyst weight = 0.1 g.

4.3.6 Influence of water

Addition of water to the dry feed decreased the reaction rate (Fig. 4-6). The effect is more pronounced for low temperatures and concentrations up to 3%, whereas for concentrations above 5% the activity was almost independent of the water concentration.

The inhibition effect of water was occasionally reported by other groups (9-12). Topsøe et al. (10) found that water hydroxylates the surface thus forming Brønsted acid sites. Moreover, water was reported to adsorb more weakly than ammonia and therefore should not inhibit NH_3 adsorption. This finding is in agreement with the observed low influence of water on activity in the higher concentration range. With models which included a competitive adsorption of ammonia and water the kinetic behavior could not be described properly. On grounds of the postulated formation of Brønsted sites, an increase in activity would be supposed which is inconsistent with the experimental results. It seems that water not only affects the number of active site but also the rate limiting step (10).

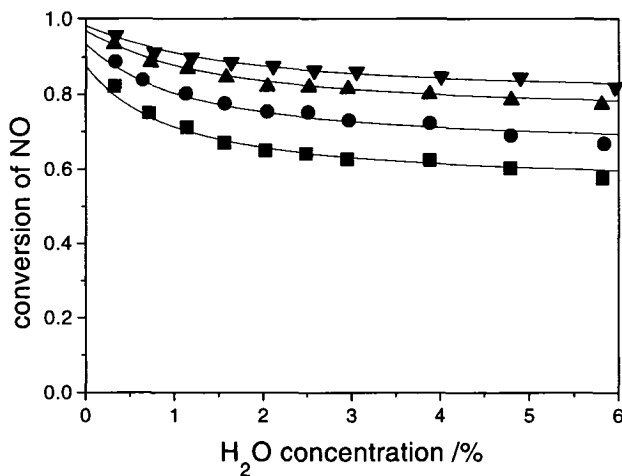


Figure 4-6. NO conversion as a function of the water concentration

■ 477 K, ● 486 K, ▲ 495 K, ▼ 501 K — simulated progress. Feed: 1000 ppm NO, 1000 ppm NH_3 , 10 % O_2 , 0- 6 % H_2O , balance N_2 . gas flow = 500 ml(NTP)/min, catalyst weight = 0.1 g.

4.3.7 Influence of oxygen

The oxygen concentration was varied in the range 0 - 15%. Without O_2 in the feed the reaction rate was almost completely suppressed due to an inhibited reoxidation of the catalyst. Figure 4-7 shows that low concentrations of oxygen strongly accelerate the reaction rate, independently whether water is present in the feed or not. The rate enhancing influence declined with increasing oxygen concentration and for higher O_2 levels the enhancement is only small (Fig. 4-7). The promoting effect of oxygen is well known for vanadia based catalysts (12, 13). Small deviations between the experimental data and the model predictions were perceptible for low oxygen concentrations. The calculated conversion was lower than the experimental value with the effect being more pronounced with water in the feed gas. The simulated progress for wet feeds shown in Figure 4-7 is an extrapolation from dry conditions as the kinetic parameters for the oxygen influence were estimated from kinetic data of experiments without water in the feed gas. The underestimation at lower oxygen concentrations is in accordance with previously reported results, which indicated that water favors the reoxidation of the catalyst (see paragraph 3.4). The small overestimation of activity observed for the wet feed at 503 K results from a loss of specific surface area.

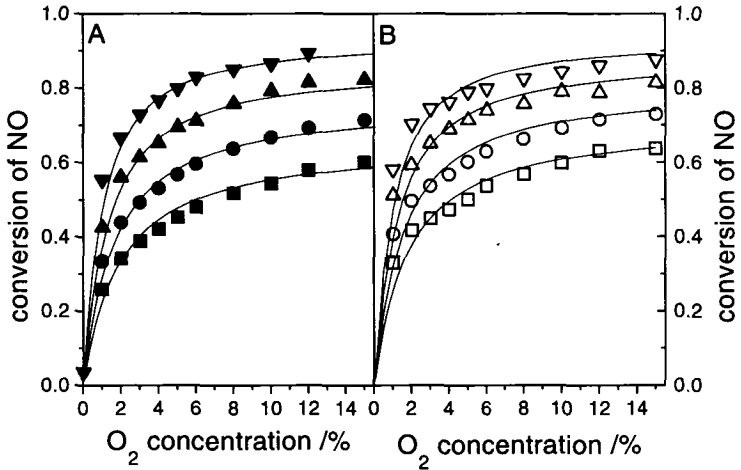


Figure 4-7. NO conversion as a function of the oxygen concentration

A = 0 % H₂O, B = 5 % H₂O, ■ 447 K, ● 456 K, ▲ 466 K, ▼ 476 K;
 □ 477 K, ○ 486 K, △ 495 K, ▽ 503 K, — simulated progress. Feed:
 1000 ppm NO, 1000 ppm NH₃, 0-15 % O₂, balance N₂, gas flow = 500
 ml(NTP)/min, catalyst weight = 0.1 g.

4.3.8 Influence of SO₂

Exposing the catalyst alternately to a dry SO₂ free feed and to a feed containing increasing concentrations of SO₂, respectively, at 500 K (Fig. 4-8) gave no indication for poisoning or deactivation processes. Moreover, the undesired formation of SO₃ was not observed. Longer exposure of the catalyst to a SO₂ containing wet and dry feed indicated a small decrease in activity for the wet feed at 500 K (Fig. 4-9). The deactivation was ascribed to the concomitant small loss of surface area induced by hydrothermal processes and not to the SO₂ content in the feed gas. Poisoning as well as

promoting effects of SO_2 are proposed in the literature. Chen (15) suggested an increase of the Brønsted acidity by SO_2 resulting in higher activity. Problems in industrial applications are generated by the oxidation of SO_2 to SO_3 although the formation of SO_3 is slow compared to the reduction of NO with NH_3 . Svachula et al. (16) proposed a steady state kinetics of the SO_2 oxidation with a reaction rate which is of variable order in SO_2 and asymptotically independent of oxygen. The oxidation is inhibited by water and ammonia and slightly promoted by NO . SO_3 reacts with ammonia and water thus forming ammonium bisulfate (NH_4HSO_4) or ammonium sulfate ($(\text{NH}_4)_2\text{SO}_4$) (see paragraph 1.3.4.1). The deposition of ammonium sulfates in pores leads to a decrease in specific surface area. The fouling depends on exhaust gas temperature and the ammonia, sulfur trioxide and water concentrations (17).

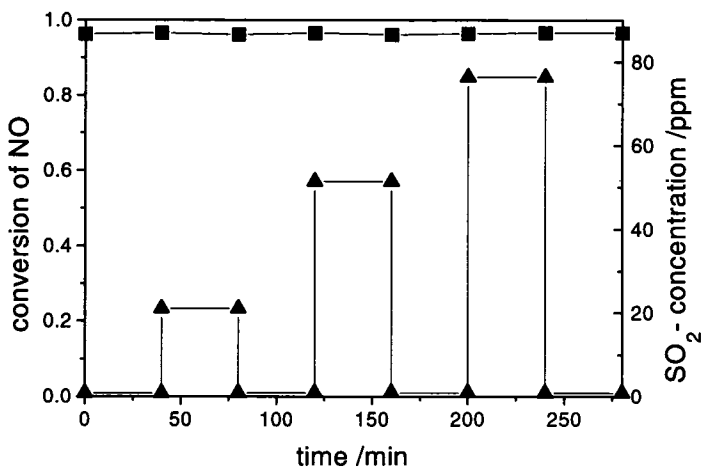


Figure 4-8. Influence of SO_2 on catalyst behavior

■ conversion of NO , ▲ SO_2 concentration. Feed: 1000 ppm NO , 1000 ppm NH_3 , 5 % H_2O , 0-76 ppm SO_2 , balance N_2 , gas flow = 800 ml(NTP)/min, $T_{\text{reactor}} = 500 \text{ K}$, catalyst weight = 0.15 g.

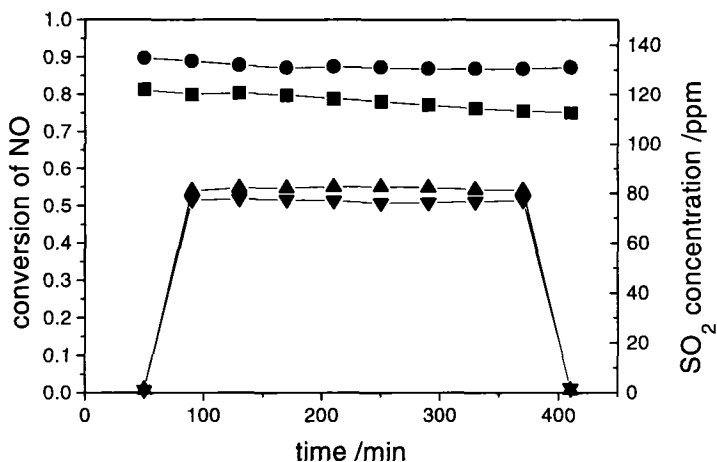
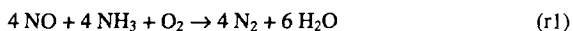


Figure 4-9. Influence of SO₂ on catalyst behavior for wet and dry feed

■ conversion of NO for wet feed at $T_{\text{reactor}} = 500 \text{ K}$, ● conversion of NO for dry feed at $T_{\text{reactor}} = 480 \text{ K}$, ▲ SO₂ concentration for wet feed, ▼ SO₂ concentration for dry feed. Feed: 1000 ppm NO, 1000 ppm NH₃, 0 or 5 % H₂O, 0 or 80 ppm SO₂, balance N₂, gas flow = 800 ml(NTP)/min, catalyst weight = 0.15 g.

4.3.9 Kinetic modeling

The selectivity to N₂ and H₂O was higher than 99 % and no significant oxidation of ammonia was observed for all experiments. For the temperature range investigated no side reaction had to be taken into account and consequently an overall stoichiometry of the reaction as shown in equation r1 can be assumed.



The kinetic behavior is well described with the following approach. The core of the model is an Eley-Rideal-mechanism which is well known from the literature. Oxygen has a strong influence on the number of active sites. The relation between the partial pressure of oxygen and the number of active sites was incorporated by a Langmuir-Hinshelwood model. Water inhibits the reaction. This effect levels off for higher water concentrations in the feed stream. This indicates that the sites still have an activity when water covers the catalyst completely. This behavior is described with a modified Langmuir adsorption model including an additional constant remainder n . The temperature dependencies of the adsorption constants were negligible in the investigated temperature range. The influence of water to the reoxidation was not significant for all experimental conditions. The best description of the experimental data was obtained with a model based on equation 4-1.

$$r = k \cdot \frac{K_{O_2} p_{O_2}}{1 + K_{O_2} p_{O_2}} \cdot \left(n + \frac{1-n}{1 + K_{H_2O} p_{H_2O}} \right) \cdot p_{NO} \quad (4-1)$$

$$k = k^0(T_{ref.}) \cdot \exp\left(\frac{-E_A}{R} \left(\frac{1}{T} - \frac{1}{T_{ref.}}\right)\right)$$

$$T_{ref.} = 450 \text{ K}$$

In order to reduce the correlation between pre-exponential factor and activation energy, the reaction rate constant was expressed as proposed by Himmelblau (18).

The model parameter estimates are listed in Table 4-1. Due to the independent estimation of the reaction rate constant, K_{O_2} and the water dependency, no correlation

exists between these parameters. The calculated correlation between n and K_{H_2O} was 0.8 and 0.2 for $k^0(T_{ref})$ and E_A , respectively.

Table 4-1 Estimated Model Parameters.

	units	parameter	standard deviation
$k^0(T_{ref})$	$m^3/kg\ s^{-1}$	0.15	$9e-4$
E_A	kJ/mol	60	0.5
K_{O_2}	Pa^{-1}	$2.8e-4$	$1e-5$
n	-	0.4	$9e-3$
K_{H_2O}	Pa^{-1}	$1.7e-3$	$1e-4$

4.4 Discussion

The proposed model is in good accordance with the findings of other groups in this field. An Eley-Rideal model is also proposed by several authors (19-21). In our experiments the reaction rate was always zeroth order in ammonia. It can be assumed that the catalyst was completely covered with ammonia even for small concentrations due to the low temperatures in all experiments. Variation in the ammonia concentration (see Figure 4-5) and calculations with adsorption constants from the literature (22) confirmed this assumption. At higher temperatures and high conversion or at unsteady operation conditions (23) ammonia adsorption has to be taken into account and could

have a significant impact on the ammonia slip which is an important parameter in industrial applications.

The activation energy found without water in the feed gives also a good fitting for the experiments with water. This is manifested in Figure 4-3 and 4-6. The main effect of water is a decrease in the pre-exponential factor (see Figure 4-9). But also an increase in the activation energy would be expected for low coverages due to exothermic adsorption of water. For low surface coverage ($K_w p_w \ll 1$), the adsorption equilibrium constant of water K_w should decrease exponentially with the increased temperature by the factor $e^{AH_w/RT}$. However, this effect is too small for a proper estimation of the adsorption energy ΔH_w . An estimation would only be possible if more experimental data in a wider temperature range and for small water concentrations would be accessible. But at the higher temperature the hydrothermal deactivation would cause a small loss in the activity which is sufficient for distorting the estimation of the adsorption energy. Furthermore, for a typical exhaust gas the water concentration is high and $K_w p_w \gg 1$, so that the modified Langmuir term for water is always about 0.4 and independent of the water content.

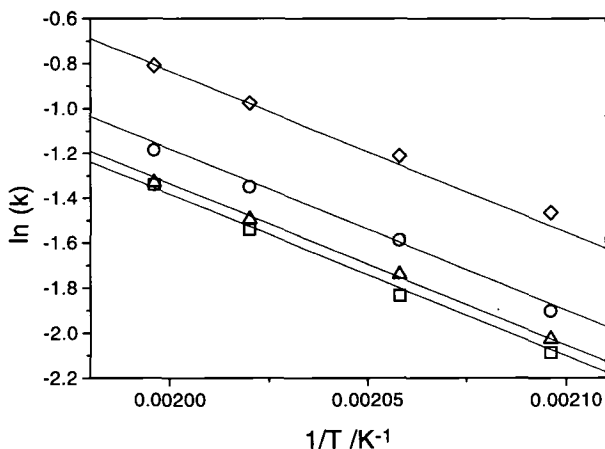


Figure 4-9. Arrhenius type plot for different water concentrations

□ 4.8 % H₂O, △ 3.9 % H₂O, ○ 1.6 % H₂O, ◇ 0.3 % H₂O, — model.

Feed: 1000 ppm NO, 1000 ppm NH₃, 10 % O₂, 0.3 - 4.8% H₂O, balance N₂, gas flow = 500 ml(NTP)/min, catalyst weight = 0.1 g.

The same restrictions as for the water adsorption constant exists for the estimation of the temperature dependence of the reoxidation. It is obvious from Figure 4-10 that the prediction of the reaction rate is too small for lower oxygen concentrations. This effect is stronger if water is present in the feed gas. Water strengthens the reoxidation of the catalysts. Similar behavior was found with an industrial vanadia based catalyst (see chapter 3). An explanation could be that water favors the adsorption of oxygen, because oxygen adsorbs hardly at the V=O sites, whose number is decreasing in the presence of water. But mechanistic interpretation of this effect needs further investigations and is not understood yet.

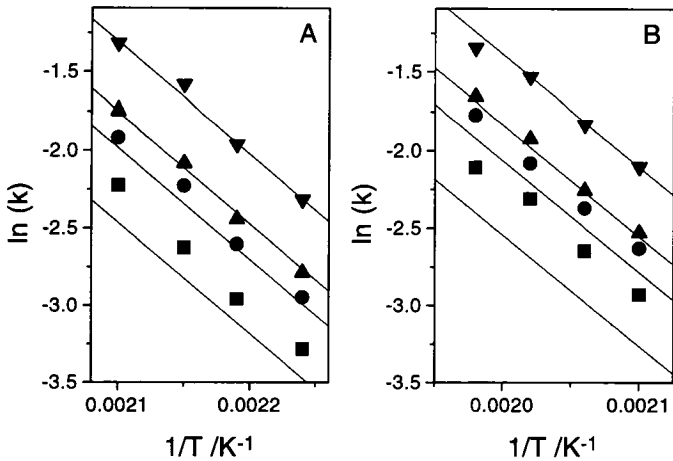


Figure 4-10. Arrhenius type plot for different oxygen concentrations

■ 1 % O₂, ● 2 % O₂, ▲ 3 % O₂, ▼ 10 % O₂, — model. Feed: 1000 ppm NO, 1000 ppm NH₃, 10 % O₂, A = 0% or B = 5 %H₂O, balance N₂, gas flow = 500 ml(NTP)/min, catalyst weight = 0.1 g.

Furthermore Figure 4-10 demonstrates that the oxygen concentration has no significant influence on the activation energy. This indicates, that the oxygen dependence depicted in Figure 4-7, is not a result of a change in the rate determining step. It must be assumed that adsorbed oxygen has an influence on the number of active sites. This was earlier proposed by Janssen et al. (20, paragraph 1.3.4.3). They suggested that molecular oxygen initially adsorbs at a single site. When there is an other vacancy next to the adsorbed oxygen molecule, the molecule dissociates and one of the atoms becomes adsorbed on the vacancy. This would be a possible explanation of the observed Langmuir behavior and clarify the underestimation for low oxygen concentration. The probability for

pairs and clusters of oxygen vacancies is assumed to increase with dropping oxygen concentrations leading to acceleration of the reoxidation. An additional factor for the underestimation in the lower concentration range could be the reoxidation with NO. This reaction path was proposed by Miyamoto et al. (24) in absence of oxygen (see paragraph 1.3.4.3).

4.5 Conclusions

It has been demonstrated that vanadia-titania aerogels are highly active catalysts for the SCR reaction in the low temperature range, due to large specific surface and the high vanadia content. Water inhibits the reduction of NO to N₂, but in the typical concentration range of exhaust gases the influence levels off. Under practical conditions the reoxidation is fast and the reaction rate is independent of the oxygen concentration. Like other vanadia based DeNO_x catalysts, the aerogel shows a good resistance to SO₂ poisoning. A hindrance for an industrial application in the near future is the high price due to the relatively demanding preparation and the high vanadia content. For preserving the high specific surface area the gel has to be dried under supercritical conditions.

With a simple model very good predictions of kinetic behavior and the parametric sensitivity were obtained. The kinetic analysis demonstrated that only a model based on Eley-Rideal mechanism can describe the kinetic behavior properly.

4.6 Notation

$m_{\text{cat.}}$ = catalyst weight, kg

V^* = gas flow, m^3/s

r = reaction rate, $\text{m}^3 \text{Pa} / \text{kg s}$

k = reaction rate constant, $\text{m}^3/\text{kg s}$

$k^0(T_{\text{ref.}})$ = pre-exponential factor, $\text{m}^3/\text{kg s}$

E_A = activation energy, kJ/mol

T = temperature, K

K_i = adsorption equilibrium constant of component i , Pa^{-1}

n = constant, -

p_i = partial pressure of component i , Pa

3.7 References

1. Lowe, P. A. "Low-Temperature Selective Catalytic Reduction NO_x Control." American Chemical Society, 1994.
2. Robie, C. P.; Ireland, P. A. and Cichanowicz, J. E. *Joint Symposium on Stationary Combustion NO_x Control, San Francisco*, (1989).
3. van der Grift, C. J. G.; Woldhuis, A. F. and Maaskant, O. L. *Catal. Today* **27**, 23 (1996).

4. Schneider, H.; Tschudin, S.; Schneider, M.; Wokaun, A. and Baiker, A. *J. Catal.* **147**, 5 (1994).
5. Schneider, M.; Maciejewski, M.; Tschudin, S.; Wokaun, A. and Baiker, A. *J. Catal.* **149**, 326 (1994).
6. Scharf, U.; Schneider, M.; Baiker, A. and Wokaun, A. *J. Catal.* **149**, 344 (1994).
7. Weisz, P. B. and Prater, C. D. *Advances in catalysis and related subjects* **6**, 144 (1954).
8. Engweiler, J. and Baiker, A. *Appl. Catal. A: General* **120**, 187 (1994).
9. Odenbrand, C. U. I.; Gabrielsson, P. L. T.; Brandin, J. G. M. and Andersson, L. A. H. *Appl. Catal.* **78**, 109 (1991).
10. Topsøe, N. -Y.; Slabiak, T.; Clausen, B. S.; Srnak, T. Z. and Dumesic, J. A. *J. Catal.* **134**, 742 (1992).
11. Duffy, B. L.; Curry-Hyde, H. E.; Cant, N. W. and Nelson, P. F. *J. Phys. Chem.* **98**, 7153 (1994).
12. Turco, M.; Lisi, L. and Pirone, R. *Appl. Catal. B: Environmental* **3**, 133 (1994).
13. Jung, J. and Panagiotidis, T. *Chemie im Kraftwerk 1990*, 1 (1990).
14. Bauerle, G. L.; Wu, S. C. and Nobe, K. *Ind. Eng. Chem. Prod. Res. Dev.* **17**, 117 (1978).
15. Chen, J. in: "Preparation, characterization, and deactivation of the catalysts for the selective catalytic reduction of NO with NH₃." Dissertation No 189, Buffalo, 1993
16. Svachula, J.; Alemany, L. J.; Ferlazzo, N.; Forzatti, P. and Tronconi, E. *Ind. Eng. Chem. Res.* **32**, 826 (1993).

17. Hums, E.; Joisten, M.; Müller, R.; Sigling, R. and Spielmann, H. *Catal. Today* **27**, 29 (1996).
18. Himmelblau, D. M. in: "Process Analysis by Statistical methods", Wiley, New York, 1970
19. Inomata, M.; Miyamoto, A. and Murakami, Y. *J. Catal.* **62**, 140 (1980).
20. Janssen, F. J. J. G.; v. den Kerkhof, F. M. G.; Bosch, H. and Ross, J. R. H. *J. Phys. Chem.* **91**, 5921 (1987).
21. Odenbrand, C. U.; Bahamondo, A.; Avila, P. and Blanco, J. *Appl. Catal. B: Environmental* **5**, 117 (1994).
22. Ruppel, W., Drews, R., Hess, K., Hölderich, W., Scheidsteger, O. in: "SCR-DeNO_x-Katalysatoren - Qualitätsicherung, Beurteilung und neue Entwicklung" (Köser, H.), 65, Vulkan-Verlag, BRD, 1992.
23. Tronconi, E.; Lietti, L.; Forzatti, P. and Malloggi, S. *Chem. Eng. Sci.* **51**, 2965 (1996).
24. Miyamoto, A.; Kobayashi, K.; Inomata, M. and Murakami, Y. *J. Phys. Chem.* **86**, 2945 (1982).

Chromia on Titania Catalyst: Modeling of the kinetic behavior and investigations of the deactivation behavior

Abstract

The kinetics and the parametric sensitivity of the selective catalytic reduction (SCR) of NO by NH₃ were investigated over a chromia on titania catalyst. The chromium oxide phase was made up predominantly of X-ray amorphous Cr₂O₃. High SCR activity and selectivity to N₂ was attained at low temperatures. The high selectivity is attributed to the absence of significant amounts of CrO₂ and crystalline α -Cr₂O₃ which favor N₂O formation. The selectivity to N₂O increased with higher temperature. Addition of up to 6 % H₂O to the dry feed reduced the rate of NO conversion and decreased the undesired formation of N₂O. The effect of water on the catalytic behavior was reversible. In the absence of oxygen, the reaction between NO and NH₃ became marginal, independently whether H₂O was present or not. Small amounts of oxygen were sufficient to restore SCR activity. Admission of SO₂ to the SCR feed resulted in a severe loss of activity. The poisoning of the catalyst by SO₂ was already notable for low SO₂ concentrations (30 ppm) and for temperatures up to 573 K. X-ray photoelectron and FTIR spectroscopy

revealed the presence of sulfate species on the catalyst surface. Analysis of the kinetic data indicated that the SCR reaction is first order in NO and zeroth order in NH₃ for temperatures in the range 400 - 520 K. The estimated activation energies for dry and wet feed amounted to 60.0 ± 1.6 kJ/mol (95% confidence limits). For temperatures in the range 400 - 520 K, and for a SO₂ free feed, the steady-state kinetic data could be well described with a model based on an Eley-Rideal type reaction between activated ammonia surface species and gaseous or weakly adsorbed NO.

5.1 Introduction

Various materials have been investigated for their application as SCR catalysts (1). One of the most effective catalyst is vanadia on titania, frequently in combination with tungsten- and/or molybdenum-oxide (see chapter 3). Other oxides have received less attention. Recently, chromia-containing catalysts have been reported to exhibit interesting properties for the reduction of nitric oxide with ammonia in the presence of excess oxygen (2, 3), especially in the low temperature range. Bulk amorphous chromium oxide was shown to be highly active at low temperatures affording nitrogen with high selectivity, whereas crystalline chromia (α -Cr₂O₃) produces substantial amounts of nitrous oxide and also exhibits significant activity for ammonia oxidation (4, 5). Differences in the catalytic behavior of these unsupported chromia catalysts are correlated with the higher density of labile oxygen species available on the surface of the amorphous sample under SCR reaction conditions (6).

In studies of supported chromium oxide catalysts it has been demonstrated that the behavior in SCR is strongly influenced by the support as well as by the nature of the

chromia surface species. Wong et al. (7) reported that TiO_2 -supported chromia catalysts were generally more active than Al_2O_3 -supported catalysts and that formation of undesired N_2O was higher for the titania supported catalyst. Previous investigations performed in our group with $\text{CrO}_x/\text{TiO}_2$ catalysts have shown that the supported chromium species are characterized by pronounced oxidation-reduction chemistry. The nature and oxidation state of the chromium oxide species depends on the Cr loading, preparation procedure, and on the pre-treatment conditions (8). It was demonstrated that the various chromium oxide phases, i.e., CrO_2 , CrOOH , and Cr_2O_3 differ markedly in their activity and selectivity (9). The highest activity combined with a high selectivity to N_2 was found for X-ray amorphous Cr_2O_3 supported on titania. Crystallization of Cr_2O_3 induced at higher temperatures reduced the activity significantly. Similar high conversion of NO is found with $\text{CrO}_2/\text{TiO}_2$, but substantial amounts of undesired N_2O are produced with this catalyst. Supported CrOOH is oxidized to CrO_2 under typical SCR conditions above 570 K and consequently exhibits similar catalytic behavior as CrO_2 (10, 11).

A limited number of studies have focused so far on the parametric sensitivity, the mechanism, and the kinetics of the SCR reaction over chromia based catalysts. For vanadia based catalysts it is well known from the literature that the presence of oxygen in the reaction mixture markedly enhances the activity for the SCR reaction (12-14), whereas water suppresses the reduction of NO (15). Duffy et al. (16) investigated the influence of oxygen on the rate and the selectivity of the SCR reaction over amorphous and crystalline chromia. A sharp rise in activity was observed for concentrations up to 1000 ppm O_2 with both forms of chromia. For higher oxygen concentrations the effect

levelled off. Willey et al. (17) similarly found higher reaction rates in the presence of oxygen for iron oxide-chromia-alumina aerogel catalysts.

Although flue gases usually contain water, most of the laboratory studies of chromia based SCR catalysts have been performed under dry conditions. The effect of water on the reaction of NO and NH₃ over amorphous and crystalline chromia catalysts has been investigated by isotopic labelling experiments by Duffy et al. (5). In the presence of excess oxygen, the addition of 1.5% H₂O decreased NO and NH₃ conversions and inhibited the formation of ammonia oxidation products N₂O and NO for temperatures up to 523 K over both forms of chromia. The authors verified that the effect of water on the activity and selectivity was reversible. Köhler et al. (8) observed significantly lower activity as well as higher selectivity to N₂O for chromium oxide supported on titania when the SCR feed gas contained water.

In low-temperature SCR applications the presence of SO₂ and its oxidation to SO₃ is of particular importance as sulfur trioxide can react with ammonia in the presence of water. The resulting ammonium sulfate and/or bisulfate can cause catalyst deactivation and can be deposited down stream in the flue gas flow (18). Yang et al. (19) prepared a Cr₂O₃-pillared interlayered clay, which exhibited a higher activity than a commercial reference catalyst, but addition of SO₂ markedly decreased its activity. Lower SCR activity and increased selectivity to N₂O was reported by Zhang et al. (20) upon deposition of SO₄²⁻ on amorphous chromia catalysts. The behavior was attributed to strong adsorption of NH₃ which prevents chromia from reacting with NO.

Several authors (21, 22) suggested for SCR on supported chromia catalysts a first order kinetics in nitric oxide and zeroth order in ammonia. Comparable reaction orders in nitric oxide and ammonia were observed for vanadia based catalysts and several

kinetic models were proposed (23-25). However, to our knowledge no model including all relevant exhaust gas components has been reported so far for chromia based catalysts.

In the present work, a 10 wt.% $\text{Cr}_2\text{O}_3/\text{TiO}_2$ catalyst has been investigated. In order to decrease the amount of CrO_2 and to minimize the formation of $\alpha\text{-Cr}_2\text{O}_3$, which both are considered responsible for N_2O formation, the method of catalyst preparation of Maciejewski et al. (10) was modified. By directly reducing the dried sample without calcination, predominantly poorly crystalline Cr_2O_3 (> 95 wt.%) was obtained. Previous studies have concentrated on chemical and structural properties as well as on the catalytic behavior of different chromium oxide phases (CrO_2 , CrOOH , Cr_2O_3) in the selective catalytic reduction of NO by NH_3 in excess oxygen. Here we are focusing on the performance and stability of $\text{Cr}_2\text{O}_3/\text{TiO}_2$ under real SCR conditions, e.g., in the presence of water in the feed. The influence of oxygen, water, and sulfur dioxide on activity and selectivity and on catalyst stability is investigated. The influence of different reaction parameters was studied and a microkinetic model has been developed, which includes the influences of all major exhaust components.

5.2 Experimental

5.2.1 Catalyst preparation

The catalyst was prepared by wet impregnation of TiO_2 (P25, specific surface area $49 \text{ m}^2/\text{g}$, supplier Degussa) with chromium(III)nitrate nonahydrate (Fluka) as described in a preceding paper (11). A chromium content of 6.84 wt% Cr, corresponding to 10 wt% Cr_2O_3 was used. After drying at $1 \cdot 10^4 \text{ Pa}$ and 363 K for two hours and at 413 K for 8 hours

the catalyst was crushed and sieved to a grain size of 180 to 300 μm . In order to avoid the formation of crystalline CrO_2 upon thermal decomposition of the chromia precursor, the dried catalyst was reduced with pure hydrogen at 523 K for 1 h without pre-calcination, thus producing mainly CrOOH (11). Heating in argon at 773 K for 5 hours resulted in the decomposition of CrOOH to a mixture of poorly crystalline Cr_2O_3 (> 95 wt.%) besides of a minor amount of undecomposed CrOOH . The BET surface area determined by N_2 -physisorption at 77 K using a Micrometrics ASAP 2000 instrument amounted to 49 m^2/g .

5.2.2 Catalytic tests

Steady-state catalytic studies were carried out in the computer controlled apparatus described in paragraph 2.1. The reaction gas mixture consisted of 200-1000 ppm NO (99.0 vol.%, PanGas), 200-1000 ppm NH_3 (99.98 vol.%, PanGas), 0-6 vol.% H_2O (bidistilled) and 0-12 vol.% O_2 (99.995 vol.%, PanGas) in N_2 -balance (99.995 vol.% PanGas). Standard experiments were carried out with a feed containing 1000 ppm NO, 1000 ppm NH_3 , 10 % O_2 in N_2 -balance using 0.35 g of catalyst (180-300 μm sieve fraction) and a reactant flow rate of 200-1000 ml (NTP) min^{-1} (60'000-300'000 h^{-1} (NTP) GHSV) at a constant pressure of 1.1 bar in the temperature range 400 - 520 K.

The selectivities to N_2 and N_2O were calculated according to equation 5-1.

$$S_i = \frac{2 \cdot F_i}{F_{\text{NOin}} + F_{\text{NH}_3\text{in}} - F_{\text{NOout}} - F_{\text{NH}_3\text{out}}} \quad (5-1)$$

Where F_i is the molar flow rate of component i and *in* and *out* refer to the reactor inlet and outlet, respectively.

5.2.3 Kinetic modeling

The model parameters were estimated from the experimental data by linear and non-linear regression analysis (see paragraph 2.3). As objective function the maximum likelihood function of the NO and N₂O partial pressures was chosen.

5.2.4 X-ray photoelectron spectroscopy (XPS)

XPS analysis of the catalyst samples was performed in a Leybold-Heraeus LHS 11 MCD instrument using Mg K α radiation (240 W) to excite photoelectrons. The analyzer was operated at 37.8 eV constant pass energy at an energy scale calibrated versus the Au 4f 7/2 signal at 84.0 eV. Under these conditions the full-width at half-maximum (FWHM) of the Ag 3d_{5/2} line was 0.9 eV. To compensate for the steady state charging effects, binding energies have been normalized with respect to the position of the C 1s signal, resulting from the adsorbed hydrocarbons.

5.2.5 Transmission FTIR spectroscopy

The transmission FTIR spectra were recorded on a Perkin Elmer System 2000 spectrometer. Mixtures of 0.5 mg catalyst sample and KBr (Fluka) were finely ground and agglomerated under pressure (15 MPa, 180 s). The transparent wafers were mounted on a special sample holder in an environmental chamber and heated at 473 K in a flow of dried nitrogen for 1 hour. Before measurements the sample was cooled to 323 K to avoid a broadening of the absorption bands. Spectra were recorded with a resolution of 4 cm⁻¹ in the range of 4000 - 450 cm⁻¹ accumulating 500 scans. Background spectra were recorded under identical conditions with a pure KBr wafer.

5.3 Results

5.3.1 Heat and mass transfer

Due to the small catalyst particle size in comparison to the reactor diameter and a quartz wool layer in front of the catalyst bed, plug flow was established over the whole catalyst bed. Theoretical calculations based on the criterion of Weisz and Prater (26) indicated that no mass transfer limitation occurred in the investigated temperature range. The calculated maximum adiabatic temperature increase for 1000 ppm NO in the feed was about 13 K. The measured experimental increase of the gas temperature for full conversion at the highest space velocity amounted to 1.5 K. Due to the negligible increase of the temperature and the small particle size, temperature gradients in the catalyst bed and catalyst particles were negligible.

5.3.2 Stability of the catalyst

The effect of time on stream on the catalytic behavior of chromia/titania in the selective reduction of NO by NH_3 with and without water in the feed is depicted in Fig. 5-1 for a temperature of 473 K. Starting with a dry feed, NO conversion and the selectivity to N_2O reached steady state within 30 min. Changing to a feed containing 5 % water resulted in an immediate sharp drop in NO conversion from 87 % to 42 %. Simultaneously a pronounced decrease of the undesired formation of N_2O from 1.9 % to 0.5 % was observed. NO conversion further decreased with time on stream to reach a new steady state value of 31 % after two hours, while N_2O selectivity remained constant. The results manifest that the formation of N_2O (73 % decrease) is slightly more inhibited in the presence of water than the reduction of NO to N_2 (64 % decrease).

The previous activity and selectivity of the catalyst was re-established within several minutes if water was removed from the feed. For a catalyst being on stream for 250 h under varying reaction conditions a decrease in catalytic activity, combined with an increase of the formation of N_2O was observed. Note that the same catalyst was used for consecutive measurements at times in the following experiments thus leading to slightly different conversion and selectivity values for similar reaction conditions. The decrease in activity is thereby reflected by the variation of the corresponding pre-exponential factors k_1^0 and k_2^0 .

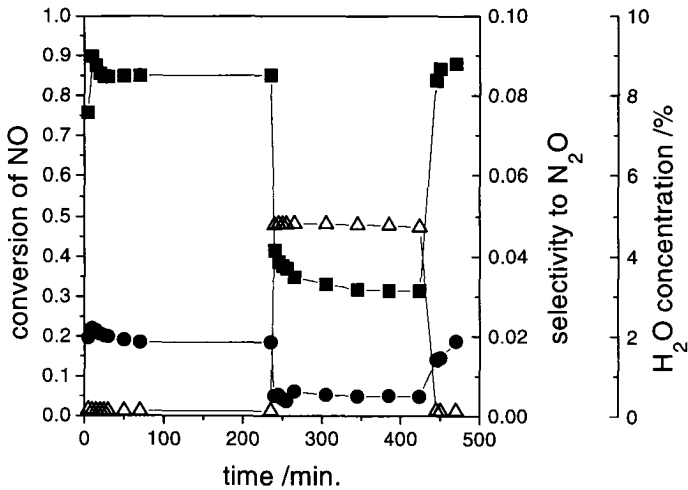


Figure 5-1. NO conversion and selectivity to N_2O as a function of time on stream for a chromia/titania catalyst being alternately exposed to dry and wet feed conditions.

■ NO conversion, ● selectivity to N_2O , △ H_2O concentration, 0 or 5%

H_2O ; gas flow rate = 300 ml/min(NTP), $T_{\text{reactor}} = 473$ K.

5.3.3 Influence of temperature

Fig. 5-2 demonstrates the dependence of the NO conversion and the selectivity to N₂O on the temperature for different gas flow rates. The symbols in this and the subsequent figures indicate measured values, whereas the curves represent the predicted conversions and selectivities from an Eley-Rideal model. A detailed description of the model is presented in a following part of this chapter. The temperature dependence of the NO conversion shows, that 90% NO are converted at 459 K for a flow rate of 300 ml(NTP)/min (Fig. 5-2). Increasing the flow rate resulted in an increase of the temperature to obtain 50% NO conversion from 424 K (300 ml/min) to 448 K (700 ml/min). Note that the amounts of NO and NH₃ converted were equal within the experimental error for all experiments (not shown). From Fig. 5-2 it is also apparent that the selectivity to N₂O is only influenced by the temperature and is independent of the gas flow rate. With raising temperature an increase of the formation of the undesired N₂O is observed.

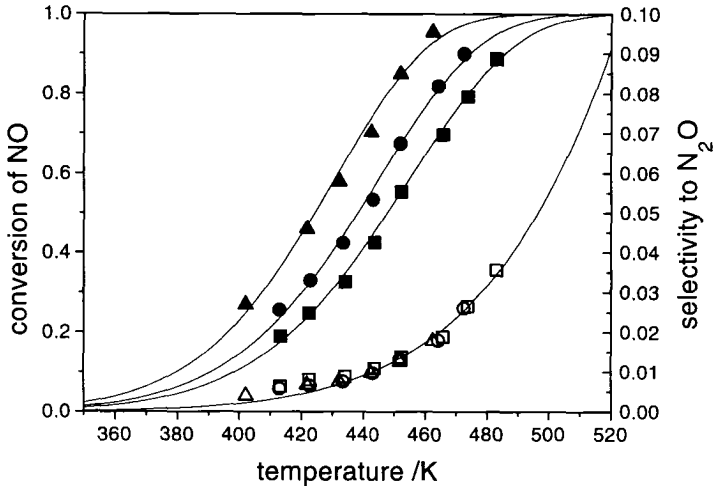


Figure 5-2. Conversion of NO (filled symbols) and selectivity to N₂O (open symbols) as a function of temperature for different gas flow rates.

▲, △ 300 ml(NTP)/min, ●, ○ 500 ml(NTP)/min, ■, □ 700 ml(NTP)/min; Symbols indicate measured values, whereas the conversion and selectivity curves (—) were calculated using the model described by Eqs. 5-2 - 5-5 and the pre-exponential factors $k_1^0 = 1.86\text{E-}2 \text{ m}^3/\text{kg s}$ and $k_2^0 = 2.4\text{E-}4 \text{ m}^3/\text{kg s}$.

5.3.4 Influence of gas flow rate

Fig. 5-3 shows the dependence of NO conversion on the ratio catalyst mass to gas flow (W/F) for different temperatures. Increasing the W/F ratio led to higher NO conversions for all temperatures. Integral analysis of the data presented in Figure 5-3 revealed reaction orders of one with respect to NO and of zero with respect to NH₃. The reaction orders were confirmed by variation of the inlet concentrations of NO and NH₃

in the range of 200 ppm to 1000 ppm. Good agreement of predicted and measured conversions was achieved over the whole experimental range with the model based on an Eley-Rideal mechanism.

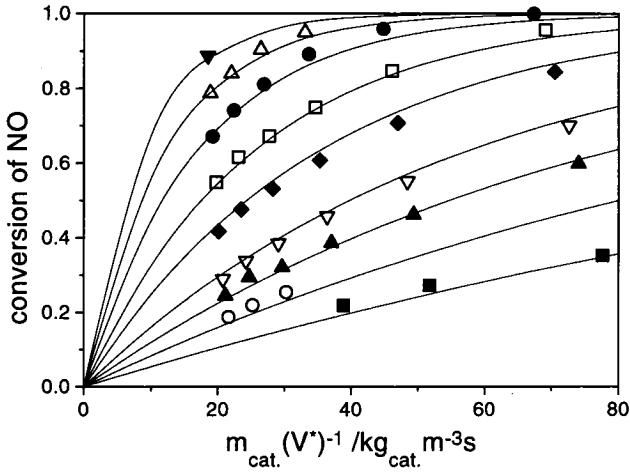


Figure 5-3. Influence of the weight/flow ratio (W/F) on the NO conversion for different temperatures.

■ 402 K, ○ 413 K, ▲ 422 K, ▼ 430 K, ◆ 443 K, □ 452 K, ● 463 K, △ 473K, ▼ 483 K; catalyst weight = 0.35g, gas flow rates = 200 ml/min - 800 ml(NTP)/min. Symbols indicate measured values, whereas the conversion and selectivity curves (—) were calculated using the model described by Eqs. 5-2 - 5-5 and the pre-exponential factors $k_1^0 = 1.86E-2 \text{ m}^3/\text{kg s}$ and $k_2^0 = 2.4E-4 \text{ m}^3/\text{kg s}$.

5.3.5 Influence of the ammonia concentration

Figure 5-4 illustrates the conversion of NO and NH₃ for different NH₃ reactor inlet concentrations. No influence to the conversion of NO was observed as long as more than 15 ppm NH₃ was present at the reactor outlet (not depicted in Figure 5-4).

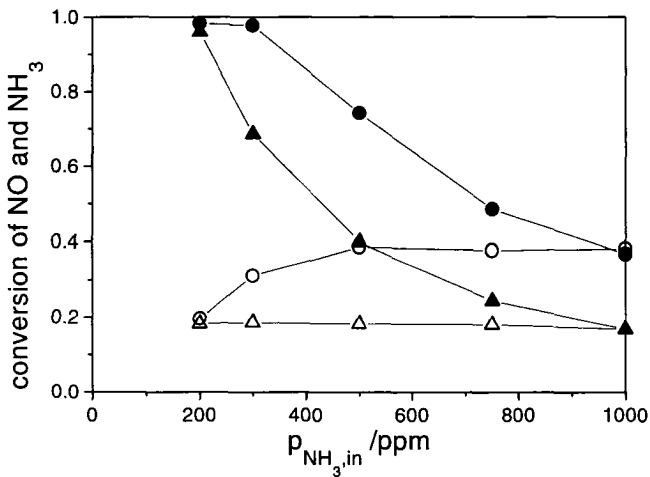


Figure 5-4. NO conversion as a function of the NH₃ reactor outlet concentration.

Δ NO conversion and \blacktriangle NH₃ conversion at 405 K, \circ NO conversion and \bullet NH₃ conversion at 424 K, Feed: 1000 ppm NO, 200 -1000 ppm NH₃, 10% O₂, balance N₂, catalyst weight = 0.4 g, gas flow rates = 500 ml(NTP)/min.

5.3.6 Effect of water

As revealed by Fig. 5-1, the addition of water substantially influenced the conversion of NO. Fig. 5-5A depicts the decrease in activity caused by water concentrations of 1 - 6 vol.% for temperatures in the range 471 K to 512 K. The effect of water on NO conversion is stronger for low temperatures and low concentrations of H₂O. The experimental data presented in Fig. 5-5B show that water has not only an impact on the conversion of NO, but also influences substantially the selectivity to nitrous oxide. Addition of water in the range 1 to 6 vol % strongly suppressed the undesired formation of N₂O, with the effect being more pronounced at higher temperatures where comparably high selectivities to N₂O would be attained in the absence of water. The deviation of measured values from the model predictions is in the range of the experimental error for both NO conversion and N₂O selectivity.

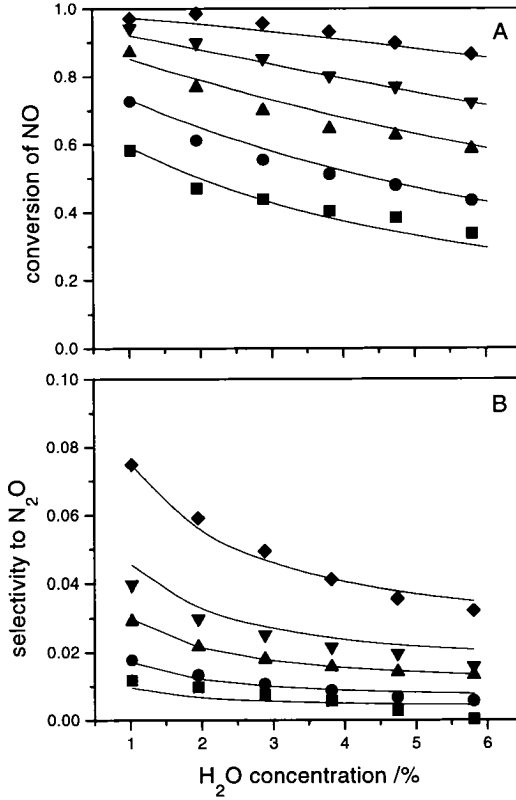


Figure 5-5. NO conversion and selectivity to N₂O as a function of the water concentration in the feed gas for different temperatures.

■ 471 K, ● 481 K, ▲ 492 K, ▼ 500 K, ◆ 512 K; gas flow rate = 500 ml(NTP)/min. Symbols indicate measured values, whereas the conversion and selectivity curves (—) were calculated using the model described by Eqs. 5-2 - 5-5 and the pre-exponential factors $k_1^0 = 1.2\text{E-}2 \text{ m}^3/\text{kg s}$ and $k_2^0 = 3.5\text{E-}4 \text{ m}^3/\text{kg s}$.

5.3.7 Influence of the oxygen concentration

The effect of oxygen on the catalytic behavior is presented in Figs. 5-6 and 5-7. In the absence of oxygen, conversion of NO was negligible in the temperature range investigated, irrespective whether dry or wet conditions were applied. Addition of a low amount of oxygen (1500 ppm) to a dry feed already substantially increased NO conversion, as revealed by the measurements at 456 K (Fig. 5-6). The increase in NO conversion was most pronounced for oxygen concentrations up to 2 vol.% for all temperatures, whereas for concentrations exceeding 2 vol.% O₂ the catalyst exhibited an almost linear raise in activity. No significant dependence of the selectivity to N₂O on the oxygen concentration was found.

In the presence of 5 vol.% water in the feed gas a similar behavior was observed (Fig. 5-7), although a linear dependence of NO conversion on oxygen concentration was only found for higher O₂ levels. Similar slopes of the linear raise were observed for oxygen concentrations higher than 6% with both dry and wet feeds.

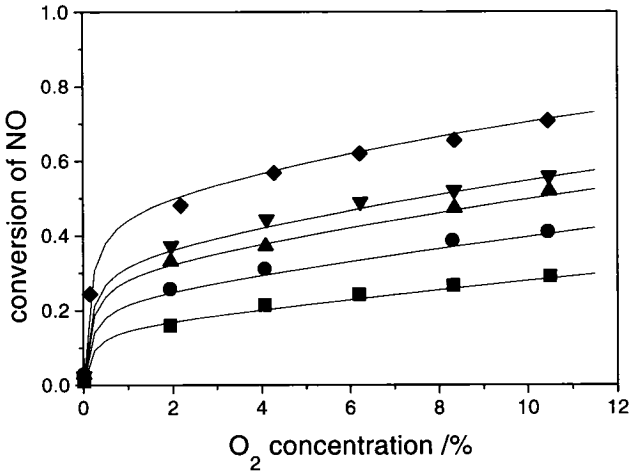


Figure 5-6. Influence of oxygen concentration in the feed gas on the NO conversion for a dry feed.

■ 420 K, ● 431 K, ▲ 440 K, ▼ 444 K, ◆ 456 K;
 gas flow rate = 500 ml(NTP)/min. Symbols indicate measured values,
 whereas the conversion and selectivity curves (—) were calculated using
 the model described by Eqs. 5-2 - 5-5 and the pre-exponential factors k_1^0
 $= 1.76E-2 \text{ m}^3/\text{kg s}$ and $k_2^0 = 5.8E-4 \text{ m}^3/\text{kg s}$.

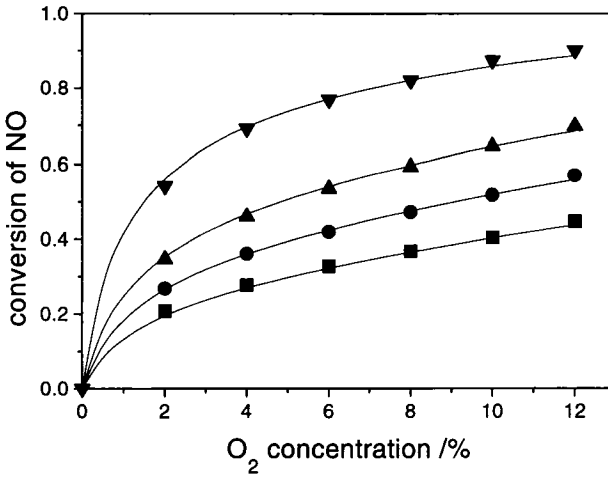


Figure 5-7. Influence of oxygen concentration in the feed gas on the NO conversion for a feed containing 5 % H₂O.

■ 489 K, ● 497 K, ▲ 505 K, ▼ 520 K; gas flow rate = 500 ml(NTP)/min. Symbols indicate measured values, whereas the conversion and selectivity curves (—) were calculated using the model described by Eqs. 5-2 - 5-5 and the pre-exponential factors $k_1^0 = 0.7E-2 \text{ m}^3/\text{kg s}$ and $k_2^0 = 7.5E-4 \text{ m}^3/\text{kg s}$.

5.3.8 Influence of the feed gas composition

The dependence of the formation of N₂O on varying the feed gas composition is illustrated in Fig. 5-8 together with the corresponding conversions of NO and NH₃. Feed A had a composition of 1000 ppm NO, 1000 ppm NH₃, 10% O₂ and 5% H₂O. Feed B contained no nitric oxide, and feed C no ammonia, respectively. Starting with feed A the conversions of NO and NH₃ were comparable within the experimental error. After switching off NO (feed B), the conversion of NH₃ dropped from 86 % to 10 % and the

N_2O concentration decreased simultaneously from 88 ppm to 10 ppm, corresponding to a constant selectivity to N_2O of 10 %. The finding shows that the direct oxidation of ammonia by oxygen is comparably small at 505 K and moreover results in a similar selectivity to N_2O . In the absence of ammonia in the feed gas (feed C) NO conversion decreased to zero and the formation of N_2O was completely inhibited. Presented results obtained with feed A and feed B demonstrate that nitrogen and nitrous oxide are predominantly produced by the reaction of NH_3 with NO at 505 K and that the contribution by direct oxidation of ammonia is negligible.

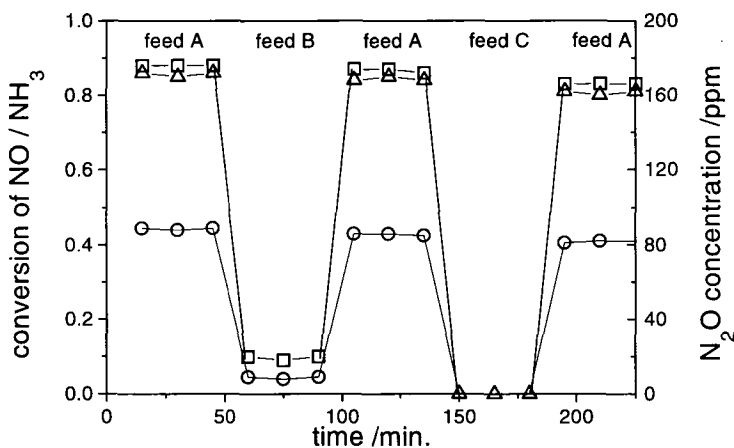


Figure 5-8. Influence of feed gas composition on the formation of N_2O and on conversion of NO and NH_3 , respectively.

□ NH_3 conversion, △ NO conversion, ○ N_2O concentration; feed A: 1000 ppm NO, 1000 ppm NH_3 , 10 % O_2 , 5 % H_2O , balance N_2 ; feed B: 1000 ppm NH_3 , 10 % O_2 , 5 % H_2O , balance N_2 ; feed C: 1000 ppm NO, 10 % O_2 , 5 % H_2O , balance N_2 . Gas flow rate = 500 ml(NTP)/min, $T_{\text{reactor}} = 505 \text{ K}$.

5.3.9 Effect of SO₂

The activity of the catalyst was irreversibly affected by the presence of sulfur dioxide in the feed gas even at low concentrations of SO₂. The poisoning effect of sulfur dioxide as a function of the SO₂ concentration is illustrated in Fig. 5-9. At a temperature of 503 K 30 ppm of SO₂ in the feed gas are sufficient for a distinct decrease of the NO conversion. The degree of deactivation is a function of the SO₂ concentration and exposure time. During the deactivation SO₂ is completely consumed. After changing to a feed without SO₂ the activity remained stable. Increasing the SO₂ concentration in steps to 60 ppm and further to 90 ppm led to a continuous decrease in NO conversion, while switching off SO₂ resulted in stable activities. No SO₃ was detected in the product stream over the whole experimental period. Running the catalyst at 503 K using the same feed stream without SO₂ for three hours revealed no change in catalytic activity and the conversion remained on the low level. Attempts were made to regenerate the catalyst by heating at 573 K in a stream of pure nitrogen for 3 hours. During this treatment compounds such as ammonium sulfates or ammonium bisulfates formed in the lower temperature range should decompose. However, neither SO₂ nor SO₃ were detected in the effluent gas stream and a subsequent conversion measurement at 503 K showed no increase in activity. If SO₂ was added at 573 K a further deactivation was observed. This indicated that the formation of ammonium sulfates or ammonium bisulfates can not exclusively explain for the poisoning effect. Moreover, no loss of specific surface area and no significant change in porosity occurred during the SO₂ poisoning experiments. Additional catalytic tests with the partly poisoned catalyst in the temperature range 523 to 573 K, showed that not only the reduction of NO to N₂

but also the undesired formation of N_2O was affected by the poisoning. At 573 K and a gas composition of 10 % O_2 , 1000 ppm NO and 1000 ppm NH_3 in N_2 balance 100% conversion and a selectivity of 98% to N_2 were obtained. Based on the assumption of different sites being responsible for the formation of N_2 and N_2O , we presume that the sites which are involved in the undesired formation of nitrous oxide are much stronger affected by SO_2 than sites which catalyze the reduction of NO to N_2 .

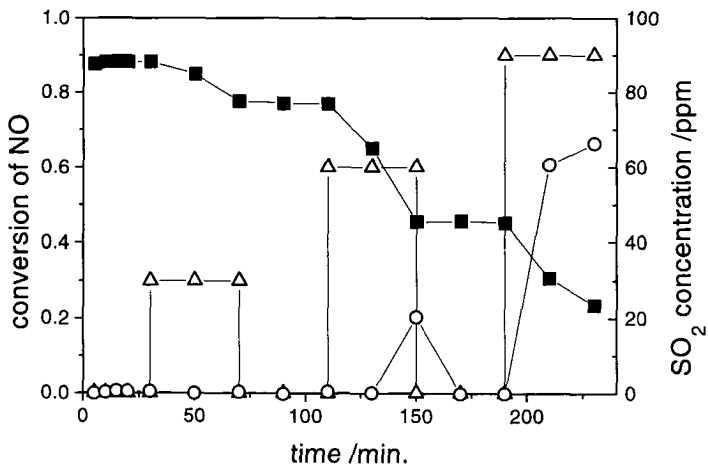


Figure 5-9. Effect of SO_2 on the conversion of NO.

△ SO_2 inlet concentration, ○ SO_2 outlet concentration, ■ NO conversion; feed composition: 1000 ppm NO, 1000 ppm NH_3 , 10% O_2 , 5% H_2O , 0-90 ppm SO_2 , balance N_2 , gas flow rate = 300 ml(NTP)/min,

$T_{\text{reactor}} = 503 \text{ K}$.

5.3.10 XPS analysis

In order to elucidate the nature of SO₂ poisoning, XPS measurements were made either with fresh catalyst samples or with catalysts exposed to SCR conditions with and without SO₂ in the feed. Part of the samples were washed three times with bidistilled water at a temperature of 353 K for 8 hours and subsequently dried under vacuum at 400K. XPS measurements were made with the washed and unwashed samples. Fig. 5-10 shows the sulfur 2p signal which was only observed for the samples exposed to feeds containing SO₂. The binding energy of 169.1 eV indicates that sulfur is present as a sulfate species (27, 28), but whether it is an adsorbed species or part of an ammonium or chromium complex is not clear. Dickinson et al. (29) reported a sulfur 2p binding energy of 169.1 eV with an asymmetric component on the higher binding energy side for chromium sulfate. The binding energy of the S 2p orbital of (NH₄)₂SO₄ is found at 168.3 eV (30), which is substantially lower than the value observed in the present work. Moreover, no significant changes in the signals for the other elements (O 1s, Cr 2p, C 1s), and especially of the N 1s signal, were observed. In addition, the signal due to sulfur is still present after treatment of the catalyst with water (Fig. 5-10B), which should eliminate soluble ammonium sulfate. This suggests that predominantly a sulfate type complex of chromium (or titanium) is present on the catalyst surface. Upon treatment of the catalyst with water at 353 K, the semiquantitative analysis revealed a decrease of the sulfur surface concentration from 1.6 at.% to 1.2 at.% and a concomitant increase of the chromium surface concentration from 7.7 to 9.3 at.%, thus indicating that the detected sulfate species could partly originate from soluble ammonium sulfates or ammonium bisulfates.

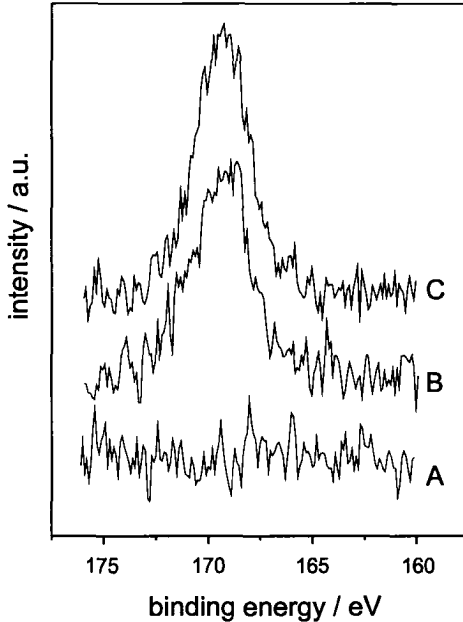


Figure 5-10. XP spectra of S 2p core level of (A) fresh catalyst, (C) catalyst after SCR reaction in a feed containing 90 ppm SO₂, and (B) the same catalyst after subsequent treatment with water at 353 K for 8 hours to remove soluble sulfate species.

5.3.11 Transmission FTIR-spectroscopy

The transmission FTIR measurements were made with catalyst samples after use in SCR with and without SO₂ in the feed. Only one weak additional band at 1115 cm⁻¹ was perceptible (Fig. 5-11) upon exposure of the catalyst to a feed containing 90 ppm SO₂. No other significant differences in the spectra were observed. The reported ranges of the characteristic absorptions of sulfates (1000 - 1420 cm⁻¹) and sulfites (980 - 1225 cm⁻¹) (31) include the observed band. This is a further indication that a sulfate or sulfite

type species was formed on the catalyst surface during the exposure to the SO_2 containing SCR-feed.

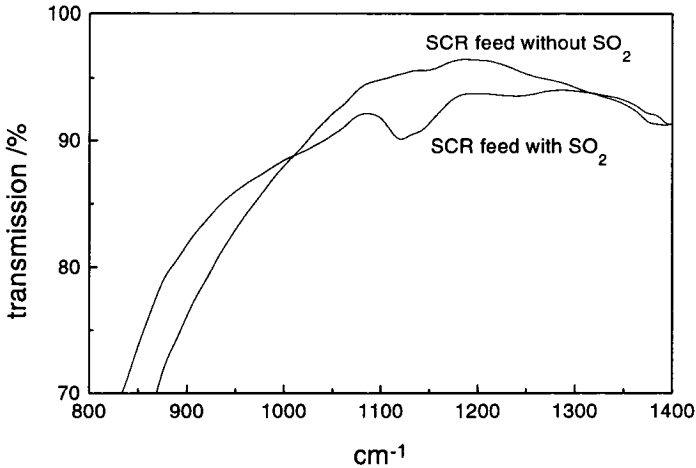
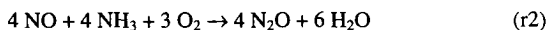
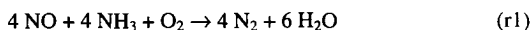


Figure 5-11. Transmission FTIR-spectra of a catalyst after SCR reaction with a SO_2 free feed and with a feed containing 90 ppm SO_2 , respectively.

5.3.12 Kinetic modeling

The kinetic model used to describe the experimental results was based on the overall stoichiometric reactions expressed by the Equations r1 and r2. Equation r1 represents the main reaction of the selective catalytic reduction of NO for an oxygen containing flue gas, whereas Equation r2 describes the side reaction responsible for the undesired formation of nitrous oxide. In all experiments the amounts of NO and NH_3 consumed during the reaction were comparable within the experimental error, indicating that NO reacts stoichiometrically with NH_3 under the reaction conditions investigated. Regarding the stoichiometry of the side reaction, the experimental results depicted in

Fig. 5-8 suggest that in the presence of water N_2O is predominantly formed by the stoichiometric reaction of NO with NH_3 in the investigated temperature range. However, substantial amounts of ammonia are oxidized directly to N_2 and N_2O in the absence of NO (Fig. 5-8). These findings support the assumption of a reaction stoichiometry according to Equations r1 and r2 under typical SCR conditions over Cr_2O_3/TiO_2 .



Different approaches based on Langmuir-Hinshelwood and Eley-Rideal models were investigated for setting up the kinetic equations. The number of kinetic parameters was minimized in order to prevent an overfitting of the obtained results. The best description of the kinetics was achieved with the following approach:

- The reaction rate is first order in NO and zeroth order in ammonia for the main and the side reaction.
- The inhibition of the main and side reaction by water is caused by a Langmuir adsorption of water on the active sites.
- The reoxidation of the catalyst determines the number of the active sites and can occur with adsorbed oxygen as well as with oxygen from the gas phase.
- Water inhibits the reoxidation by a competitive Langmuir type adsorption

The reaction orders of NH_3 and NO were established by varying the inlet concentrations of NO and NH_3 in the range of 200 ppm to 1000 ppm and by integral analysis, which involves a comparison of the experimental data with values predicted by the model. The zeroth order in ammonia suggests a strong adsorption of ammonia. The assumption that the main and the side reaction have the same reaction orders implies that a variation of the NO or NH_3 concentration has no effect on selectivity. Figure 5-2 indeed shows that the same selectivity is observed for different conversions upon varying the gas flow rate at a constant temperature. As different conversions involve different concentrations of NO and NH_3 , this finding confirms our assumption.

The inhibition by water could be caused by the competitive adsorption of water and ammonia, but no sufficient fitting was achieved under this assumption. Good fitting was obtained on condition that part of the active sites are covered independently by water. The temperature dependencies of the adsorption equilibrium constants $K_{\text{H}_2\text{O}_{(1)}}$ and $K_{\text{H}_2\text{O}_{(2)}}$ were significant which allowed us to estimate the heats of adsorption ($\Delta H_{\text{H}_2\text{O}}$) and the pre-exponential factors ($K^0_{\text{H}_2\text{O}}$) for the main and the side reaction (Table 5-1).

For the reoxidation of the catalyst gaseous as well as adsorbed oxygen were taken into account. This can be justified by the observed sharp increase of NO conversion in the range of low oxygen concentrations and the linear dependence in the higher O_2 concentration range. Worse fitting was obtained if only one type of reoxidation was considered. An empirical weighing factor was introduced to account for the different influence on reoxidation by either gaseous or adsorbed oxygen. The promoting effect of oxygen has to be the same for the main and the side reaction because the selectivity was independent of the oxygen concentration. The observed inhibiting effect of water on the

adsorption of oxygen was considered in the model by taking into account competitive adsorption of O₂ and H₂O.

In order to prevent any distortion of the parameter estimation by the observed slow decrease of catalytic activity and the simultaneous slight increase of the selectivity to N₂O with time on stream, the pre-exponential factors were adjusted according to the aging of the catalyst. Separate parameter estimation with used and fresh catalysts showed that only the pre-exponential factors $k_i^0(T_{ref.})$ and $k_2^0(T_{ref.})$ changed. Based on this assumption the reaction rates for the reduction to N₂ (r_1) and for the formation of N₂O (r_2), respectively, are described by the following equations:

$$r_1 = k_1 \left(np_{O_2} + \frac{K_{O_2} p_{O_2}}{1 + K_{O_2} p_{O_2} + K_w p_{H_2O}} \right) \frac{1}{1 + K_{H_2O(i)} p_{H_2O}} p_{NO} \quad (5-2)$$

$$r_2 = k_2 \left(np_{O_2} + \frac{K_{O_2} p_{O_2}}{1 + K_{O_2} p_{O_2} + K_w p_{H_2O}} \right) \frac{1}{1 + K_{H_2O(i)} p_{H_2O}} p_{NO} \quad (5-3)$$

$$k_i(T) = k_i^0(T_{ref.}) \exp \left(\frac{-E_{A_i}}{R} \left(\frac{1}{T} - \frac{1}{T_{ref.}} \right) \right) \quad (5-4)$$

$$K_{H_2O(i)}(T) = K_{H_2O(i)}^0(T_{ref.}) \exp \left(\frac{-\Delta H_{H_2O(i)}}{R} \left(\frac{1}{T} - \frac{1}{T_{ref.}} \right) \right) \quad (5-5)$$

$$T_{ref.} = 450K$$

To reduce the correlation between the pre-exponential factors ($k_i^0(T_{ref.})$, $K_{H_2O}^0(T_{ref.})$), the activation energies (E_{A_i}), and the enthalpies of adsorption (ΔH_i), the reaction rate constants (k_i) and the equilibrium constant of adsorption ($K_{H_2O(i)}$) were expressed as proposed by Himmelblau (32). All estimated parameters of the kinetic model are listed in Table 5-1.

Table 5-1. Estimated parameters for kinetic model described by Eqs. 5-2 - 5-5.

parameter	value	standard deviations	units
k_1^0	1.9e-2 - 0.7e-2	0.01e-2 - 0.06e-2	m ³ /kg s
E_{A_1}	60	0.8	kJ/mol
k_2^0	2.4e-4 - 7.5e-4	0.04e-4 - 0.6e-4	m ³ /kg s
E_{A_2}	115	1.6	kJ/mol
$K_{H_2O_{(l)}}^0$	6.0e-4	0.7e-4	Pa ⁻¹
$\Delta H_{H_2O_{(l)}}$	-43	4	kJ/mol
$K_{H_2O_{(g)}}^0$	1.5e-2	0.3e-2	Pa ⁻¹
$\Delta H_{H_2O_{(g)}}$	-77	4	kJ/mol
n	8.9e-5	0.7e-5	Pa ⁻¹
K_{O_2}	4.8e-3	0.6e-3	Pa ⁻¹
K_w	1.2e-3	0.3	Pa ⁻¹

5.4 Discussion

The kinetic behavior of the 10 wt.% Cr₂O₃/TiO₂ catalyst is comparable with findings of Wong and Nobe (22) for titania supported vanadia and chromia catalysts for which a reaction rate first order in NO and zeroth order in NH₃ is proposed. The integral analysis of the experimental data revealed a zeroth order reaction with respect to NH₃, suggesting that the catalyst is completely covered by ammonia under reaction conditions, which is reasonable for low temperatures. At higher temperatures and for low ammonia concentrations the coverage is not complete and ammonia adsorption has

to be considered in the model (33). Based on temperature-programmed desorption and *in situ* diffuse reflectance FTIR measurements, Schneider et al. (34) proposed that the presence of Brønsted bound ammonia is a necessary requirement for the reduction of NO to N₂ over CrO_x/TiO₂.

The observed first-order reaction with respect to NO indicates that gaseous NO is involved in the rate limiting step. This finding would support an Eley-Rideal mechanism, as proposed similarly for vanadia based catalysts. The same reaction order in NO would be expected if the adsorption of NO is involved in the rate limiting step. As opposed to vanadia based catalysts, where the adsorption of NO has only been reported under reducing conditions (35, 36), the adsorption of NO on chromia was observed by several authors. Kugler et al. (37) suggested that nitric oxide adsorbs on reduced chromia surface in the form of a *cis*-N₂O₂ dimer and as an NO₂ chelate surface complex. The same surface species were observed on α-Cr₂O₃ but not on amorphous chromia (38). On α-Cr₂O₃, these two species are discussed to be formed by oxidation of adsorbed NH₃ molecules and are intermediates on the reaction pathway to N₂O (38). Schneider et al. (9) observed by FTIR bands due to surface bound NO under reaction conditions on CrO₂/TiO₂, but not on Cr₂O₃/TiO₂. The question whether adsorbed or gaseous NO reacts with ammonia on the surface of chromium based catalysts is still unresolved and no conclusive statement can be given based on experimental evidence.

In analogy with supported vanadia catalysts, Schneider et al. (9) observed Brønsted sites even at higher temperatures for Cr₂O₃/TiO₂ catalysts. During SCR, N₂O is formed by oxidation of Lewis-bound ammonia with NO and/or oxygen present in the feed gas. In the case of Cr₂O₃, with no adsorbed NO, oxidation of ammonia to N₂O occurs at temperatures higher than 450 K (9). In the absence of NO only Lewis bound

ammonia is observed above 420 K, which is oxidized to N_2 and N_2O (34). At higher temperatures ammonia oxidation to NO is favoured in the presence of oxygen. In our experiments we observed in the presence of NO that N_2O was mainly formed by the reaction of NH_3 with NO (Fig. 5-8). The direct oxidation of NH_3 by O_2 to N_2 , N_2O and H_2O was negligible in comparison to the main reaction. However, based on our results it can not be excluded that NH_3 is oxidized to NO in a first step, followed by subsequent reaction to N_2 and N_2O under certain conditions. The fact that differences in the selectivity of used and fresh catalysts have only an influence on the pre-exponential factors indicates that the reaction to N_2 and N_2O , respectively, occur on different sites in accordance with findings by Schneider et al. (34, 9). The estimated adsorption enthalpy of water amounted to -43 kJ/mol for the reaction to N_2 , and -77 kJ/mol for the reaction to N_2O , respectively, which is a further indication of different sites being responsible for the main and the side reaction. Taking into account the estimated adsorption enthalpies and the observed inhibition of the NO conversion, it can be assumed that water adsorbs stronger on a Lewis site than on a Brønsted site.

The role of water in the reversible inhibition of the SCR reaction is not fully understood yet. Water can be involved in the rate limiting step or block the active sites. If the inhibition by water is due to a competitive adsorption between water and ammonia, the reaction order of ammonia should not equal zero in the presence of water. In the model we assumed kinetics of first order in NO and zeroth order in NH_3 in the presence and absence of water. These assumptions necessitate a linear temperature dependency of the reaction rate in the Arrhenius-type plot. The data depicted in Figure 5-12 confirm our assumption of the reaction orders for NO and NH_3 in presence and absence of water in the feed gas.

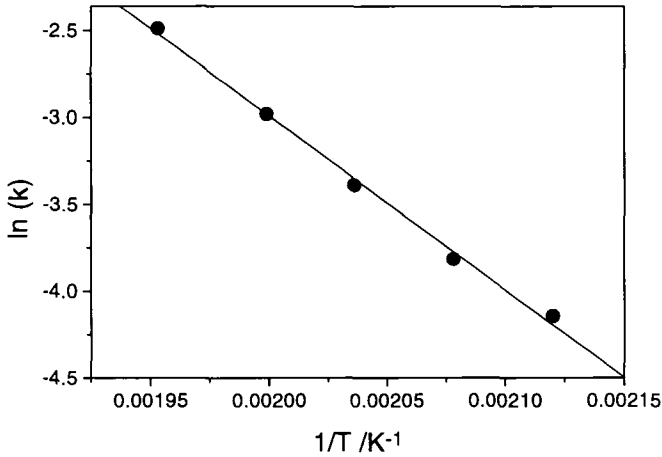


Figure 5-12. Arrhenius type plot for kinetic tests under standard conditions with a feed containing 5 % H_2O ; gas flow rate = 500 ml(NTP)/min.

The variation of ammonia concentration in the feed gas led to small changes of the NO conversion, which were in the range of the experimental error and could also be caused by the observed slow deactivation of the catalyst in the presence of water at high temperatures. An estimation of the adsorption constant of ammonia in a statistically significant way was not possible due to the lack of accurate data at low NH_3 concentrations. No successful fitting was achieved with models based on an assumption of a competitive adsorption between water and ammonia.

Oxygen plays a crucial role in SCR for vanadia and chromia based catalysts (16, 39). Schneider et al. (34) demonstrated by TPD experiments that CrO_x/TiO_2 reduced by ammonia is inactive for the selective catalytic reduction of NO. They suggested that a partially oxidized state of the surface must be maintained for SCR. A marked increase in activity and a concomitant decrease in the selectivity to N_2O upon addition of 0.1 % O_2

to the SCR feed was also reported for amorphous chromia by Duffy et al. (16). In accordance with these results we found that in the absence of oxygen the reaction rate collapsed. Below 1 vol.% oxygen in the dry feed, and below 2 vol.% oxygen for a feed containing 5 vol.% water, a sharp raise in activity was observed with increasing oxygen concentration. For higher oxygen concentrations, a smaller linear increase was found (Figs. 5-6 and 5-7). The description of the kinetic conversion curves by a power law approach, implementing a Freundlich isotherm, was not satisfactory. By using a Temkin isotherm good fitting was only achieved for the range between 2 and 10 vol.% oxygen and by assuming a pure Langmuir isotherm, only the concentration range below 5 vol.% could be fitted properly. The linear dependence of NO conversion on oxygen concentration led us to the assumption that an additional path of reoxidation of the catalyst takes place, which involves gas phase oxygen and which is significant for higher oxygen partial pressures. This assumption in combination with the model based on a Langmuir-type adsorption resulted in the best description of the oxygen dependency for the investigated experimental range. Water in the feed gas inhibited the path of the reoxidation via adsorbed oxygen. The inhibition was significant and was taken into account by a competitive adsorption of oxygen and water. The adsorption equilibrium constant was about four times smaller for water than for oxygen.

The nature of SO₂ poisoning of the chromia on titania catalyst differs from fouling effects caused by ammonium sulfate deposition observed on vanadia based catalysts, where the effect is reversible (18). Ammonium sulfate or bisulfate decomposes at higher temperatures and no fouling is expected for reaction temperatures above 530 K. In our case the catalyst was also poisoned at temperatures of 573 K, as well as in the presence of low SO₂ concentrations. Attempts to reactivate the catalyst either by heating in pure

nitrogen at 573 K, or by washing with water failed. Note that *no significant change* of the specific surface area and the pore size distribution was perceptible after the SO₂ poisoning experiments. Observed changes of the selectivity after the exposure to SO₂ indicate that the process of poisoning may be different for the sites responsible for N₂ and N₂O formation, respectively. The sites which produce N₂O are mainly poisoned by SO₂. XPS as well as FTIR measurements revealed the presence of sulfate species on the catalyst surface. The affinity of these species to the Lewis acid sites seems to be stronger than to the Brønsted sites. This is in accordance with the stronger inhibition by water and the postulated stronger adsorption of ammonia on Lewis acid sites (36). Lower SCR activity upon deposition of sulfate ions on amorphous chromia was attributed by Zhang et al. (20) to strong adsorption of NH₃ which prevents chromia from reacting with NO.

5.5 Conclusions

Chromia supported on titania exhibits high activity and selectivity to N₂ in the catalytic reduction of NO in the temperature range 400 - 520 K. Applying a modified preparation procedure resulted in a catalyst containing > 95 wt.% poorly crystalline Cr₂O₃, which shows significantly lower tendency for N₂O formation compared to CrO₂ or crystalline α -Cr₂O₃.

The addition of water decreases NH₃ and NO conversion and increases the selectivity to N₂. The effect of water on activity and selectivity is reversible. Similar as with vanadia based catalysts, the activity collapsed in the absence of O₂ in the feed gas. Low amounts of oxygen resulted in a sharp increase of the reaction rate. The addition of

SO₂ led to irreversible poisoning of the catalyst, which restricts application of this catalyst to SO₂ free waste gases.

With a model based on an Eley-Rideal mechanism good prediction of the kinetic behavior was obtained for the temperature range 400-520 K and for a SO₂ free feed gas.

5.6 Notation

m_{cat} = catalyst mass, kg

V^* = gas flow (NTP), m³/s

r_i = reaction rate, Pa m³ / kg s

k_i = reaction rate constant, m³ / kg s

K_A = adsorption equilibrium constant of component A, Pa⁻¹

k_i^0 = pre-exponential factor of the reaction rate constant, m³ / kg s

$K_{\text{H}_2\text{O}(g)}^0$ = pre-exponential factor of the adsorption equilibrium constant of H₂O, Pa⁻¹

$\Delta H_{\text{H}_2\text{O}(g)}$ = adsorption enthalpie of water, kJ/mol

n = empirical weighting factor for the reoxidation, -

5.7 References

1. Bosch, H. and Janssen, F., *Catalysis Today* **2**, 369 (1988).
2. Curry-Hyde, E. and Baiker, A., *Ind. Eng. Chem. Res.* **29**, 1985 (1990).
3. Engweiler, J.; Nickl, J.; Baiker, A.; Köhler, K.; Schläpfer, C. W. and von Zelewsky, A., *J. Catal.* **145**, 141 (1994).

4. Curry-Hide, H. E.; Musch, H. and Baiker, A., *Appl. Catal.* **65**, 211 (1990).
5. Duffy, B. L.; Curry-Hyde, H. E.; Cant, N. W. and Nelson, P. F., *J. Catal.* **154**, 107 (1995).
6. Schraml-Marth, M.; Wokaun, A.; Curry-Hyde, H. E. and Baiker, A., *J. Catal.* **133**, 415 (1992).
7. Wong, W. C. and Nobe, K., *Ind. Eng. Chem. Prod. Res. Dev.* **25**, 179 (1986).
8. Köhler, K.; Engweiler, J.; Viebrock, H. and Baiker, A., *Langmuir* **11**, 3423 (1995).
9. Schneider, H.; Maciejewski, M.; Köhler, K.; Wokaun, A. and Baiker, A., *J. Catal.* **157**, 312 (1995).
10. Maciejewski, M.; Köhler, K.; Schneider, H. and Baiker, A., *J. Solid State Chem.* **119**, 13 (1995).
11. Köhler, K.; Maciejewski, M.; Schneider, H. and Baiker, A., *J. Catal.* **157**, 301 (1995).
12. Bauerle, G. L.; Wu, S. C. and Nobe, K., *Ind. Eng. Chem. Prod. Res. Dev.* **17**, 117 (1978).
13. Inomata, M.; Miyamoto, A. and Murakami, Y., *J. Catal.* **62**, 140 (1980).
14. Jung, J. and Panagiotidis, T., *Chemie im Kraftwerk 1990*, 1 (1990).
15. Odenbrand, C. U. I.; Gabrielsson, P. L. T.; Brandin, J. G. M. and Andersson, L. A. H., *Appl. Catal.* **78**, 109 (1991).
16. Duffy, B. L.; Curry-Hyde, H. E.; Cant, N. W. and Nelson, P. F., *Appl. Catal. B: Environmental* **5**, 133 (1994).
17. Willey, R. J.; Lai, H. and Peri, J. B., *J. Catal.* **130**, 319 (1991).
18. Kittrell, J. R.; Eldridge, J. W. and Conner, W. C., *Catalysis* **9**, 126 (1992).

19. Yang, R. T.; Chen, J. P.; Kikkinides, E. S. and Cheng, L. S., *Ind. Eng. Chem.* **31**, 1440 (1992).
20. Zhang, G.; Buckingham, S.; Curry-Hyde, H. E. and Cant, N., *APCChE* **3**, 31 (1993).
21. Niiyama, H.; Murata, K. and Echigoya, E., *J. Catal.* **48**, 201 (1977).
22. Wong, W. C. and Nobe, K., *Ind. Eng. Chem. Prod. Res. Dev.* **25**, 179 (1986).
23. Nam, I. S.; Eldridge, J. W. and Kittrell, J. R., *Ind. Eng. Chem. Prod. Res. Dev.* **25**, 186 (1986).
24. Robinson, W. R. A. M.; van Ommen, J. G.; Woldhuis, A. and Ross, J. R. H., *Proceedings of the 10th International congress on Catalysis, 19-24 July, Budapest, Hungary*, 2673 (1992).
25. Tufano, V. and Turco, M., *Appl. Catal. B: Environmental* **2**, 133 (1993).
26. Weisz, P. B. and Prater, C. D., *Advances in catalysis and related subjects* **6**, 144 (1954).
27. Briggs, D. and Seah, M. P., "Practical Surface Analysis by Auger and X-Ray Photoelectron Spectroscopy." J. Wiley, Chichester, 1985.
28. Wagner, C. D. et al., "Handbook of X-Ray Photoelectron Spectroscopy.", Perkin Elmer (Physical Electronics Division), Eden Prairie, 1978.
29. Dickinson, T.; Povey, A. F. and Sherwood, P. M. A., *J. Chem. Soc. Faraday Trans. I* **72**, 686 (1976).
30. Barbaray, B.; Contour, J. P. and Mouvier, G., *Env. Sci. Technol.* **12**, 1294 (1978).
31. Pretsch, E.; Seibl, J.; Simon, W. and Clerc, P. D., "Strukturaufklärung organischer Verbindungen mit spektroskopischen Methoden", Springer-Verlag, Berlin, 1981.

32. Himmelblau, D. M., "Process Analysis by Statistical Methods" Wiley, New York, 1970.
33. Efstathiou, A. M. and Fliatoura, K., *Appl. Catal. B: Environmental* **6**, 35 (1995).
34. Schneider, H.; Scharf, U.; Wokaun, A. and Baiker, A., *J. Catal.* **147**, 545 (1994).
35. Odriozola, J. A.; Heinemann, H.; Somorjai, G. A.; la :Banda, J. F. G. d. and Pereira, P., *J. Catal.* **119**, 71 (1989).
36. Srnak, T. Z.; Dumesic, J. A.; Clausen, B. S.; Törnqvist, E. and Topsøe, N.-Y. *J. Catal.* **135**, 246 (1992).
37. Kugler, E. L.; Kadet, A. B. and Gryder, J. W., *J. Catal.* **41**, 72 (1976).
38. Schraml-Marth, M.; Wokaun, A.; Curry-Hyde, H. E. and Baiker, A., *J. Catal.* **134**, 75 (1992).
39. Janssen, F. J. J. G.; v. den Kerkhof, F. M. G.; Bosch, H. and Ross, J. R. H., *J. Phys. Chem.* **91**, 5921 (1987).

Leer - Vide - Empty

Comparison of the investigated catalysts

6.1 Catalytic performance in the low temperature range

The comparison of the performance of the catalysts was carried out using the proposed kinetic models to calculate NO conversion and selectivities to N_2O for the different catalysts. In the case of the CrO_x/TiO_2 catalyst the kinetic parameters estimated with fresh catalyst samples were used to exclude deactivation effects. It is obvious from Figure 6-1 that for a dry feed the vanadia-titania aerogel exhibited the highest NO conversion rate, followed by the titania supported chromium oxide catalyst and the commercial vanadia based catalyst. The commercial catalyst was less and the chromoxide catalyst most affected by water. Significant formation of the undesired nitrous oxide was only observed for the chromium oxide on titania catalyst. The addition of 5% water to the dry feed suppressed NO conversion for all catalysts (Fig. 6-2). The comparison of the temperature dependence of the undesired formation of nitrous oxide for CrO_x/TiO_2 shows a lower selectivity for the feed containing 5% water.

The highest estimated activation energy was obtained for the vanadia based commercial catalyst with 99 kJ/mol for the wet feed, and 87 kJ/mol for the dry feed, respectively. The higher activation energy in the presence of water, may be due to the adsorption of water. Considering a Langmuir type adsorption the adsorption equilibrium

constant of water decreases exponentially with increasing temperature (1). Due to this temperature dependence, the adsorption of water can cause an increase of the apparent activation energy.

For the aerogel catalyst with a several times higher vanadia content than the commercial catalyst the estimated activation energy amounted to 60 kJ/mol. This is in accordance with the findings of Amiridis and Solar (2), who found a significant decrease in activation energy with increasing vanadia surface concentration in presence and absence of H_2O and SO_2 . A similar activation energy of 60 kJ/mol was observed for $\text{CrO}_x/\text{TiO}_2$.

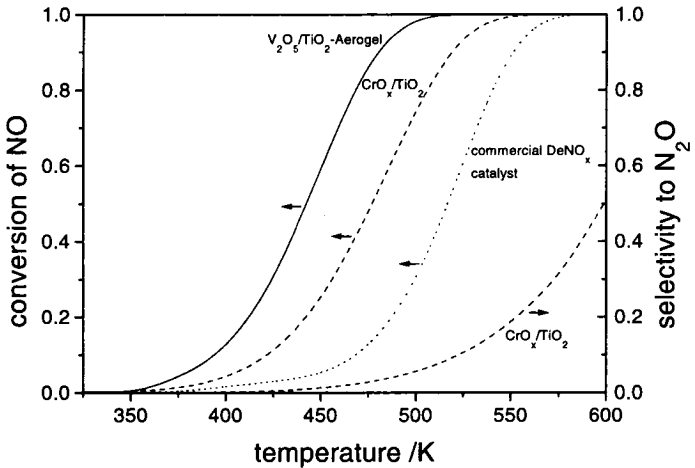


Figure 6-1. NO conversion and N_2O selectivity versus temperature for the different catalysts in the absence of water.

Simulation conditions: feed: 10% O_2 , 1000 ppm NO, 1000 ppm NH_3 , balance N_2 , 1.1 bar pressure, gas flow = 500 ml(NTP)/min, catalyst weight = 0.1g.

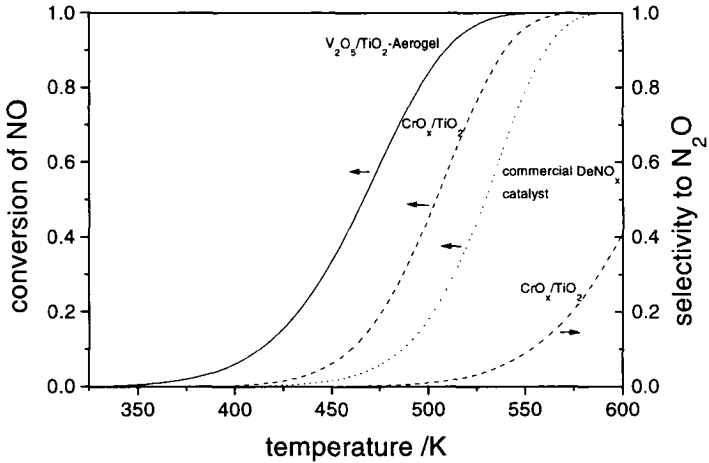


Figure 6-2. NO conversion and N₂O selectivity versus temperature for the different catalysts in the presence of water.

Simulation conditions: feed: 10% O₂, 5% H₂O, 1000 ppm NO, 1000 ppm NH₃, balance N₂, 1.1 bar pressure, gas flow = 500 ml(NTP)/min, catalyst weight = 0.1g.

6.2 Influence of the exhaust composition on the kinetics

All investigated catalysts showed similar dependencies on the oxygen and water concentration, respectively. O₂ accelerated and H₂O decreased the reaction rate. The effects were less pronounced for higher water and oxygen concentrations. Carbon dioxide showed no significant influence on the kinetic behavior for all catalysts. Sulfur dioxide poisoned the CrO_x/TiO₂ catalyst markedly, whereas the vanadia based catalysts showed a sufficient resistance to SO₂.

6.3 Conclusions

The comparison of the catalysts under real SCR conditions, i.e. in the presence of water, showed a distinct improvement of the catalytic performance in the lower temperature range for the newly developed catalysts. Due to the high specific surface and the high vanadia content compared with the other catalysts, the V_2O_5/TiO_2 aerogel exhibits a high activity at very low temperatures.

6.4 References

1. Satterfield C. N. "Heterogeneous Catalysis in Industrial Practice", 2nd edition, McGraw-Hill, New York, 1991.
2. Amiridis D. M., Solar J. P., *Ind. Eng. Chem. Prod.* **35**, 978 (1996).

Final Remarks

The aim of this study was to investigate and model the kinetic behavior of new promising SCR catalysts, which were developed in our laboratory during the last few years.

It has been shown that vanadia-titania aerogels are highly active and selective for the selective catalytic reduction of NO by NH₃, particularly in the low temperature range. It was possible to improve the chemical properties of the chromoxide based catalysts using a new pretreatment without calcination. A significantly lower selectivity to N₂O was achieved, improving the efficiency for the removal of nitrogen oxides at low temperature.

In the future, the elimination of the hindrances to an industrial application has to be in the focus of the research. In the case of the vanadia-titania aerogel catalyst, the preparation has to be modified to lower the costs, and proper methods to manufacture the catalyst in a geometric form, which has sufficient mechanical strength against abrasion and erosion and low pressure drop, has to be developed. The main hindrance for the CrO_x/TiO₂ catalyst is the lack of resistance to the poisoning by SO₂. In the case of a successful improvement of the resistance to poisoning, this type of catalyst would be an interesting alternative to the existing commercial vanadia based catalysts especially in the lower temperature range.

The investigations of the commercial catalysts showed that with simple models the kinetic behavior can be explained. However a proper scale up needs further investigations of the makrokinetics, which also include mass and heat transfer. In the future the dynamic behavior during the start up and the shut down procedure, will have growing importance. The control of the NO_x emission and the ammonia slip during these sequences needs further research and is in the focus of the present research in our laboratory.

List of Publications

The following list summarizes the papers which resulted from this study.

"Selective reduction of NO_x by NH_3 over commercial DeNO_x catalyst: Parametric Sensitivity and kinetic modeling", Willi R., Roduit B., Köppel R. A., Wokaun A. and Baiker A., Chem. Eng. Sci. **51**, 2897 (1996).

"High Performance Aerogel DeNO_x Catalyst: Catalytic Behavior and Kinetic Modeling", Willi R., Köppel R. A. and Baiker A., submitted to Ind. Eng. Chem. Res..

"Selective Reduction of NO by NH_3 over Chromia on Titania Catalyst: Investigation and Modeling of the Kinetic Behavior", Willi R., Maciejewski M., Göbel U., Köppel R. A. and Baiker A., submitted to J. Catal..

Curriculum Vitae

Name : Willi, René
Date of birth : November 11, 1967
Place of birth : Zurich
Nationality : Swiss, citizen of Mels (SG)

Education :

1974 - 1980 Primary School, Mels (SG)
1980 - 1982 Intermediate School, Mels (SG)
1982 - 1986 Grammar School Type C, Sargans (SG)
1987 - 1992 Chemical Engineering studies at the Swiss Federal Institute of
Technology (ETH), Zurich
1993 - 1996 Ph.D. Thesis under the supervision of Prof. Dr. A.
Baiker at the Department of Chemical Engineering
and Industrial Chemistry of the ETH Zurich